



AALBORG UNIVERSITY  
DENMARK

Aalborg University Esbjerg

Department of Civil Engineering

# **Numerical Lower Bound Limit Analysis of Static Loaded Plates by Nonlinear Programming**

– Optimization of Steel and Reinforced Concrete Plates

by

Bo Rasmussen, Ermin Sehovic & Rasmus Urhøj Hansen

Master's Thesis

June 2016

Esbjerg



MASTER'S THESIS 2016

**Numerical Lower Bound Limit Analysis of Static  
Loaded Plates by Nonlinear Programming**

Long Master's Thesis within Structural and Civil Engineering

Esbjerg, 09/06/2016

Total number of pages: 79

---

(Bo Rasmussen)

---

(Ermin Sehovic)

---

(Rasmus Urhøj Hansen)



Department of Civil Engineering  
Division of Structures, Materials and Geotechnics  
Aalborg University Esbjerg  
Esbjerg, Denmark 2016



# Abstract

Two efficient programs for optimizing perfect plastic steel plates and reinforced concrete plates, subjected to static, in-plane forces, are developed. The first program deals with optimization of steel plates by developing a submodeling technique with the purpose of verifying critical stress spots caused by numerical errors in the finite element method. The submodeling approach is possible to conduct as a result of the implementation of an efficient self-developed script in ANSYS. The second program concerns load and material optimization of reinforced concrete structures. The reinforced concrete program is capable of dealing with different plate geometries, based on the restriction of nonlinear yield criterions with regard to reinforced concrete and concentrated reinforcement.

Both programs concern on determining the load bearing capacity of plate structures based on an interaction between a stress-based finite element method and the lower bound theorem. Stress-based plate, beam, and bar elements are introduced as a part of the finite element method. The lower bound limit analyses are conducted by nonlinear optimization algorithms based on the interior point method, which leads to a scalar load multiplier  $\alpha$  defining the load bearing capacity. For enhanced optimization performance, the nonlinear yield criterions in both programs are reformulated to second-order cones.

Finally, the efficiency of the submodeling technique to verify critical stress spots is demonstrated by means of an example of a steel plate subjected to in-plane forces resulting in a geometrical stress singularity.

The efficiency and versatility of the reinforced concrete program is presented by examples of an end wall and casted u-stirrups in the load optimization, whereas a material optimization example resulting in material reduction is presented. When considering the end wall in the load optimization case, it is seen that a 32.5 % higher load multiplier is obtained in comparison to the stringer method when the load is applied in the reinforcement. For the load case where the load is applied in the concrete a 15.9 % higher load multiplier is obtained in comparison to the approach in [1], which is a result of the implementation of nonlinear yield criterions for both the plate element and reinforced bar elements. In the material optimization, the total reinforcement volume is reduced by 30 % when applying the limit load, and this shows the potential of the numerical approach in the thesis.



# Preface

This report is a result of a Masters's Thesis conducted in the period of September 2015 to June 2016 at the Department of Civil Engineering at the Aalborg University Esbjerg. The project has been under the supervision of Professor Lars Damkilde and PhD Fellow Niels Dollerup, both are affiliated to the department of Civil Engineering at Aalborg University Esbjerg. Furthermore, the authors give a special thanks to Sven Krabbenhøft for his help regarding Mosek.

The report concerns optimization of both steel plates and reinforced concrete plates. The theory behind of formulations is presented simultaneously, whereas the application of the described theories is demonstrated separately at the end of the report.

Esbjerg, June 2016

Bo Rasmussen, Ermin Sehovic & Rasmus Urhøj Hansen

# Notation

## Mathematical symbols

[ ]	Rectangular matrix or square matrix
{ }	Column vector, row vector

## Latin Symbols

$A$	area of element
$a_i, b_i$	coordinate difference in x- and y-direction for element side $i$
$B$	number of outer boundary sides
$C$	constraint matrix
$C_s$	strength vector
$d$	direction vector
$E$	number of elements
$f_c$	Compressive strength in concrete
$f_j$	yield condition
$f_t^x, f_t^y$	tensile strength in concrete
$f_y$	yield strength
$g$	constraint function
$h$	element equilibrium matrix
$H$	assembled system equilibrium matrix, Hessian of Lagrangian
$k$	strength parameter
$l, l_i$	length of element and element side $i$
$M_p$	plastic momentum of resistance
$N$	shape functions
$N_p$	plastic resistance regarding normal forces
$p_x, p_y$	load intensity in the $x$ - and $y$ -direction
$q$	generalized external nodal forces
$Q$	element nodal force vector
$R$	system load vector
$R_c$	self-weight load vector
$S$	number of inner boundary sides
$S$	diagonal matrix containing slack variables
$s$	number of shared sides
$s_j$	slack variable
$v$	displacements, (Lagrange multipliers)
$x$	x-coordinate
$y$	y-coordinate
$W^e$	external work
$W^i$	Internal work

$t$	thickness
$T$	matrix containing partial derivatives of Lagrangian
$z$	diagonal matrix containing the Lagrange multipliers

## Greek Symbols

$\alpha$	scalar load multiplier
$\beta$	system stress parameter vector
$\beta^*$	optimized system stress parameter vector
$\gamma$	duality gap, difference between primal and dual solution
$\varepsilon$	strain
$\lambda$	strain rate of each plastic strain (Lagrange multiplier)
$\theta$	rotational angle
$\mu$	barrier parameter
$\Phi$	reinforcement degree
$\sigma_x, \sigma_y, \tau$	in-plane stresses
$\sigma_1, \sigma_2$	principal stresses
$\mathcal{L}$	Lagrange function



# Contents

<b>1. Introduction.....</b>	<b>1</b>
1.1 Material Models .....	3
1.2 Applied Material Models.....	5
1.3 Scope of this Study .....	6
1.4 Overview of the Thesis.....	7
<b>2. Theorems of Limit State Analysis .....</b>	<b>9</b>
2.1 Extremum Principles.....	9
2.2 Existing Limit State Analysis Approaches.....	11
2.3 Yield Conditions.....	12
2.4 Lower Bound Formulation .....	14
<b>3. Finite Element Formulation .....</b>	<b>17</b>
3.1 Triangle Plate Element .....	18
3.2 Bar and Beam Element.....	27
<b>4. Yield Criteria .....</b>	<b>33</b>
4.1 Yield Criterion for Reinforced Concrete Plates .....	33
4.2 Yield Criterion for Concentrated Reinforcement .....	35
4.3 Yield Criterion for Steel Plates.....	36
<b>5. Numerical Limit State Analysis .....</b>	<b>39</b>
5.1 Interior Point Method versus Simplex Method.....	39
5.2 Path-following Interior Point Method.....	40
5.3 Numerical implementation in MATLAB – fmincon.....	46
5.4 Numerical implementation in Mosek (SOCP).....	49
<b>6. Program for Verification of Critical Stress Spots .....</b>	<b>51</b>
6.1 Procedure for Stress Verification .....	53
6.2 Submodeling Technique .....	54
6.3 Submodeling in ANSYS Workbench.....	54
6.4 Parameters Influencing the Load Multiplier .....	57
6.5 Example of Application – Plate with Stress Singularity.....	58
<b>7. Load Optimization of Reinforced Concrete Plates.....</b>	<b>63</b>
7.1 Problem Formulation .....	63
7.2 Example – End Wall Exposed to Wind Load .....	64
7.3 Example – Plate with Curved Reinforcement.....	68
<b>8. Reinforced Concrete Plates – Material Optimization .....</b>	<b>73</b>
8.1 Problem Formulation .....	73
8.2 Weighted Object Function.....	74
8.3 Example – End Wall Exposed to Wind Load .....	75
<b>9. Conclusion .....</b>	<b>79</b>

<b>Appendix A: Upper and Lower Bound Solution of a Statically Indeterminate Beam .....</b>	<b>80</b>
<b>Appendix B: Primal-dual Formulation for Load Optimization .....</b>	<b>83</b>
<b>Appendix C: Example of Path Following Interior Point Method .....</b>	<b>86</b>
<b>Appendix D: Steel Plate Optimization – fmincon Study.....</b>	<b>88</b>
<b>Appendix E: Reformulation of Yield Criteria to Second-Order Cones.....</b>	<b>94</b>
E.1 Reformulation of von Mises Yield Criterion .....	94
E.2 Reformulation of M.P. Nielsen’s Yield Criterion .....	95
E.3 Reformulation of the Nonlinear MN-relation.....	95
<b>Appendix F: Program for Global Steel Plate Optimization .....</b>	<b>97</b>
F.1 Full Plate Model Optimization .....	97
F.2 Convergence Study of a Global Model.....	97
<b>Appendix G: Verification of Critical Stress Spots in Steel Plates – Studies..</b>	<b>101</b>
G.1 Study of Submodel Size .....	101
G.2 Study of Submodel Mesh Refinement.....	106
G.3 Study of Boundary Stresses in ANSYS .....	110
G.4 Study of Cut Boundary Stresses for different Global Meshes .....	113
<b>Appendix H: Interaction of Elements.....</b>	<b>123</b>
H.1 Example with Pure Shear Stress States.....	123
H.2 Compressive Stress State .....	126
<b>Appendix I: Appended Paper .....</b>	<b>129</b>
<b>Bibliography.....</b>	<b>142</b>

# 1. Introduction

Reinforced concrete is the most widely used structural material in the world. A lot of constructions within different fields of civil engineering is nowadays build by use of reinforced concrete, and two typical examples of application are shown in Figure 1.1



(a) *Bridge pier.* [2]



(b) *Axel towers in Copenhagen.* [3]

**Figure 1.1.** *Examples of application of reinforced concrete.*

Different theories for mathematically deriving the strength of reinforced concrete plates have been presented during the history, including the theory of plasticity. Plasticity is a widely approved principle regarding the design of structures, especially when it comes to steel and reinforced concrete structures as they possess ductile properties. By utilizing the theory of plasticity in structural analysis, better proportioned and more economical structures can be designed as the theory represents reality better than the conventional elastic method [4]. Within the field of plasticity, the assumption of perfect plastic material behaviour has often been used in combination with the extremum principles in order to obtain the ultimate load bearing capacity of steel and reinforced concrete structures. When considering a perfect plastic material model, the assumption of sufficient deformation capabilities in the structure is valid. This assumption is necessary in order to obtain stress redistributions. The extremum principles are used in both analytical and numerical mathematics, and especially numerical limit state analyses have gained more attention over the last decades as a result of improved computers, and the invention of new optimization methods. Thus, nowadays highly complex structures are solved efficiently based on numerical methods. The application of a perfect plastic material model for assessing the load bearing capacity of reinforced concrete plates has been treated by numerous engineers, including M.P. Nielsen, and the approach is widely accepted since perfect plasticity is also as a part of the Eurocodes [5].

In a finite element context, it has been more challenging to implement plasticity models of reinforced concrete plates in comparison to reinforced concrete slabs because the contribution from the concentrated reinforcement has to be included [1]. Different methods, based on the extremum principles, for obtaining the load bearing capacity of plates have been utilized, and among these is the widely used stringer method [6]. The stringer method is

characterized as being an idealized representation of the concentrated reinforcement [6]. In the stringer method, the plate is defined as a rectangular shear panel, while the orthogonal concentrated reinforcement is capable of obtaining normal stresses. The demand for rectangular elements and the assumption of a pure shear stress state in the shear panel makes the stringer method disadvantageous for complex problems.

An enhanced numerical method for conducting optimization of reinforced concrete plates is presented in [1]. The method is seen as a more efficient alternative to the stringer method, and it has proven to be more advantageous in comparison to the stringer method as the assumption of a pure shear stress state in the shear panels is not needed. Thereby, a much more refined stress distribution can be obtained, and a higher load can be applied in the design. The approach has proven to be more efficient than the stringer method regarding both the ultimate load bearing capacity and material design. However, in [1] a linear programming approach has been presented, which is not preferable as the yield criteria are convex. This makes room for improvement of the method as both the yield criterion for concrete and reinforcement, respectively, is linearized. By implementing nonlinear yield criteria in the approach, a higher load bearing capacity and more economical structures can be obtained. The advantages in our approach is the implementation of nonlinear criteria for both the reinforced concrete and concentrated reinforcement bar, which makes it possible to obtain a higher load bearing capacity. Furthermore, the nonlinear yield criteria are reformulated to second-order cones, and thereby a time-efficient optimization is obtained.

The presented theory in [1] for optimization of reinforced concrete plates give rise to a wider application. By excluding the concentrated reinforcement in the formulation, and by implementing von Mises yield criterion in the method as a substitution to M.P. Nielsen yield criterion, it is possible to develop an algorithm for optimizing steel plates defined by triangular, stress-based elements. This leads to a program capable of verifying critical stress spots in two-dimensional plates. In the finite element method, it is frequently seen that fulfilling the ultimate limit state becomes a problem when designing static loaded structures by the theory of elasticity [1].

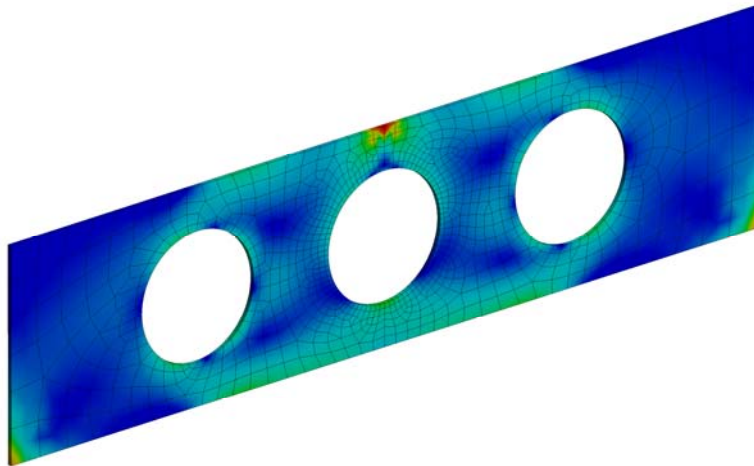


**Figure 1.2.** *Example of a plane structure with a critical stress singularity spot.*

More specific, numerical errors in terms of stress singularity spots (see Figure 1.2) often induce stresses exceeding the elastic load bearing capacity. As a consequence, the verification of critical stress spots often has to be conducted by means of a nonlinear plasticity analysis of the entire structure, which is both time-demanding, in terms of iterations and model size, and furthermore unsafe. To accommodate this problem, the study aims for an efficient method to verify critical stress spots by the theory of plasticity. The objective of the calculation is to efficiently provide a scalar load multiplier that defines the optimal safety level. The advantage of the approach in this study is that only a subarea is considered and that the solver not only gives a lower bound solution, but it calculates the optimal stress distribution. Thereby, it is possible to determine whether critical stress spots lead to structural collapse.

For solving numerical plate problems with a perfect plastic material model in this study, the lower bound method is implemented. The lower bound method has several advantages over the upper bound method, including the fact that the collapse load is on the safe side. The element formulation is stress-based in contrast to elastic finite element formulations that are displacement based. A linear stress field is described in the calculations, which is based on a finite element discretization where each element has a certain number of stress parameters. As only statically underdetermined structures are considered, it gives rise to stress redistributions at yielding spots in the structure. In the lower bound method, it corresponds to that only a part of the stress parameters has to secure equilibrium, whereas the rest of the stress parameters are used to redistribute the load in order to obtain the maximum load bearing capacity. The calculations are based on nonlinear optimization programming since M.P. Nielsen yield criterion and von Mises yield criterion are utilized.

Thereby, the focus of the thesis is to develop a numerical tool, which enables the engineer to efficiently conduct verification of critical stress spots in static loaded steel plates. Secondly, the aim is to develop an efficient program for reinforced concrete plates by implementing nonlinear yield criterions.

## 1.1 Material Models

Through centuries various loading scenarios have been used to examine the response of materials. The purpose was to set up mathematical material models that could forecast the material response. In this thesis two materials are considered; namely, concrete and steel.

### 1.1.1 Concrete

Concrete is a composite material as it consists of at least two materials; namely, cement paste and aggregate particles. The strength and properties of concrete is obtained by mixing aggregate particles with cement and water, which results in a hydration process. A stiffness difference appears in concrete as aggregate typically has a larger stiffness compared to cement paste. This means that the stress field becomes complex when a concrete structure is subjected to loading. As a result of the material compound, stress concentrations occur at the interface between the aggregate and cement paste, which leads to formation of cracks.

Typically, the cracks are so small and occur at stresses much lower than the compressive concrete strength. The internal cracks are so small that they cannot be seen and they are often referred to as microcracks [7]. As a result of crack formation, concrete cannot be considered as an isotropic material in a mechanical point of view.

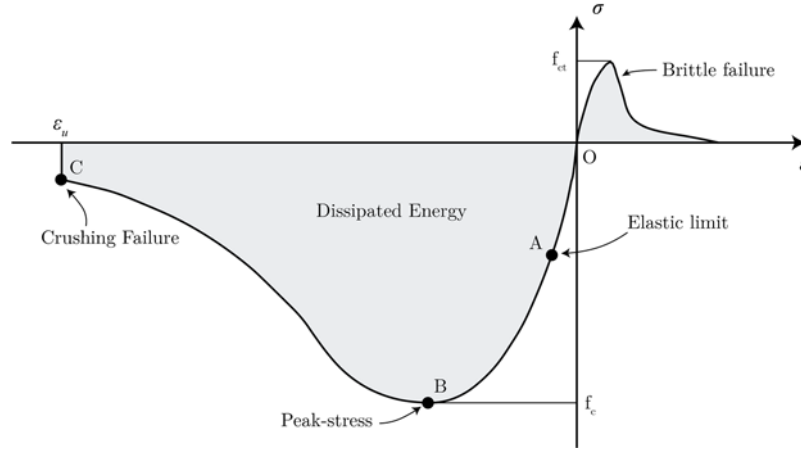


**Figure 1.3.** Stress-strain curve for concrete subjected to uni-axial loading. Illustration from [7].

An example of a stress-strain curve for a concrete structure subjected to uni-axial loading is shown in Figure 1.3. From the figure it can be seen that the compressive strength is much higher in comparison to the tensile strength. The first part in the compressive zone ( $\sigma < 0$ ), that is going from O to A, is the elastic region, and the area beneath is the elastic energy absorbed in the material. When a structure is loaded beyond the elastic limit, the material is subjected to irreversible deformation, which is referred as plastic deformations in this thesis. A hardening process takes place in the transition from the elastic limit at point A to the peak load at point B. After the peak, the structure undergoes a softening process, which is a results of strength weakening because of damages inside the structure. The last stage in the stress-strain curve is point C where the material undergoes global crushing and failure has occurred [7]. When concrete is subjected to tension, a similar material behaviour is seen, see Figure 1.3. The tensile strength of concrete is often neglected as it is highly dependent on the crack formation which makes it unreliable. Thus, steel reinforcement is typically casted into the concrete to establish a reliable tensile strength in the structure. When combining the two materials it is often referred to as a reinforced concrete, and both a ductile compressive and tensile strength is obtained. In both tension and compression, the concrete structure will absorb energy corresponding to the area under the stress-strain curve.

### 1.1.2 Steel

Steel is a common material in many structural designs, and it is characterized by having a ductile behaviour in both compression and tension. The first part of the stress-strain curve describes the elastic progression until reaching the elastic limit, see Figure 1.4.

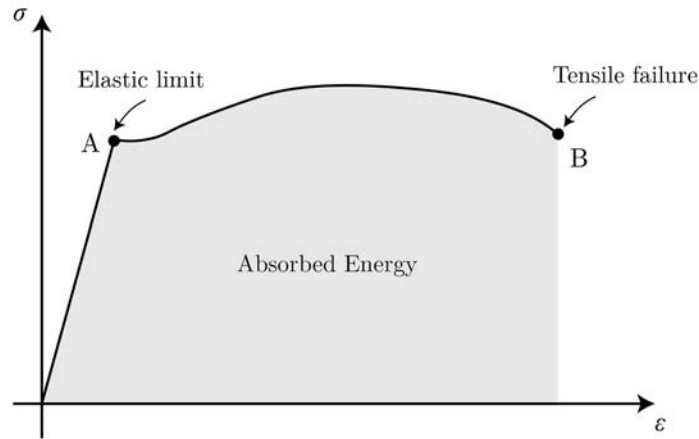


**Figure 1.4.** *Stress-strain for steel subjected to uni-axial loading.*

When exceeding the elastic limit, steel shows plastic properties and irreversible deformations are obtained. Steel is characterized by the ability to increase the strain level even though the maximum level of stress is achieved, which is also illustrated in the figure above.

## 1.2 Applied Material Models

As the actual material behaviour is complex to describe mathematically, an idealized model is used in order to formulate the constitutive relations elaborated in chapter 2. Thus, the aim in this section is to describe and determine the material models appealing to the limit state analyses in this thesis.

When optimizing a limit state problem, the basic concept is to estimate the most optimal solution that satisfies a number of constraints. For that purpose, it is often preferable to make an idealization of the actual material models. The idealization is achieved by a linearization of the plastic region, and it is especially convenient in a numerical perspective where the implementation is more straightforward compared to a full nonlinear stress-strain correlation. Similarly, the numerical approach is more time-efficient as hardening is not an issue, which is a great advantage in large scale problems. In this thesis it is chosen to idealize the material models for both concrete and steel, such that a perfect plastic material behaviour is obtained, see Figure 1.5.

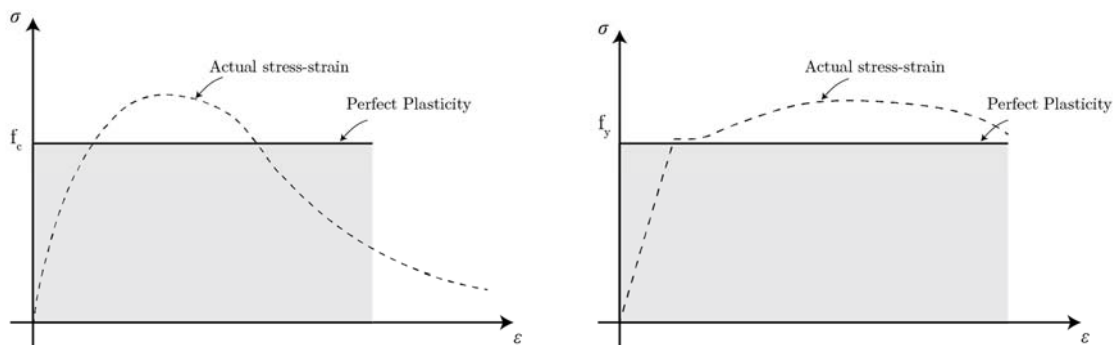


**Figure 1.5.** *Perfect plastic material models for concrete and steel, respectively.*

The perfect plastic material model is without question a coarse idealization in some respect. First of all, no information about the deformation is known before reaching the yield value. Secondly, the unloading scenario corresponds to linear elastic progression. Thus, the material obtains the same stress level for different strain levels, which implies that the cumulative strain is unknown when loading and unloading the structure into the plastic region more than once. The potential to allow deformations going towards infinity is therefore present, why the perfect plastic material model is normally only used to examine the ultimate limit state where the deformational influence is of no interest or importance. In reality, however, testing have proven the perfect plastic material model as being well suited for both steel and reinforced concrete structures in the ultimate limit state, why this model in overall is seen as reasonable for the limit analyses treated in the thesis. Yet, an effective strength is normally added to reinforced concrete structures, which is also the case in this thesis. An effective strength is often added to the concrete in order to use the perfect plastic material model. The effective strength is a reduction factor, which downsizes the load bearing capacity, and it is found by experiments that are hold against the perfect plastic material model. The primary reason for using the factor is to account for the deviation between the actual material model and the perfect plastic model. Similarly, the concrete strength is affected by cracks, which is also included in this factor. This implies a different reduction factor as each concrete strength various, see e.g. [8].

### 1.3 Scope of this Study

The scope of the thesis is to develop two engineering programs; the first program should enable engineers to quickly determine whether stress singularities in two-dimensional steel plates lead to structural collapse, whereas the other program should be capable of conducting load and material optimization of reinforced concrete plates. Both programs are based on the lower bound theorem.

In the first program the aim is to set-up a stress-based finite element model based on a submodeling technique and the lower bound theorem. The convex optimization is solved by an interior point algorithm, and a load bearing capacity is obtained. On behalves of the load bearing capacity it is possible to conclude whether the most critical stress state in the submodel is allowable.

The second program is a further development of the first program since it uses the same plate element formulation. By including bar and beam elements, the aim is to be capable of efficiently optimizing reinforced concrete structures with regard to both material and load optimization.

## 1.4 Overview of the Thesis

This thesis describes the theory and application of both steel plates and reinforced concrete plates. The application for steel plates describes the problem posed when critical stress spots appear in plane structures, while the theory of reinforced concrete plates concerns load and material optimization.

The theory and presumptions are presented from chapter 1 to chapter 5, while the application of the theory is described from chapter 6 to chapter 8.

This chapter describes the issue regarding plate structures in a numerical context. The actual material response when subjecting steel and reinforced concrete to loading is described, and the chapter is concluded by describing different methods for conducting limit analyses.

Chapter 2 introduces the extremum principles, which forms the basis for optimizing structures in this thesis. Furthermore, the yield conditions and the lower bound formulation are presented, which are fundamental for the work in the later chapters. Alternative approaches based on the extremum principles are also evident.

Chapter 3 describes the finite element formulation of plate, beam, and bar elements, and it gives an introduction to the difference between the stiffness-based finite element method and the stress-based finite element method with regard to the lower bound formulation. Furthermore, an explanation of the equilibrium equations is given, and the assembling principle is illustrated.

Chapter 4 deals with the yield criterion for steel plates, reinforced concrete, and concentrated reinforcement, respectively. The expression for the yield criteria are later formulated in terms of constraints in the optimization in order to obtain an allowable lower bound solution.

Chapter 5 initiates with an explanation of the differences between the simplex method and interior point method, and the reason for choosing the interior point method is given. Furthermore, the theory behind the path following primal-dual interior point method is derived. Finally, the implementation of the lower bound theorem and finite element approach in `fmincon` and `Mosek` is described.

Chapter 6 describes the procedure and theory of the developed program for optimization of steel plates by a submodeling approach. The chapter is ended with an example of application.

Chapter 7 and 8 focuses on reinforced concrete plates with regard of load and material optimization. In both chapters the application of the program is presented by examples.



## 2. Theorems of Limit State Analysis

### 2.1 Extremum Principles

A lot of studies have taken place in the field of limit state analysis during the last century in order to assess the load bearing capacity of structures [7]. Common for most of the studies is that they are based on the extremum principles which were formulated by A. Gvozdev in 1936. The extremum principles assume a perfect plastic material model, and this leads to three theorems, which are described in the followings, see Figure 2.1.

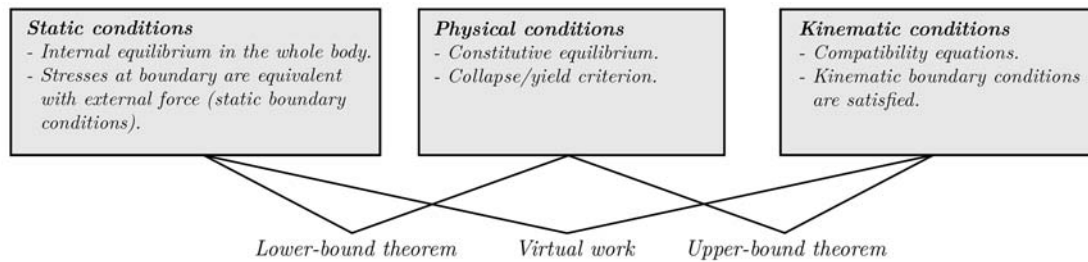


**Figure 2.1.** Extremum principles in relation to the fundamental conditions.

#### 2.1.1 Lower Bound Theorem

The lower bound theorem is restricted by static conditions and physical conditions, see Figure 2.1. An admissible lower bound solution has to satisfy both the static and physical conditions, and this leads to the following lower bound sentence

*The structure will be able to sustain a load if there exists a stress field that is in equilibrium with the load, satisfies all boundary conditions, and is not violating the yield criterion at any point in the structure.*

When statically indeterminate structures are considered, multiple solutions exist and thereby multiple stress fields that satisfies the conditions. This gives rise to an optimization problem where the purpose is to find the largest possible collapse load.

In the lower bound theorem, it is assumed that the structure naturally finds the optimal stress distribution. This implies the utmost load bearing capacity, even though the most optimal stress field might not be chosen. The assumption for allowing stress redistributions is an infinite strain capacity, why the lower bound theorem excludes itself from kinematic conditions and the size of the deformations. The argument for neglecting the deformations is often related to designs where structures are designed with respect to the ultimate limit state. This entails that plastic deformations appear rarely. However, using the lower bound method to estimate the collapse load for the ultimate limit state always leads to a load equal to or lower than the strength of the given structure [9]. This is simply illustrated in 0, where a static indeterminate beam system is calculated by means of the lower bound method.

From this it can be seen that only optimum (the highest load) corresponds to the collapse load.

### 2.1.2 Upper Bound Theorem

The upper bound theorem is based on kinematic collapse mechanisms and is restricted by kinematic and physical conditions, see Figure 2.1. The upper bound sentence reads

*At all possible kinematic collapse mechanisms, the internal plastic work will be higher than the external work caused by the actual collapse load.*

From the sentence it can be understood that the most critical collapse mechanism is always found among all possible collapse mechanisms. [9] In the upper bound theory, the collapse mechanism resulting in the smallest possible collapse load is to be found. That leads to an optimization problem just as it is the case in the lower bound theorem. The upper bound method is thus consistently unsafe when estimating the load bearing capacity since there is a risk of overestimating the collapse load if the proper collapse mechanism isn't determined. The upper bound theorem has a great advantage in simple hand calculations since it is often easy to imagine the collapse mechanisms. In contrast to the upper bound theorem, the stress distribution in the lower bound method is much more difficult to predict as it involves large optimization problems [6]. However, the upper bound method does not appeal for finite element implementation due to time-consuming computational costs.

The indeterminate beam from the example in Appendix A: is likewise calculated by the upper bound method, and it is seen that only one solution corresponds to the lower bound solution.

### 2.1.3 Exact Solution

In order to obtain an exact solution in a structural term, the three fundamental conditions illustrated in Figure 2.1 must be satisfied. Regarding limit analysis, this implies that an exact solution is only obtained if the lower and upper bound solution corresponds to each other. This is due to the conditional difference of each approach, which only together satisfy all three conditions.

The exact solution can thus be understood uniquely, since only one lower and upper bound solution is identical. This is also illustrated in the figure below, where the purpose is to find the collapse load.

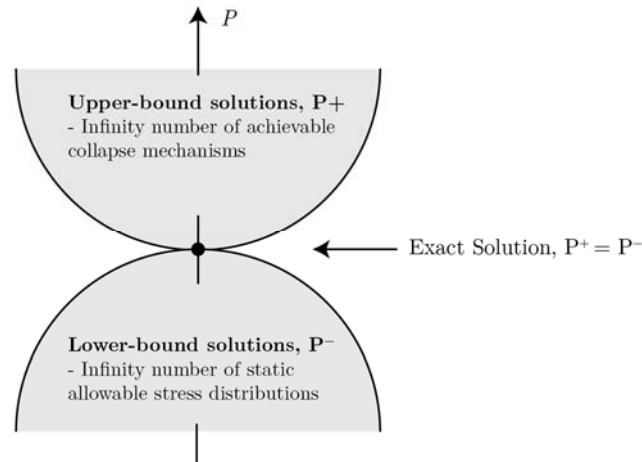


**Figure 2.2.** Illustration of lower and upper bound solutions.

As earlier mentioned the lower bound solution provides estimates of a collapse load that is smaller than or equal to the actual load bearing capacity, while the upper bound solution is vice versa. However, in practice the exact solution is not always accessible by the optimization method applied to the problem. A duality gap can reveal the difference between the lower and upper bound solution and thereby the error of an accepted solution. This is further elaborated when considering the actual optimization algorithm later in this thesis.

## 2.2 Existing Limit State Analysis Approaches

Different approaches, based on the extremum principles, have been developed in order to predict the response of structures. Among these approaches are the *strut-and-tie model*, *yield line method*, and the *stringer Method*.

The Strut-and-Tie method dates back to 1922 [10], and it is based on the lower bound theorem. In the strut-and-tie method the compression bars (struts) are connected to the tension bars (tie) in order to redistribute the load. An optimization problem regarding the connection of the struts and ties has to be maximized in order to obtain the collapse load.

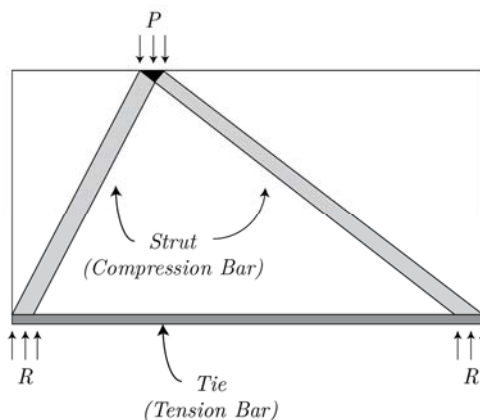


**Figure 2.3.** Example of a Strut-and-Tie model.

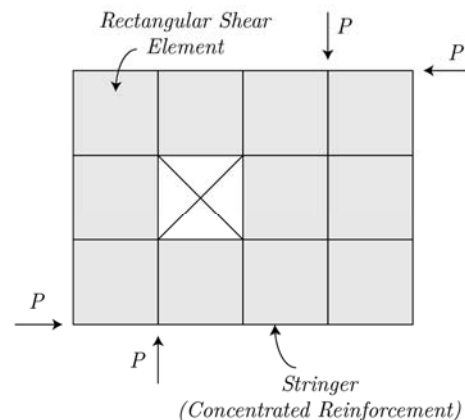


**Figure 2.4.** Example of a Stringer model.

The yield-line theory, based on the upper bound theorem, was formulated by Johansen in 1943 [11] [12]. In manual limit state analysis, the method is widely used for estimating the collapse load of slabs, even though it can lead to an underestimation of the load bearing capacity. The yield-line method can be used for calculating the collapse load of both slabs subjected to bending, and plates subjected to in-plane forces. Despite the wide application in manual limit state analysis, the method isn't suited for finite element implementation.

The stringer method was formulated by Lundgren in 1949, and it is based on the lower bound theorem [13]. In the stringer method, the rectangular fields are defined as shear elements, while the stringers (orthogonal concentrated reinforcement) are capable of carrying normal forces. The demand for rectangular shear panels and the assumption of a pure shear stress state leads to an underestimating of the collapse load. Furthermore, complex models can't be treated due to the geometrical restrictions in the method. An example of a structure modelled by the stringer method is illustrated in Figure 2.4.

A numerical approach for optimizing plates subjected to in-plane forces was proposed in [1]. The approach is based on the lower bound theorem and it is considered as an enhanced strut-and-tie method. In the approach, the stress field is approximated in terms of triangular fields. Their approach has an advantage over the stringer method as the triangular stress fields are capable of carrying both normal stresses and shear stresses, whereas it is only possible to carry shear stresses in the stringer method. Another advantage of the method is the possibility to handle complex structures as the geometry doesn't necessarily has to be of rectangular shape. The method in [1] is also emphasized in this thesis.

## 2.3 Yield Conditions

A yield criterion is a mathematical model that defines the transition from elastic to plastic material behaviour. The yield condition is also called a *yield surface* since it makes a convex boundary as seen in Figure 2.5.

$$f(\sigma_x, \sigma_y, \tau_{xy}) = 0 \quad \forall \quad f(\sigma_1, \sigma_2) = 0, \quad (2.1)$$

When assuming a perfect plastic material behaviour, it leads to a yield criterion with a non-expanding boundary. The yield criterion consists of three stress components for plane structures as indicated in Eq. (2.1).

The yield criterion has a significant role when the extremum principles are considered in the limit analysis. In the lower bound limit analysis, the yield criterion is used to tell whether a given stress state is safe. A model is said to have an allowable stress state if all stresses within the model lies inside or on the yield surface, i.e.  $f(\sigma) \leq 0$ . A visualization of the general considerations can be seen in the figure below.

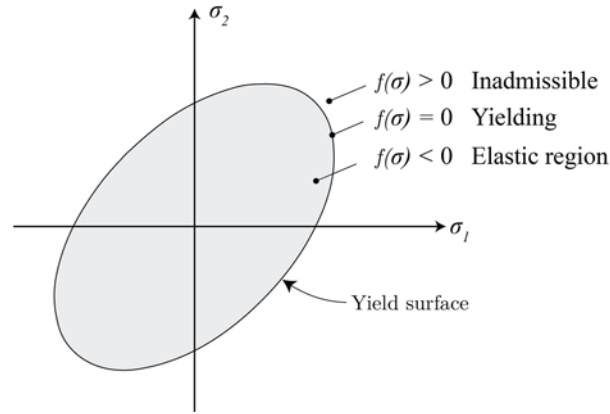


**Figure 2.5.** General yield condition by principal stresses.

When loading the construction into the plastic region the stress state can solely be modified by a stress rearrangement leading to a stress point located along or inside the yield surface. A load normally resulting in hardening will therefore not expand the yield surface and the stress point must for this reason still be located at the yield boundary. Although no expansion of the yield surface can occur due to the perfect plastic material behaviour, the stress point will still relocate when increasing the load.

In the upper bound theorem, the yield condition is used to describe the collapse mechanism for a given strain field. The plastic strain  $\varepsilon^p$  is expressed by von Mises flow rule where the strain state is described as an outward normal to the yield surface [7]

$$\varepsilon_{ij}^p = \lambda \frac{\partial f}{\partial \sigma_{ij}}, \quad (2.2)$$

where the plastic multiplier  $\lambda$  has to be greater or equal to zero, i.e.  $\lambda \geq 0$ . The geometrical interpretation of the strain vector is seen in the figure below.

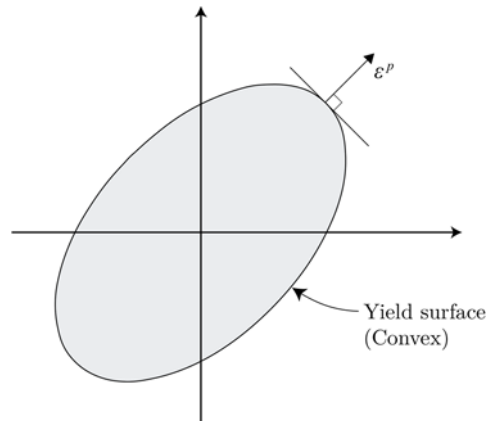


**Figure 2.6.** Flow rule.

Most yield criteria in engineering are based on empirical test that are conducted based on hypotheses.

## 2.4 Lower Bound Formulation

The lower bound method is to be applied in the limit state analysis, where the aim is to determine an optimized stress distribution by maximizing the intensity of the predefined external load. In the lower bound method two conditions have to be satisfied in order to obtain a feasible stress state

- Equilibrium equations (Local equilibrium and equilibrium of stresses across element boundaries)
- Yield criterion

In this case the problem is accommodated by the finite element method with stress-based elements. Stress-based elements are used instead of the traditional displacement-based elements since the problem is formulated as a lower bound method. In the finite element method, the discretized equilibrium equations are written as

$$\mathbf{H}\beta = \mathbf{R}_c + \alpha\mathbf{R}, \quad (2.3)$$

where  $\beta$  is a column vector containing the variables and  $\mathbf{H}$  is the global, assembled equilibrium matrix. The external load is divided into two parts; namely, a constant part  $\mathbf{R}_c$  describing the self-weight of the structure and a part  $\mathbf{R}$  that is proportional to the scalar load multiplier  $\alpha$ . The global equilibrium matrix  $\mathbf{H}$  consists of contributions from all individual elements of a model. When the global equilibrium matrix  $\mathbf{H}$  is set up, the number of stress parameters should be higher than the number of equilibrium equations, which results in a statically underdetermined structure.

The discretized equilibrium equations in Eq. (2.3) can be rewritten to Eq. (2.4), which is later written in a more conventional way

$$\mathbf{H}\beta - \alpha\mathbf{R} = \mathbf{R}_c. \quad (2.4)$$

Two types of constraints have to be set up. The first set of constraints has the purpose of satisfying equilibrium equations, whereas the second set of constraints has to secure that the yield criterion is not violated. The constraint securing that the yield criterion is not violated has to be checked in a number of points in each element. For all elements in a structure, the yield criterion can be expressed as

$$f_j(\beta, k) \leq 0, \quad j = 1, 2, \dots, p, \quad (2.5)$$

where  $k$  is the strength parameter. The nonlinear optimization problem becomes a maximization problem since the lower bound method is considered.

### 2.4.1 Load Optimization

Load optimization has to be conducted for both the steel plates and the reinforced concrete plates. A scalar load multiplier  $\alpha$  has to be determined, which describes the optimal stress distribution in the structure.

The nonlinear lower bound load optimization problem is expressed as

$$\begin{aligned} & \text{maximize:} && \alpha \\ & \text{subject to:} && \mathbf{H}\beta - \alpha\mathbf{R} = \mathbf{R}_c \\ & && f_j(\beta, k) \leq 0, \quad j = 1, 2, \dots, p \end{aligned} \quad (2.6)$$

As it is expressed in Eq. (2.6), the maximization problem is subjected to both equality constraints, since the elements are formulated in terms of equilibrium equations, and inequality constraint in terms of the yield criterions.

By solving the maximization problem in Eq. (2.6) with the corresponding linear and non-linear constraints, it is possible to obtain the optimal value for the load multiplier  $\alpha$  and the corresponding stress parameters  $\beta$ .

In many cases it is convenient to convert the inequality constraints to equality constraints. This is done by implementing slack variables, which only takes positive values. When adding slack variables, the maximization problem in Eq. (2.6) takes the following form

$$\begin{aligned} & \text{maximize:} && \alpha \\ & \text{subject to:} && \mathbf{H}\beta - \alpha\mathbf{R} = \mathbf{R}_c \\ & && f_j(\beta) + s_j = 0, \quad s_j \geq 0, \quad j = 1, 2, \dots, p. \end{aligned} \quad (2.7)$$

This maximization problem has to be solved in order to determine the scalar load multiplier and thereby the collapse load. In the mathematical optimization theory, the primal problem in Eq. (2.7) is reformulated in order to obtain the dual problem. The primal and dual problem can be related to lower and upper bound theorem, and thereby the solution can be obtained in terms of a gap. The mathematical expressions of the primal-dual formulation for load optimization of steel plates is derived in Appendix B:.

### 2.4.2 Material Optimization of Reinforced Concrete Plates

Material optimization has to be conducted for the reinforced concrete plate. The objective is to minimize the total amount of reinforcement volume in order to obtain a more economically advantageous plate structure. Similar to the load optimization, a scalar has to be determined, which in the case of material optimization is the sum of multiple material parameters. The formulation of the material optimization, including slack variables, can be expressed as

$$\begin{aligned}
& \text{minimize} && \{0^T \quad \dots \quad 0^T \quad \mathbf{w}^T\} \begin{Bmatrix} \beta^1 \\ \vdots \\ \beta^n \\ \mathbf{d} \end{Bmatrix} \\
& \text{subject to} && \mathbf{H}\beta = R \\
& && f_j(\beta, d) + s_j = 0, \quad s_j \geq 0, \quad j = 1, 2, \dots, p \\
& && d > 0 .
\end{aligned} \tag{2.8}$$

The minimization problem is subjected to both equality constraints and inequality constraints, where the objective is to minimize the material parameter  $d$ , which is a column vector consisting of the material parameters. The material parameters  $d$  are positive since a strength parameter by nature can't be negative.  $\mathbf{w}$  is a row vector containing the material weighting factors, which include the relative cost of of the different material groups. The equality constraints ensure equilibrium between the internal work and external work. In the material optimization approach, the stress variables are fixed with regard to the external work  $R$  in contrast to the load optimization. The inequality constraints are a funtion of both the stess variables and the material parameters. The application of the theory is presented later in the thesis by means of an example.

### 3. Finite Element Formulation

The lower bound formulation is accommodated by using stress-based elements as a part of an equilibrium based finite element method. In equilibrium based finite element methods, the stress field is approximated and not the structural displacement field as is the case in displacement-based finite element methods. Stress-based elements are used instead of displacement-based elements even though displacement-based elements are the most widely used elements within the finite element method today. The advantage of using stress-based elements in the limit state analysis is that the formulation of the extremum principles is more direct [7].

In the optimization of steel plates only the linear triangle plate element is considered, whereas a combination of the plate element, bar element, and beam element is considered when optimizing reinforced concrete plates.

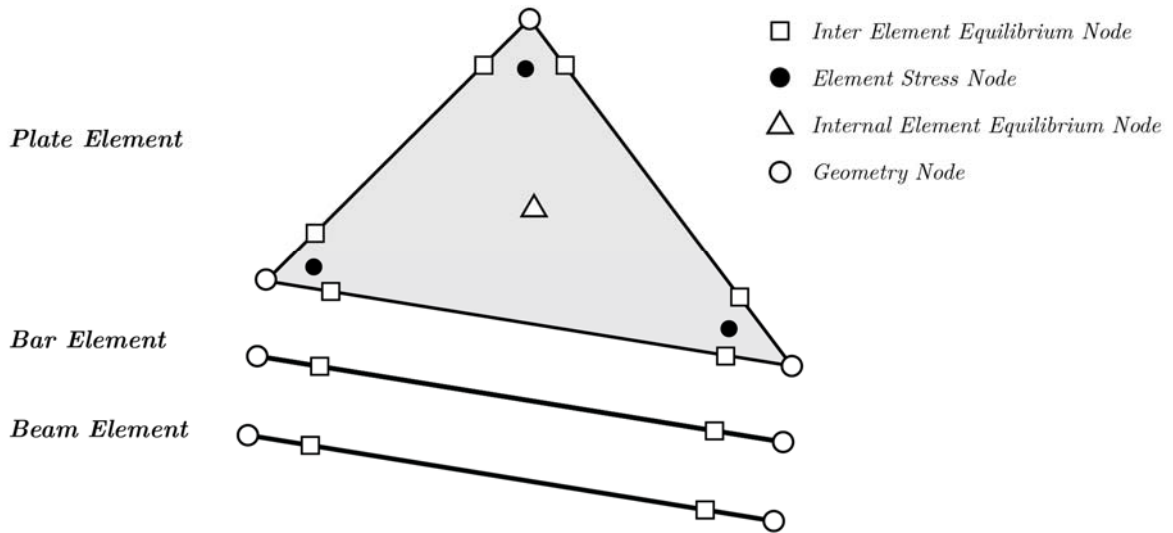


**Figure 3.1.** *Equilibrium based triangle element, bar element, and beam element.*

In the optimization of reinforced concrete, a formulation of a reinforcing bar (rebar) element is introduced as a tension device for concrete plates. In order to compensate for the relatively weak concrete tensile strength, rebars are casted into concrete to obtain a tensile strength capacity. Since the material behavior is assumed perfect plastic, the rebars only guarantee a resistance needed for the design load, whereas the size of the deformations is unknown.

In order to set up the global equilibrium matrix  $\mathbf{H}$  of a structure it is necessary to express the equilibrium equations for a single element. In Eq. (3.1) the equilibrium equations are given in a compact form as

$$\mathbf{q} = \mathbf{h}\beta , \tag{3.1}$$

where  $\mathbf{h}$  is the local equilibrium matrix for an element,  $\beta$  is a vector containing the variables, and  $\mathbf{q}$  are the generalized nodal forces. The nodal forces can either be stresses, forces or moments. [1]

When each local equilibrium element  $\mathbf{h}$  of a structure is formulated, it is necessary to assemble each element  $\mathbf{h}$  into the global equilibrium matrix  $\mathbf{H}$  just as it is the case in the finite element method. The assembly procedure is described later in this chapter.

### 3.1 Triangle Plate Element

A stress-based triangle plate element is formulated, and it is to be used for optimizing both steel plates and reinforced concrete plates. The stress state of each triangular plate element is described by the stresses at each element node. In contrast to the displacement-based methods, the nodal values are unique to each element, which means that stresses don't necessarily take the same value at the same node for the adjacent element. For linear stress elements the admissible stress field is secured at two points on each element side. If higher order stress-based elements were used, an additional node should have been included along each element side. Furthermore, the internal equilibrium of each element must be satisfied in order to obtain a statically admissible solution. This is done by satisfying the equilibrium equations in a number of points lying within each element. For the linear stress triangle, the internal equilibrium equations have to be satisfied at a single point in each element as shown in Figure 3.1.

The stress variation in the element is chosen to be linear, which means that the stresses within the element are interpolated linearly between the nodes. Each plate element consists of three stress parameters  $\sigma_x$ ,  $\sigma_y$ , and  $\tau$  at each node, and thereby a total number of nine stress parameters for each element is obtained, see Figure 3.2.

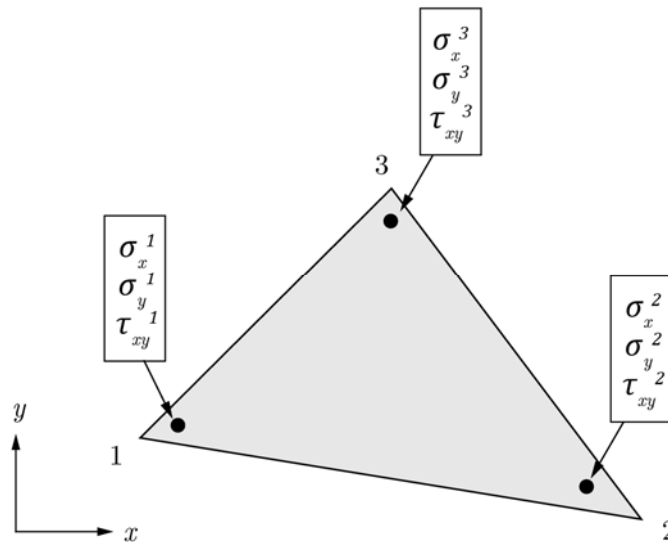


Figure 3.2. Stress parameters for a plate element.

The equilibrium equation from Eq. (3.1) is formulated for a plate element in terms of the following compact form

$$\mathbf{q}_{plate} = \mathbf{h}_{plate} \boldsymbol{\beta}_{plate}. \quad (3.2)$$

The formulation in Eq. (3.2) can be extended to the following matrix form

$$\begin{Bmatrix} \mathbf{q}_1 \\ \mathbf{q}_2 \\ \mathbf{q}_3 \\ \mathbf{q}_c \end{Bmatrix} = \begin{bmatrix} \mathbf{h}_1 & & & \\ & \mathbf{h}_2 & & \\ & & \mathbf{h}_3 & \\ \mathbf{h}_{c1} & \mathbf{h}_{c2} & \mathbf{h}_{c3} & \end{bmatrix} \begin{Bmatrix} \beta_1 \\ \beta_2 \\ \beta_3 \end{Bmatrix}, \quad (3.3)$$

where the subscripts 1, 2 and 3 refer to the nodes shown in Figure 3.2, and the letter  $c$  refers to the center of the element.

The local equilibrium matrix  $\mathbf{h}_{plate}$  in Eq. (3.3) is a  $14 \times 9$  matrix, and it has the purpose of satisfying all equilibrium equations, which is fundamental in the lower bound method.

Some of the equilibrium equations secure continuity in the stresses across element sides, whereas other has the purpose of securing internal element equilibrium [1]. The first twelve rows in the equilibrium matrix  $\mathbf{h}$  has the purpose of securing continuity in the stresses across element sides, whereas the last two rows secure equilibrium between forces from intersecting line elements, also called internal element equilibrium.

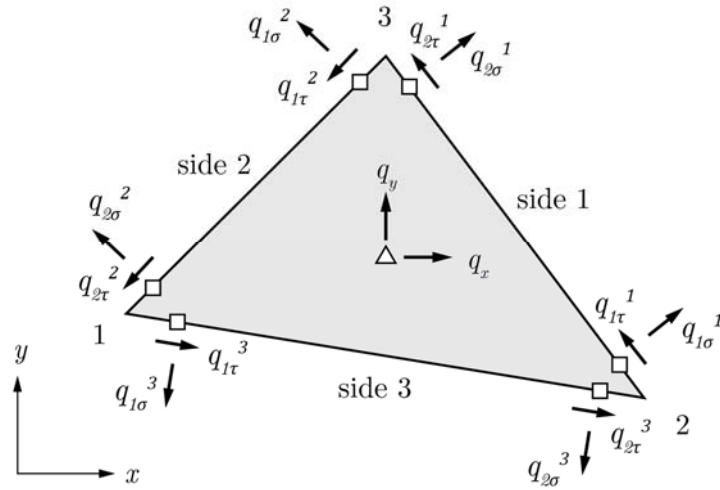


**Figure 3.3.** Generalized nodal forces for the stress-based plate element.

### 3.1.1 Internal Element Equilibrium

The three stress variables at each element node, as seen in Figure 3.2, has to fulfil internal equilibrium in the  $x$ - and  $y$ -direction as given in Eq. (3.4).

$$\begin{aligned} \frac{\partial \sigma_x}{\partial x} + \frac{\partial \tau_{xy}}{\partial y} &= q_x \\ \frac{\partial \sigma_y}{\partial y} + \frac{\partial \tau_{xy}}{\partial x} &= q_y, \end{aligned} \quad (3.4)$$

where  $q_x$  and  $q_y$  are the distributed loads per unit area (body forces) in the gravitational direction. Since the stresses are assumed to vary linearly across the element, the stresses throughout the element are expressed by linear shape functions [14]

$$\sigma_x = \sum_{i=1}^3 N_i \sigma_{xi}, \quad \sigma_y = \sum_{i=1}^3 N_i \sigma_{yi}, \quad \tau_{xy} = \sum_{i=1}^3 N_i \tau_{xi}, \quad (3.5)$$

where  $\sigma_{xi}$ ,  $\sigma_{yi}$  and  $\tau_{xyi}$  are the stress parameters, and  $N_i$  are the linear shape functions. The generalized nodal forces  $q_c$  corresponding to local equilibrium consists of contributions from each element node [1]

$$q_c = \begin{Bmatrix} q_x \\ q_y \end{Bmatrix} = q_{c1} + q_{c2} + q_{c3}. \quad (3.6)$$

The stress contribution from each corner is formulated in both the  $x$ - and  $y$ -direction by substituting Eq. (3.5) into Eq. (3.4), and thereby the following expression is established for the generalized nodal forces

$$q_{ci} = \begin{Bmatrix} 0 \\ q_y \end{Bmatrix} = \begin{bmatrix} \frac{b_i}{2A} & 0 & -\frac{a_i}{2A} \\ 0 & -\frac{a_i}{2A} & \frac{b_i}{2A} \end{bmatrix} \begin{Bmatrix} t\sigma_x^i \\ t\sigma_y^i \\ t\tau^i \end{Bmatrix} = h_{ci} \beta_i, \quad (3.7)$$

where  $h_{ci}$  is depending on the geometry of the element as  $a_i$ ,  $b_i$ , and  $A$  are included in the formula, see Figure 3.4. In Eq. (3.7) it is seen that  $q_x = 0$ , which is due to that it is assumed that the gravitational force only acts in the  $y$ -direction.

The area of the plate element  $A$  is calculated by means of the coordinates of the three element nodes

$$A = \frac{1}{2} \det \begin{bmatrix} 1 & x_i & y_i \\ 1 & x_j & y_j \\ 1 & x_k & y_k \end{bmatrix}, \quad (3.8)$$

where  $i$ ,  $j$  and  $k$  are indices 1, 2 and 3.

The element is numbered such that side  $i$  is opposite node  $i$  (see Figure 3.3 and Figure 3.4), and the length of side  $l_i$  is expressed by the vector  $(a_i, b_i)$

$$a_i = x_k - x_j, \quad b_i = y_k - y_j, \quad l_i = \sqrt{a_i^2 + b_i^2}. \quad (3.9)$$

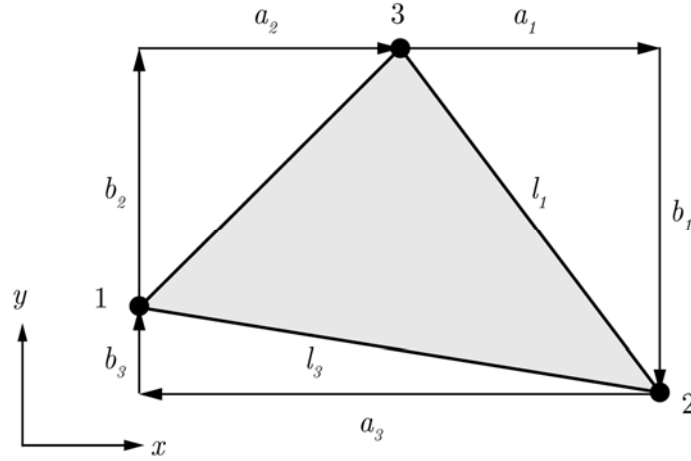


Figure 3.4. Area coordinates.

### 3.1.2 Equilibrium of Stresses across Element Boundaries

As described earlier the equilibrium of stresses across element boundaries also have to be secured. This regard the stresses normal to the plate sides and the shear stresses. Since the stresses are assumed to vary linearly, the equilibrium has to be satisfied at two points along an element side [1]. In this case the nodes at the side ends are chosen as reference points for fulfilling equilibrium, see Figure 3.3.

The generalized nodal forces at node  $i$  are expressed by the internal stresses at node  $i$ . At node  $i$  the four generalized forces are expressed as

$$q_i = \begin{Bmatrix} q_{2\sigma}^j \\ q_{2\tau}^j \\ q_{1\sigma}^k \\ q_{1\tau}^k \end{Bmatrix} = \begin{bmatrix} \frac{b_j^2}{l_j^2} & \frac{a_j^2}{l_j^2} & -\frac{2a_j b_j}{l_j^2} \\ \frac{a_j b_j}{l_j^2} & -\frac{a_j b_j}{l_j^2} & \frac{(b_j^2 - a_j^2)}{l_j^2} \\ \frac{b_k^2}{l_k^2} & \frac{a_k^2}{l_k^2} & -\frac{2a_k b_k}{l_k^2} \\ \frac{a_k b_k}{l_k^2} & -\frac{a_k b_k}{l_k^2} & \frac{b_k^2 - a_k^2}{l_k^2} \end{bmatrix} \begin{Bmatrix} t\sigma_x^i \\ t\sigma_y^i \\ t\tau^i \end{Bmatrix} = h_i \beta_i, \quad (3.10)$$

where  $a$ ,  $b$  and  $l$  are given from Figure 3.4. The constants in the local equilibrium matrix  $\mathbf{h}$  are made from the general continuum stress transformation equations based on equilibrium between forces

$$\begin{aligned} \sigma_n &= \sigma_x \sin^2 \theta + \sigma_y \cos^2 \theta - 2\tau_{xy} \cos \theta \sin \theta \\ \tau_{nt} &= \frac{1}{2}(\sigma_x - \sigma_y) \sin 2\theta + \tau_{xy} \cos 2\theta. \end{aligned} \quad (3.11)$$

The establishment of the equilibrium matrix  $\mathbf{h}_{plate}$  for a plate element is done by combining Eqs. (3.3), (3.7) and (3.10), which thereby satisfies the equilibrium equations.

### 3.1.3 Assembling of the Plate Equilibrium Matrix

Unlike displacement-based elements, each node is unique to the element, and equilibrium is obtained between shared element sides by summarizing the local load contribution  $q_i$  and thereby obtaining equality. If two element sides are united, the equality is satisfied when the equality constraint equals to zero, see Figure 3.5 (b). This is also the case for the outer boundaries, which has to be in equilibrium with the static boundary conditions.

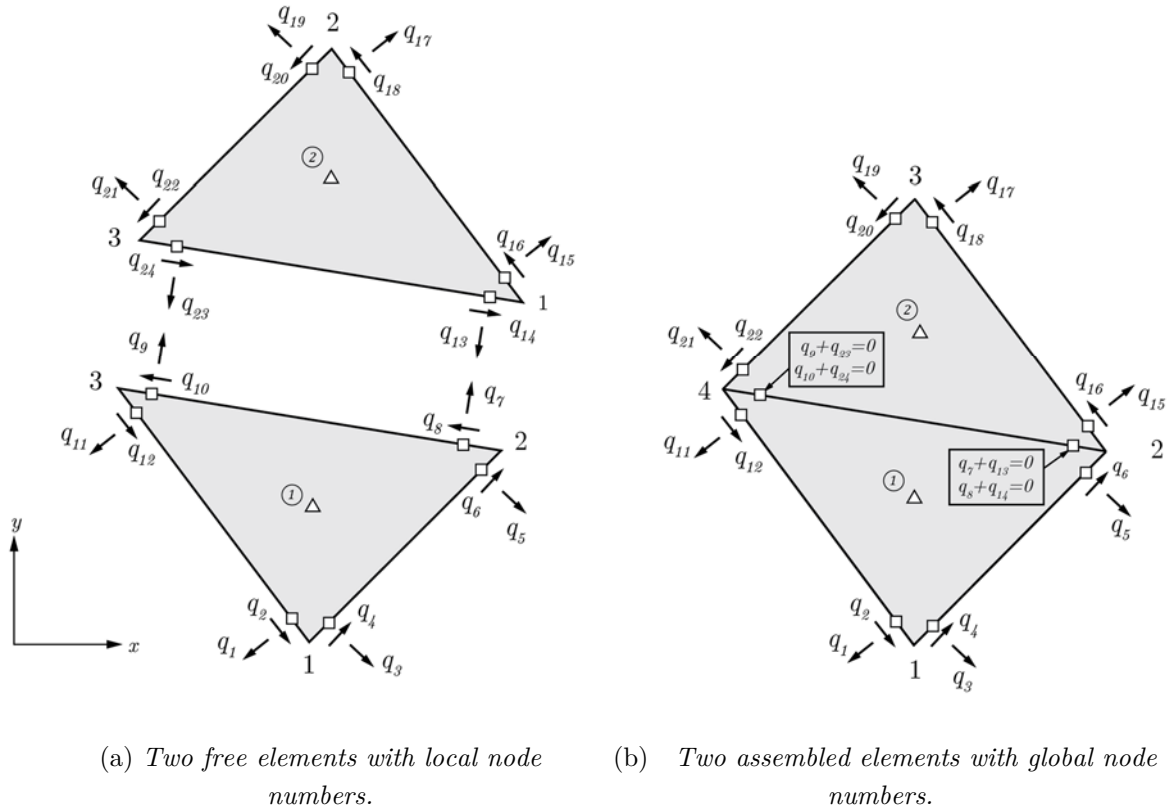
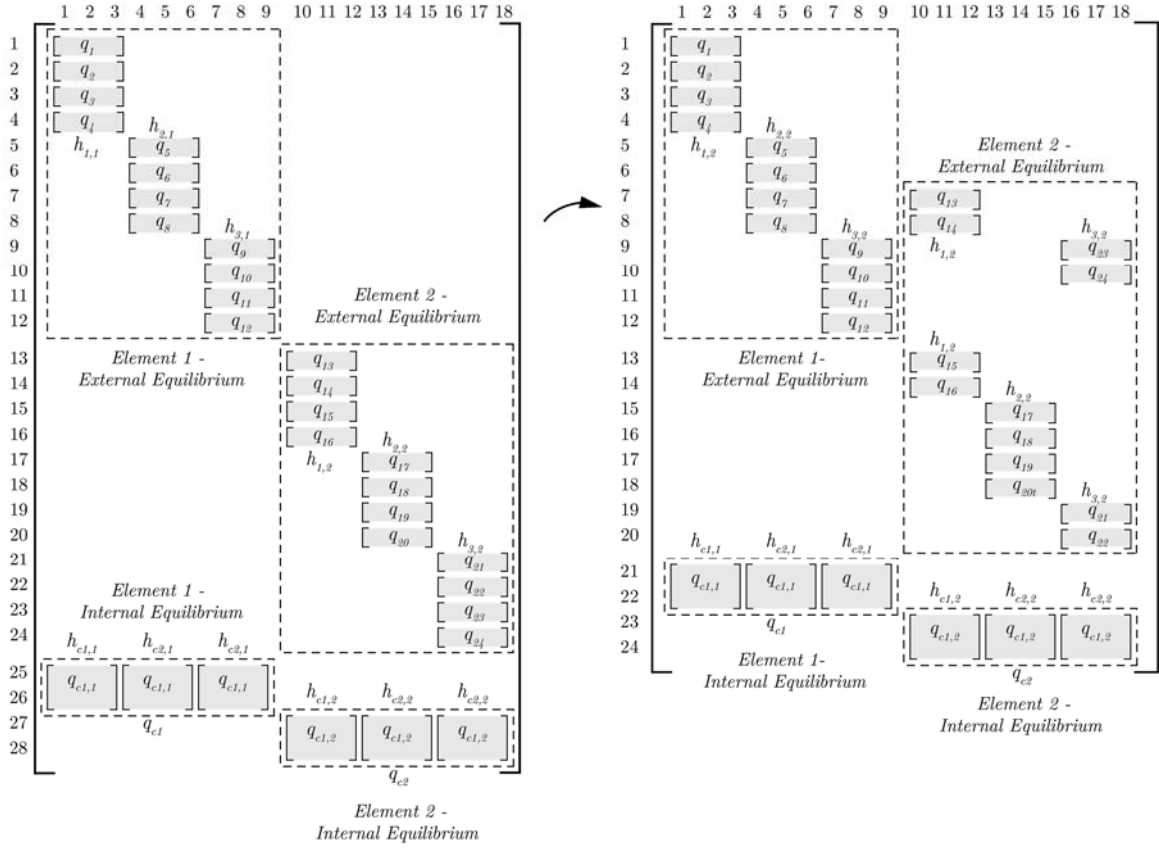


**Figure 3.5.** Before and after assembling of two plate elements.

The stress variables located at the corners are implicitly considered infinitesimal close to the corner nodes, see Figure 3.2. The connection between the stress variables and the generalized nodal forces on the element sides is made from the equilibrium matrix, see Eq. (3.10).

The assembling principle for the global equilibrium matrix  $\mathbf{H}$  is shown in terms of the example given in Figure 3.5. The equilibrium matrices for the example is as shown in Figure 3.6.



(a) Two free elements

(b) Assembled elements

**Figure 3.6.** Global equilibrium matrix  $H$  for example (a) and (b) given in Figure 3.5.

The numbers in Figure 3.6 on the vertical left side and the horizontal top denotes the row and column number, respectively. When having a model consisting of two or more assembled plate elements, the total number of equilibrium equations  $n_q$  becomes

$$n_q = 14E - 4s, \tag{3.12}$$

where  $E$  is the number of elements and  $s$  is the number of shared sides. It should be noted that the number of columns is constant regardless of the connection between elements, which means that only the number of equilibrium equations is reduced and not the number of stress variables.

### 3.1.4 Kinematic Boundary Conditions

Kinematic boundary conditions are implemented in the finite element structure by removing the equilibrium equations that correspond to given generalized nodal forces  $q$ . In the example given in Figure 3.5 (b), simple supports are introduced in the geometrical node 1 and 2, as seen in the figure below.

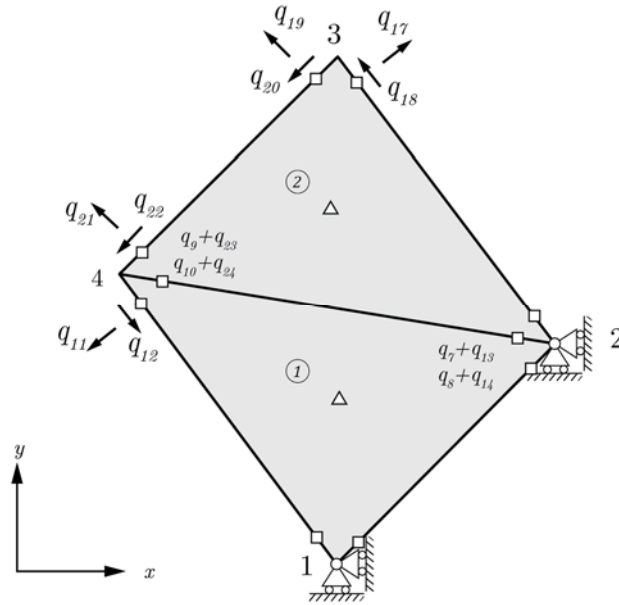


Figure 3.7. Kinematic boundary conditions for example in Figure 3.5 (b).

For the example in Figure 3.7 the global equilibrium matrix  $\mathbf{H}$  is reduced by removing the equilibrium equations related to the following generalized nodal forces;  $q_1, q_2, q_3, q_4, q_5, q_6, q_{15},$  and  $q_{16}$ . The resulting equilibrium matrix  $\mathbf{H}$  after assembling and implementing kinematic boundary conditions is seen in Figure 3.8.

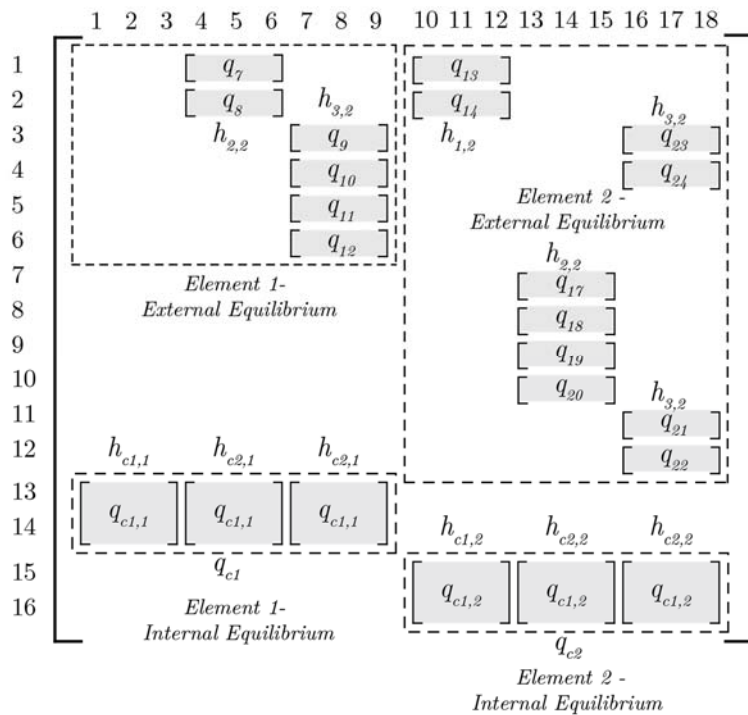


Figure 3.8. Resulting equilibrium matrix  $\mathbf{H}$  including internal equilibrium.

It should be noticed that  $m < n$ , where  $m$  is the number of rows and  $n$  is the number of columns of the equilibrium matrix. From the figure it is seen that the resulting equilibrium matrix consists of 16 equations and 18 stress variables, which means that the system is two

times statically indeterminate ( $18 - 16 = 2$ ). Thereby, it is possible to make a rearrangement of the stresses.

### 3.1.5 Outer Boundary Conditions

The load vector is assembled by the same principles as the global equilibrium matrix,  $H$ . The task in a finite element context is to apply the outer boundary load  $q_b$  to the corresponding equilibrium equation (see Eq. (3.1)), and thereby prescribe the equality constraints on the global outer boundary. The boundary load is given from the three stresses  $\sigma_x$ ,  $\sigma_y$  and  $\tau_{xy}$ , which vary linearly along the element boundary. In Figure 3.9 a simplification is made by showing the stress variation acting normal to an outer boundary.

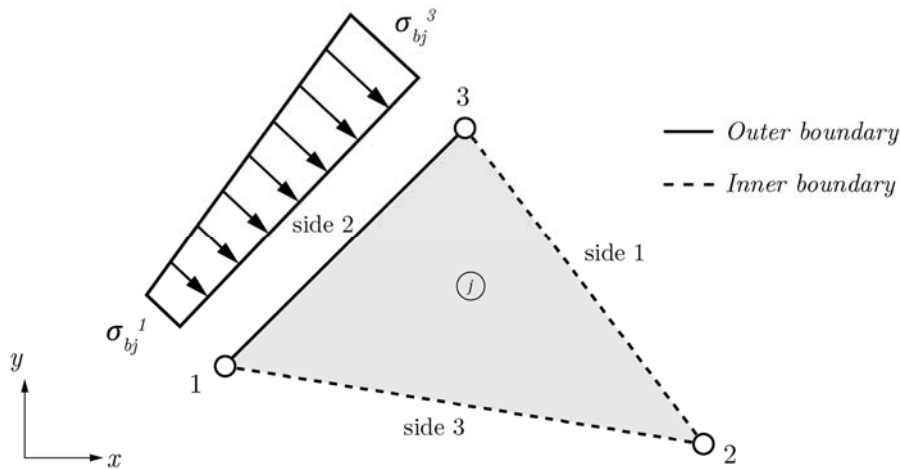


Figure 3.9. Boundary condition for element  $j$ .

In Figure 3.9 the three external stresses are acting linearly on side 2, which is located on an outer boundary. The dashed sides, 1 and 3, are located on an inner boundary and they have to be in equilibrium with the adjacent elements. The nodal stress parameters that are located at a node with one side belonging to an outer boundary have two equality constraints, which means that a side on a boundary produces four equality constraints, see the figure below.

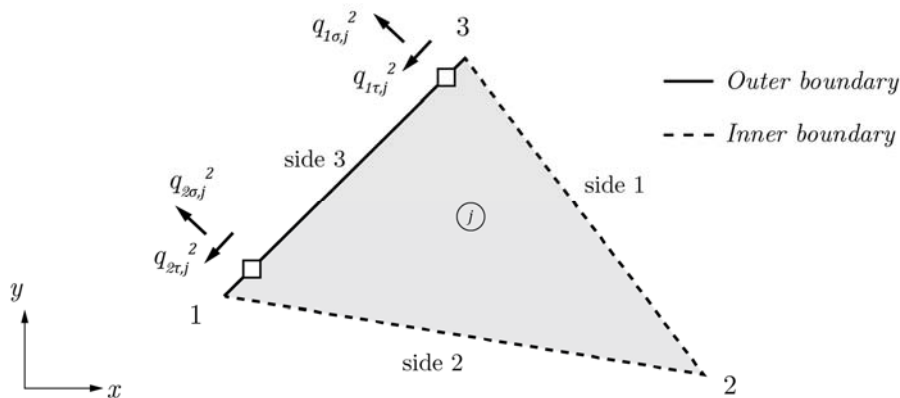
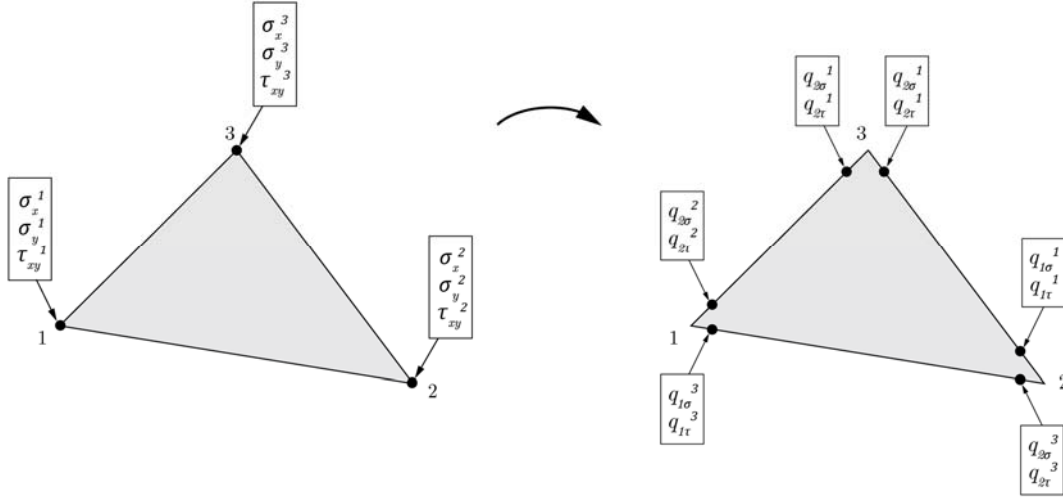


Figure 3.10. Generalized outer boundary loads for element  $j$ .

The boundary stresses are transformed to equality constraints by the following expression

$$\{q_{b,j}^i\} = \begin{Bmatrix} q_{\sigma,j}^i \\ q_{\tau,j}^i \end{Bmatrix} = [h_{b,j}^i] \{\sigma_{b,j}^i\}, \quad (3.13)$$

where  $i$  is the node number,  $j$  is the element number,  $q_b$  is the generalized boundary load, including  $q_\sigma$  and  $q_\tau$ ,  $h_b$  is the boundary transformation matrix, and  $\sigma_b$  are the boundary stresses  $\sigma_x, \sigma_y$ , and  $\tau_{xy}$ .



**Figure 3.11.** Transformation from outer stresses to generalized forces.

By use of the same parameters given in Figure 3.4, the transformation matrix,  $h_b$ , referring to the equality constraints at node 1 on side 2 can be written as

$$[h_{b,j}^1] = \begin{bmatrix} \frac{b_2^2}{l_2^2} & \frac{a_2^2}{l_2^2} & -\frac{2a_2b_2}{l_2^2} \\ \frac{a_2b_2}{l_2^2} & -\frac{a_2b_2}{l_2^2} & \frac{(b_2^2 - a_2^2)}{l_2^2} \end{bmatrix}, \quad (3.14)$$

where the boundary stresses at node 1 are arranged as

$$\{\sigma_{b,j}^i\}^T = \{\sigma_{x,b}^1 \ \sigma_{y,b}^1 \ \tau_{xy,b}^1\}. \quad (3.15)$$

The procedure applies to node 3, which together with node 1 produces 4 equality constraints to the 6 stress variables on the outer boundary (side 2), see Figure 3.10.

### 3.1.6 Assembling of Load Vector

The load vector  $R$  is assembled with respect to all the equalities that have to be fulfilled in the finite element formulation. The load vector contains the three different equality constraints, which are determined from Eq. (3.7), (3.10) and (3.13). The equalities have to be inserted in the appropriate rows in order to satisfy all the equilibrium equations. The assembling of the load vector can then be summarized by

$$\{R\} = \sum_{j=1}^B \{q_{b,j}\} + \sum_{k=1}^E \{q_{c,k}\} + \sum_{l=1}^S \{q_{i,l}\}, \tag{3.16}$$

where  $R$  is the global load vector/equality constraints,  $B$  is the number of outer boundary nodes,  $E$  is the number of elements, and  $S$  is the number of inner boundary sides.

### 3.2 Bar and Beam Element

A formulation of a beam and bar element (rebar element) is introduced with the main purpose of acting as a tension device in concrete plates. In a finite element perspective, the rebar element is a combination of a bar and beam element, and thus the rebar element holds both beam and bar properties. Since concrete is assumed having no tensile strength, the purpose is to obtain all the tensile stresses in the reinforcement, whereas the compressive stresses have to be obtained in the concrete.

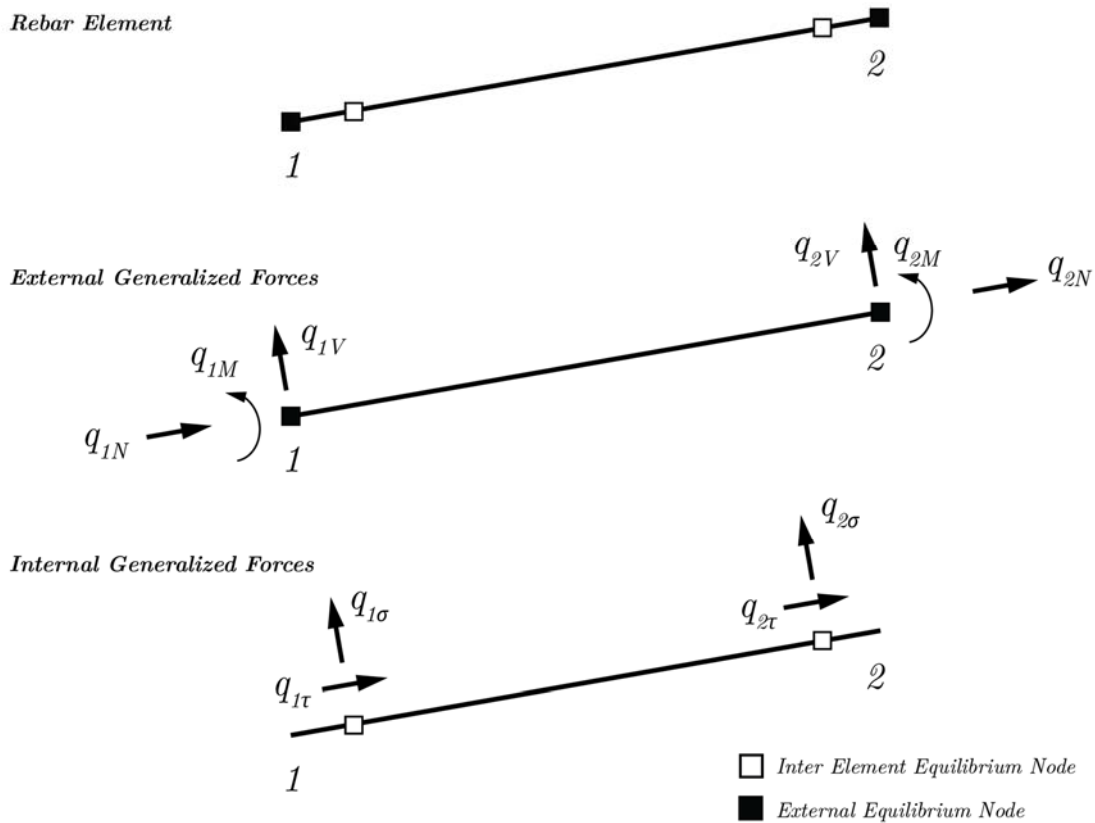


**Figure 3.12.** External and internal generalized nodal forces for a rebar element.

The forces in the formulated concrete structure are transferred by an interaction between the plate elements and the rebar elements. The rebar element must ensure equilibrium between adjacent plate elements as well as adjacent rebar elements. In order to secure interaction between two adjacent rebar elements external generalized forces are introduced, whereas equilibrium between rebar elements and plate elements is secured by the internal generalized forces. The external generalized forces acting on the rebar element are equivalent

to the well-known displacement-based element formulation, where three degrees of freedom are acting at each node, see Figure 3.12.

To obtain equilibrium in the rebar element ten equality constraints for each rebar element has to be fulfilled, where the 6 equality constraint corresponds to the interaction between the adjacent rebar elements, and the last 4 equality constraints corresponds to the interaction between rebar and plate elements, see Figure 3.12.

### 3.2.1 Equilibrium across Rebar Element Boundaries

Since the force varies linearly along the plate element boundary, the normal force has a quadratic variation and the moment has a cubic variation. The normal force in the bar element is interpolated by an equally spaced 3-point arrangement with two nodes, see Figure 3.13.

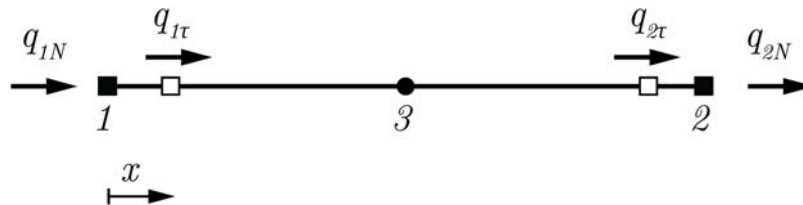


**Figure 3.13.** Quadratic bar element with generalized nodal forces.

The moment in the beam element is interpolated by an equally spaced 4-point arrangement with 2-nodes, see Figure 3.14.

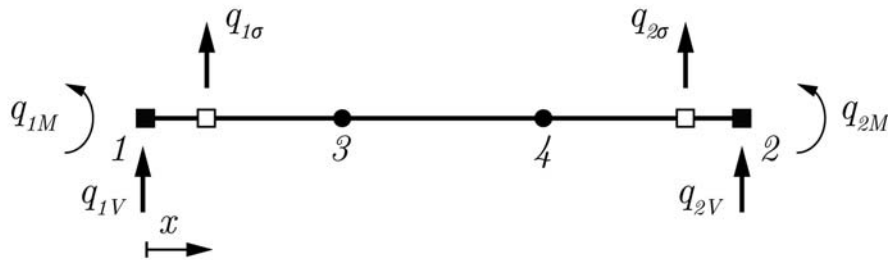


**Figure 3.14.** Cubic beam element with generalized nodal forces.

To fulfil the continuity requirements of the stress variation over the entire element, the quadratic stress variation is described through three stress variables, which is related to a 2nd order polynomial. Similarly, the cubic stress variation is described through four stress variables, which is related to a 3rd order polynomial.

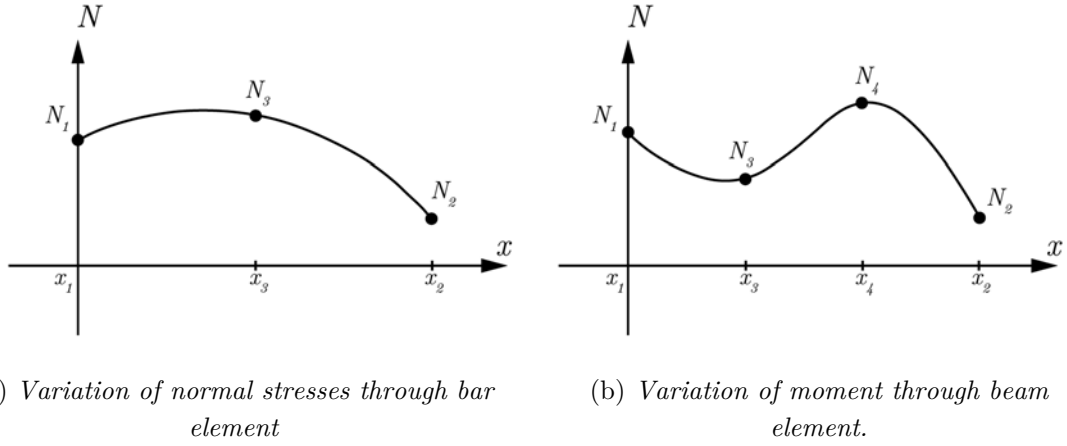


**Figure 3.15.** Variation of normal stresses and moments.

The quadratic interpolation fits a parabola to the points  $(x_1, N_1)$ ,  $(x_2, N_2)$ , and  $(x_3, N_3)$ , where  $x$  is the position and  $N$  is the normal force acting in the bar. The cubic interpolation fits 3th order polynomial to the points  $(x_1, M_1)$ ,  $(x_2, M_2)$ ,  $(x_3, N_3)$  and  $(x_4, N_4)$ . The quadratic and cubic shape function are made from Lagrange's interpolation formula, which in the physical coordinate system is expressed by

$$q_N(x) = \sum_{i=1}^3 L_i(x)N_i \quad (3.17)$$

$$q_M(x) = \sum_{i=1}^4 L_i(x)M_i,$$

where  $L_i$  is the Lagrange shape function expressed in physical coordinates.

The generalized axial stresses  $q_\tau$  are determined by the first derivative of the internal normal stresses, which in the physical coordinates can be determined from Eq. (3.18).

$$q_\tau(x) = \frac{d}{dx} q_N(x) \quad (3.18)$$

In order to have a proper interaction between beam elements, it is necessary to formulate the internal distribution. Due to the cubic varying moment, the shear force  $q_V$  must be quadratic. The variation of shear stresses is determined by the first derivative of the moment. In the physical coordinate system it can be expressed as

$$q_V(x) = \frac{d}{dx} q_M(x). \quad (3.19)$$

Equally the generalized transverse load is of a linear varying form due to the moment variation and it can be determined by the second derivative, which in the physical coordinate system can be expressed from

$$q_\sigma(x) = \frac{d^2}{d^2x} q_M(x). \quad (3.20)$$

The equilibrium matrix which ensure equilibrium between the bar element, beam element and plate element is in compact form expressed by

$$q_{beam} = h_{beam}\beta_{beam}, \quad (3.21)$$

where  $q_{beam}$  is a vector with generalized forces, and  $h_{beam}$  is a matrix that ensures equilibrium between internal and external stresses. The equilibrium matrix,  $h_{beam}$ , is divided into two parts, in which the first part only includes the generalized forces from Eq. (3.18) and Eq. (3.20). The two equations express the equilibrium between bar elements, beam elements and plate elements.

$$\begin{Bmatrix} q_{1\sigma} \\ q_{1\tau} \\ q_{2\sigma} \\ q_{2\tau} \end{Bmatrix} = \begin{bmatrix} 0 & 0 & 0 & -\frac{18}{l^2} & \frac{9}{l^2} & \frac{45}{l^2} & -\frac{36}{l^2} \\ \frac{3}{l} & \frac{1}{l} & -\frac{4}{l} & 0 & 0 & 0 & 0 \\ 0 & 0 & 0 & \frac{9}{l^2} & -\frac{18}{l^2} & -\frac{36}{l^2} & \frac{45}{l^2} \\ -\frac{1}{l} & \frac{3}{l} & \frac{4}{l} & 0 & 0 & 0 & 0 \end{bmatrix} \begin{Bmatrix} N_1 \\ N_2 \\ N_3 \\ M_1 \\ M_2 \\ M_3 \\ M_4 \end{Bmatrix} \quad (3.22)$$

The other part includes the nodal forces from Eq. (3.17) and Eq. (3.19) and ensures equilibrium between beam/bar elements.

$$\begin{Bmatrix} q_{1N} \\ q_{1V} \\ q_{1M} \\ q_{2N} \\ q_{2V} \\ q_{2M} \end{Bmatrix} = \begin{bmatrix} -1 & 0 & 0 & 0 & 0 & 0 & 0 \\ 0 & 0 & 0 & -\frac{11}{2l} & \frac{1}{l} & \frac{9}{l} & -\frac{9}{2l} \\ 0 & 0 & 0 & -1 & 0 & 0 & 0 \\ 0 & 1 & 0 & 0 & 0 & 0 & 0 \\ 0 & 0 & 0 & \frac{1}{l} & -\frac{11}{2l} & -\frac{9}{2l} & \frac{9}{l} \\ 0 & 0 & 0 & 0 & 1 & 0 & 0 \end{bmatrix} \begin{Bmatrix} N_1 \\ N_2 \\ N_3 \\ M_1 \\ M_2 \\ M_3 \\ M_4 \end{Bmatrix} \quad (3.23)$$

The rotation is obtained in the concrete by directly transferring the stresses perpendicular to beam in the plate generalized nodal forces.

Finally, moments and shear stresses in the beam are small in order to fulfil the static boundary condition, why it is assumed to be negligible to control yielding due to shear stresses.

### 3.2.2 Assembling of the Concrete Equilibrium Matrix

The assembling procedure when including rebar elements is similar to the procedure described earlier in this chapter. An example of assembling a rebar element with a plate element is seen in the figure below.

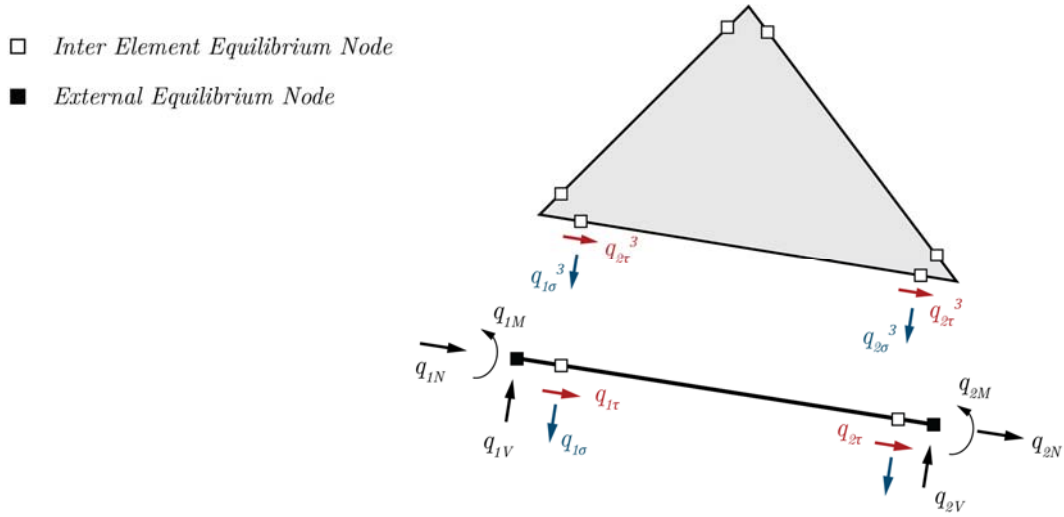


**Figure 3.16.** Principle of assembling a rebar element with a plate element.

The generalized nodal forces,  $q_\sigma$  and  $q_\tau$ , in the inter element equilibrium node for the rebar element has to be added up with the corresponding nodal forces for the plate element. The sum of the generalized nodal forces in the inter element equilibrium node has to equal zero. Two rebar elements are assembled with by adding the three external generalized nodal forces with the corresponding forces in the adjacent rebar element. The total number of equations  $n_q$  describing the rebar nodal forces becomes

$$n_q = 6N_r - 3s_n, \quad (3.24)$$

where  $N_r$  is the number of rebar elements, and  $s_n$  is the number of shared nodes. It should be noted that the number of columns is constant regardless of the connection between elements, which means that only the number of equilibrium equations is reduced and not the number of normal force and moment variables.



## 4. Yield Criteria

The objective function in the lower bound formulation in section 2.4 is constrained by a yield criterion, which has to be fulfilled in order to obtain an allowable lower bound solution. Hence, this chapter presents the criteria used to define the limit of steel plates and reinforced concrete plates with regard to load optimization and material optimization.

### 4.1 Yield Criterion for Reinforced Concrete Plates

In order to optimize reinforced concrete plates, a yield criterion is needed to describe the capacity of the composite material. [5] M.P. Nielsen suggested a yield criterion that defines the shear capacity of reinforced concrete plates with respect to normal stresses. Fundamental for the understanding of the criterion is the assumption of zero tensile capacity in the concrete, perfect plastic material behaviour of the reinforcement, and no shear capacity in the reinforcement. For the concrete this implies that the yield condition in a plane of principal stresses can be visualized as a modified Coulomb material, see Figure 4.1.

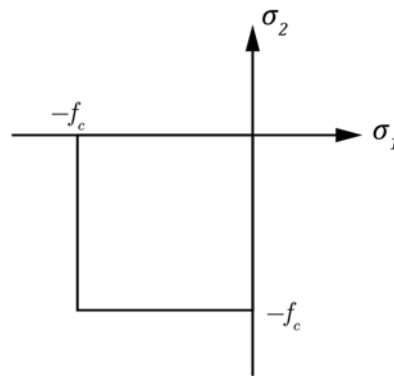


**Figure 4.1.** In-plane yield condition of concrete by principal stresses ( $f_c$  is the compressive strength).

Reinforcement in concrete is needed since a pure shear stress state will result in cracking since the tensile strength of concrete is assumed zero, see Figure 4.2.

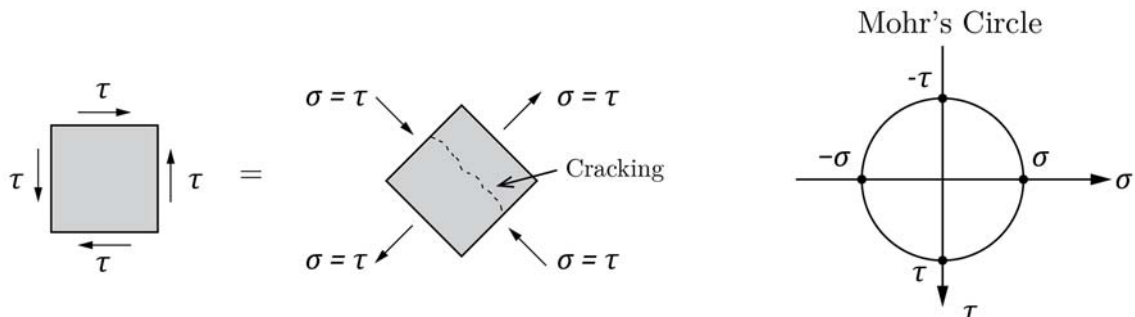


**Figure 4.2.** Pure shear stress state transformed to pure tension/compression by Mohr's Circle.

Hence, the plate structure needs reinforcement, which is most clearly seen by the shear stress example. The inclusion of reinforcement to concrete provides either an isotropic or

anisotropic tensile strength to the material. This tensile strength of the composite concrete material is given by

$$f_t^x = \frac{A_x f_y}{t} \quad \wedge \quad f_t^y = \frac{A_y f_y}{t}, \quad (4.1)$$

where  $A_x$  and  $A_y$  are the areas of reinforcement per length unit,  $f_y$  is the yield stress of the reinforcement, and  $t$  is the thickness of the concrete. In reality, the reinforcement adds a compressive strength to the plate structure as well, but as this contribution in many cases is small compared to the compressive strength of concrete it is chosen to be neglected. The plane yield condition of reinforced concrete plates is illustrated in Figure 4.3.

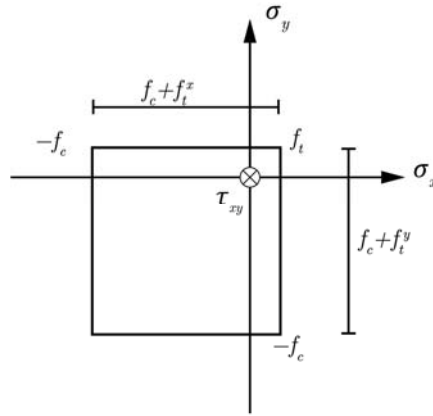


**Figure 4.3.** *In plane yield condition of reinforced concrete plates.*

Consequently, the normal stresses must be located within the following intervals

$$-f_c \leq \sigma_x \leq f_t^x \quad (4.2)$$

$$-f_c \leq \sigma_y \leq f_t^y \quad (4.3)$$

In a finite element aspect, the stress-based elements are assumed to have both compressive and tensile properties. An illustration of the element is seen in Figure 4.4.

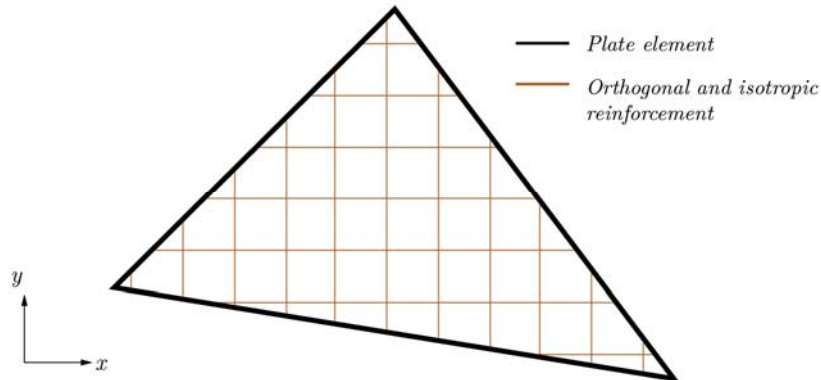


**Figure 4.4.** *Plate element with properties from composite material.*

In order to formulate the three-dimensional M.P. Nielsen yield surface, the shear capacity,  $\tau_{xy}$ , has to be described as a function of the normal stresses,  $\sigma_x$  and  $\sigma_y$ , that are located inside the contour of Figure 4.3. By realizing that the three-dimensional yield surface can

only be described by two functions, it is possible to use the expressions for principal stresses to derive M.P. Nielsen yield criterion

$$-(f_t^x - \sigma_x)(f_t^y - \sigma_y) + \tau_{xy}^2 \leq 0 \quad (4.4)$$

$$-(f_c + \sigma_x)(f_c + \sigma_y) + \tau_{xy}^2 \leq 0 . \quad (4.5)$$

If considering the above equations, it can be seen that the constraints restrict each other with respect to the allowable shear capacity.

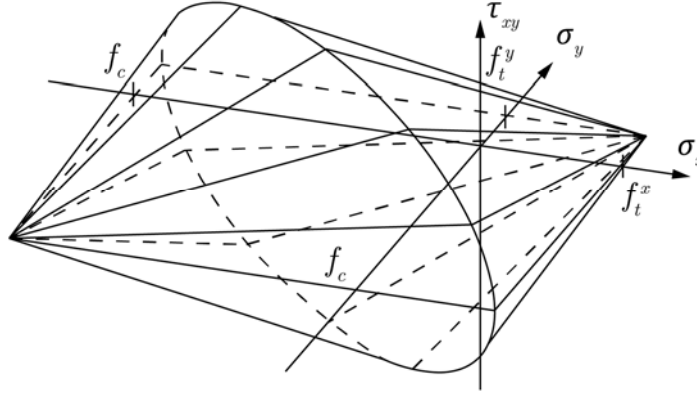


**Figure 4.5.** *M.P. Nielsen's yield criterion for reinforced concrete plates. Illustration from [1].*

The full derivation of Eq. (4.4) and (4.5) can be seen in e.g. [5], and it is important to notice that the above equations are only allowed for reinforcement degrees,  $\Phi$ , less than 0.3.

$$\Phi = \frac{A_x f_y}{t f_c} \wedge \frac{A_y f_x}{t f_c} \leq 0,3 \quad (4.6)$$

When  $\Phi \geq 0.3$ , a bound for the shear capacity needs to be added to the system

$$-0.5f_c \leq \tau_{xy} \leq 0.5f_c , \quad (4.7)$$

which can be seen as a simplification of the high reinforcement degree. This limit is needed as the shear capacity is only related to the concrete as a start. Hence, for small reinforcement degrees,  $\Phi \leq 0.3$ , the influence is considered small and therefore no limit is introduced.

## 4.2 Yield Criterion for Concentrated Reinforcement

The concentrated reinforcement capacity in reinforced concrete plates is established by a yield locus that accounts for the plastic bending moment and the normal force (MN-relation). The limit of the plastic MN-relation is given by the following two expressions [15]

$$f(M, N) = \left( \frac{M}{M_p} \right) + \left( \frac{N}{N_p} \right)^2 - 1 = 0 \quad (4.8)$$

$$f(M, N) = \left( \frac{M}{M_p} \right) - \left( \frac{N}{N_p} \right)^2 + 1 = 0 , \quad (4.9)$$

where  $M_p$  and  $N_p$ , denotes the plastic resistance with respect to the moment and the plastic normal force capacity, respectively. The full derivation of the above equation can be seen in [16], and common is that shear is not accounted for in the concentrated reinforcement as the shear capacity is considered despairingly small. This is further explained in [5].

The corresponding elastic limit is given by

$$f(M, N) = \pm \left( \frac{M}{M_{el}} \right) \pm \left( \frac{N}{N_{el}} \right) - 1 = 0, \quad (4.10)$$

where  $M_{el}$  and  $N_{el}$  are the elastic moment and normal force capacity, respectively.

The fractions in Eq. (4.9) and (4.10) are restricted to be located in the interval of

$$-1 \leq \left( \frac{M}{M_p} \right) \wedge \left( \frac{N}{N_p} \right) \wedge \left( \frac{M}{M_{el}} \right) \wedge \left( \frac{N}{N_{el}} \right) \leq 1. \quad (4.11)$$

An illustration of the plastic and elastic limit is shown in Figure 4.6 a). As perfect plasticity is assumed for the limit state problems, optimization of the reinforced concrete plates naturally follows the plastic limit. For that reason, the moment and normal force values acting on the beam and bar elements must be located inside or along the plastic yield surface. Hence, the cross-sections of the reinforcement have a stress distribution dictated by the yield function, which depends on the observation point. This is illustrated in Figure 4.6 b).

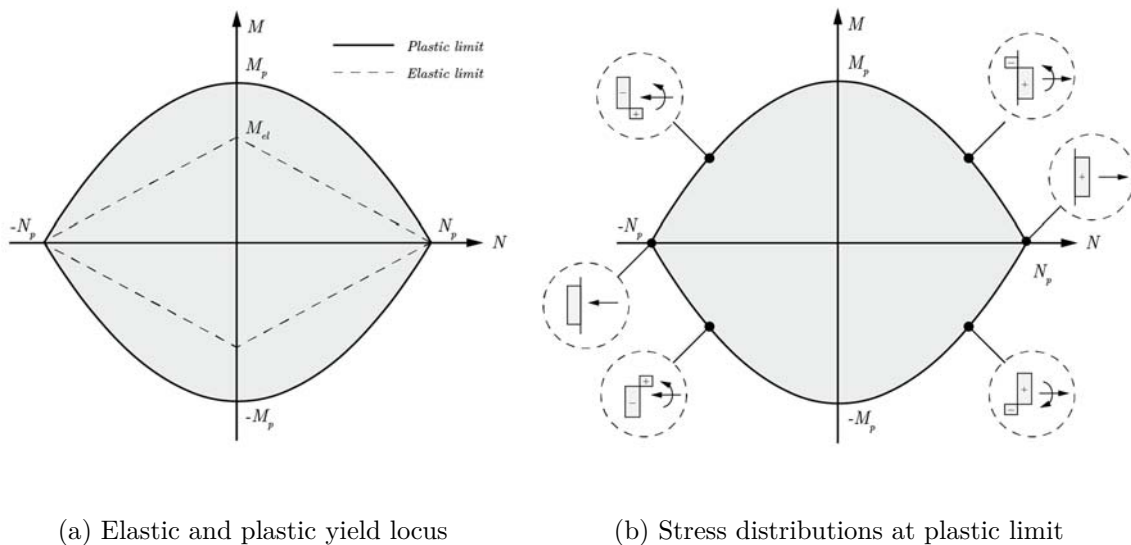


**Figure 4.6.** Yield criterion for reinforcement in concrete plates.

### 4.3 Yield Criterion for Steel Plates

A perfect plastic material behaviour is considered for the steel plates and thereby the assumption of sufficient deformation capabilities in the structure is valid. The assumption is necessary in order to obtain stress redistributions and a limit for this distribution must be defined, that is, the von Mises yield criterion. This criterion is well known for suiting a

ductile material behaviour and is often expressed by the so-called von Mises stress  $\sigma_v$ , which in a plane case is defined as

$$\sigma_v = \sqrt{\sigma_x^2 - \sigma_x\sigma_y + \sigma_y^2 + 3\sigma_{xy}^2}, \quad (4.12)$$

and for principal stress states by

$$\sigma_v = \sqrt{\sigma_1^2 - \sigma_1\sigma_2 + \sigma_2^2}. \quad (4.13)$$

Optimization of the steel plates must obey von Mises yield criterion, which means that every stress state in the optimized structure has to be located in the feasible domain of the convex yield locus.

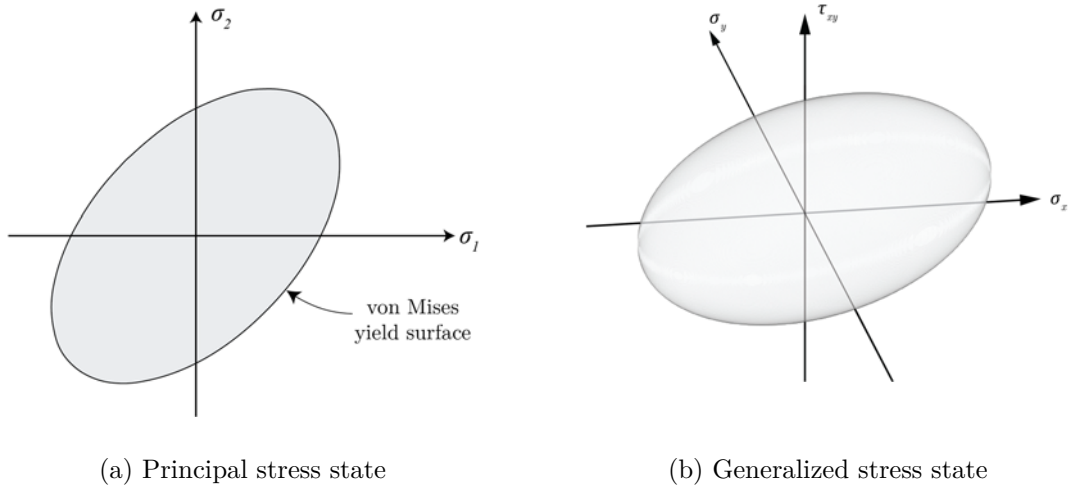


**Figure 4.7.** *von Mises yield criterion.*

If the limit is violated no information is known about the stress state and it is considered inadmissible. By taking the material yield strength into account it is possible to define a function that can be utilized in the optimization

$$f(\sigma, Y_s) = \sigma_v - Y_s \leq 0, \quad (4.14)$$

where  $Y_s$  defines the initial yield strength of the material.



## 5. Numerical Limit State Analysis

Optimization is a well-known problem in calculus, which for centuries has been studied with great interest. As many other mathematical topics, the invention of computers made a significant breakthrough in the way of conducting optimization, and nowadays highly complex problems are optimized by numerical methods. Thus, the lower bound limit analysis problems presented in section 2.4 can be optimized using one of several numerical approaches.

### 5.1 Interior Point Method versus Simplex Method

The yield criteria associated with each limit analysis is defined in chapter 4, and common for all optimization problems treated in this thesis, is the nonlinearity due to a convex yield surface. The nonlinear aspect is worth noticing as the numerical approach is chosen on this behalf. Within the field of mathematical optimization two optimization approaches are widely used; namely, the simplex method and the interior point method. The simplex method was developed by Dantzig in 1947 and is strictly related to linear problems, while the interior point method invented by Karmarkar in 1984 [17] can be seen as a solving type capable of handling both linear and nonlinear problems. Thus, an interior point method requires no linearization of a convex yield surface unlike the simplex method. The search of optimum is diverse, and the major difference is found in the way the methods traverses the feasible region.

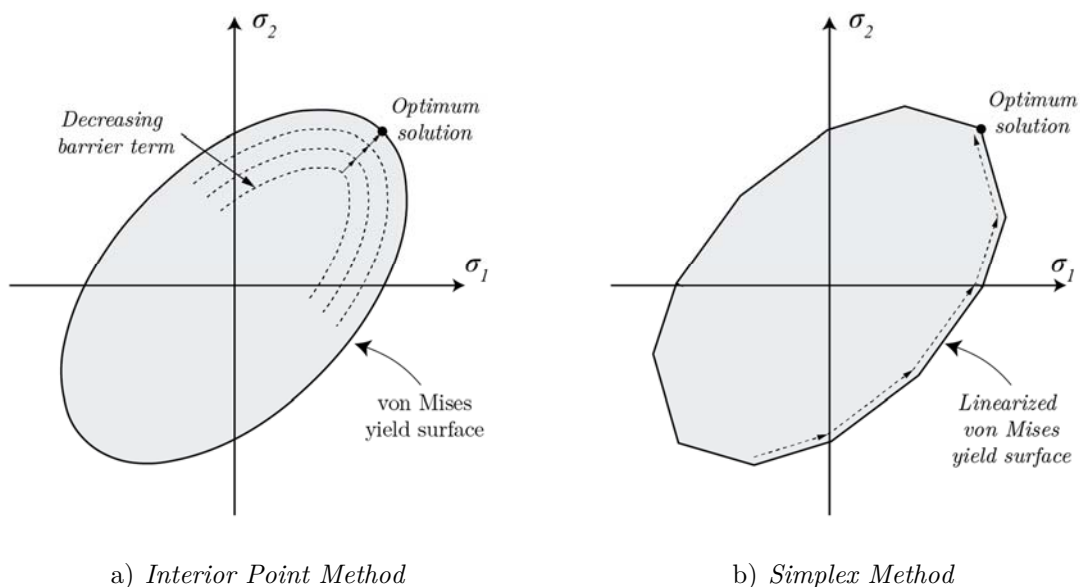


**Figure 5.1** Searching principle for the interior point method and simplex method.

As illustrated in Figure 5.1, the simplex method traverses along linearized boundaries, whereas the interior point method traverses the interior region by the restriction of a decreasing barrier term, which is further elaborated later in this chapter. Previously studies

have proven that the interior point method is effective in limit analyses as the number of iterations is only minimal affected by the size of the problem, see e.g. [18].

The yield criterion is linearized by a few number of linear constraints in Figure 5.1 b), and it would require a higher degree of discretization to obtain a more accurate optimum. This would lead to more iteration steps if utilizing the simplex method, and thereby more computational time. Consequently, the interior point method is found to be more suitable for optimizing the limit state problems in this thesis.

## 5.2 Path-following Interior Point Method

A number of interior point methods has been developed, and the choice of algorithm for a given problem depends on the problem type. [15] In this section the path-following interior point method is covered since it is suitable for large scale optimizations. The derivation is accomplished by standard notation for nonlinear problems as the limit state problem in this thesis can be transformed to this notation. When considering the path-following interior point method three major topics are fundamental for the understanding

- the barrier term,
- the method of Lagrange multipliers and the Lagrange function,
- Newton's method.

In order to make the notation more general and help understanding the numerical implementation issue, it is chosen to reformulate the original equations from section 2.4 to the following problem

$$\text{maximize} \quad \mathbf{b}^T \mathbf{y} \quad (5.1)$$

$$\text{subjected to} \quad \mathbf{A} \mathbf{y} = \mathbf{c} \quad (\text{Equilibrium}) \quad (5.2)$$

$$\mathbf{f}(\mathbf{y}) \leq \mathbf{0} , \quad (\text{Yield Criterion}) \quad (5.3)$$

where the above notation corresponds to the lower bound formulation of the load optimization problem in section 2.4 since

$$\begin{aligned} \mathbf{b} &= [\mathbf{0} \ 1]^T \\ \mathbf{y} &= [\boldsymbol{\beta} \ \alpha] \\ \mathbf{A} &= [\mathbf{H} - \mathbf{R}] \\ \mathbf{c} &= \mathbf{R}_c . \end{aligned} \quad (5.4)$$

The first operation in obtaining the optimum solution is to convert the yield criterion inequality constraint in Eq. (5.3) into an equality constraint by introducing a slack variable,  $s$ , for each inequality constraint

$$\mathbf{f}(\mathbf{y}) + s_j = \mathbf{0} , \quad s_j \geq 0, \quad j = 1, 2, \dots, p . \quad (5.5)$$

The value of the slack variable,  $s$ , expresses the additional stress capacity before reaching yielding. This operation is solely allowed by the restriction of a non-negative slack variable.

### 5.2.1 Barrier Term

[15] Fiacco and McCormick developed a barrier term, which has the purpose of replacing the inequality constraints ( $s \geq 0$ ) by a penalizing term in the objective function. The objective function including the barrier term is given as

$$\mathbf{b}^T \mathbf{y} + \mu \sum_{i=1}^k \log(s_i), \quad \mu > 0, \quad (5.6)$$

where  $\mu$  denotes a decreasing barrier parameter greater than zero. The parameter is worth noticing since the additional logarithmic expression will imply that the objective decreases, when the slack variable approaches zero. To visualize this fact, the logarithmic expression is illustrated in the figure below.

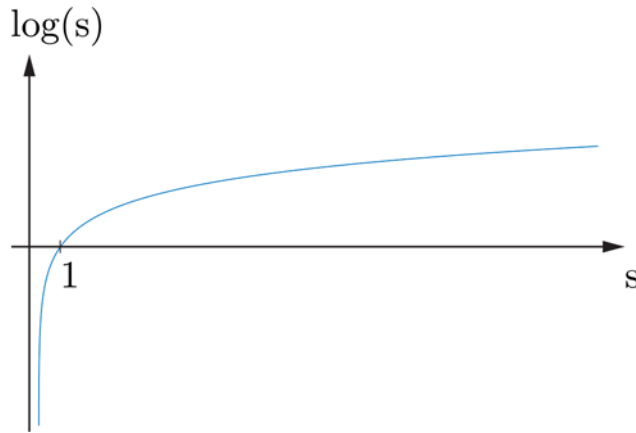


**Figure 5.2.** Illustration of the log contribution to the objective function.

The issue with the barrier term is that if the constrained optimum is located at the boundary, meaning that one or more slack variables are equal to zero at optimum, then the logarithmic expression will prevent the objective from reaching optimum. Thus, the barrier parameter  $\mu$  is needed in order to balance the contribution of the true objective function in Eq. (5.1), with that of the barrier term in Eq. (5.6). This implies that  $\mu$  determines the quantity of the barrier term, which must go towards zero such that the objective function corresponds to the original objective expression at the optimum solution. [15] Seen from a visual point of view it implies that as  $\mu$  decreases, the feasible domain expands and eventually corresponds to the entire feasible domain, see e.g. Figure 5.1 a).

The total expression in Eq. (5.6) has to be maximized, and it leads to an algorithm favouring feasible stress points located as far away from the yield surface as possible. This fact leads to a more optimal search direction that converges towards optimum faster than starting by considering the entire space.

### 5.2.2 Lagrange Multipliers

The method of Lagrange multipliers is an optimization strategy for finding maximum and minimum of an equality constrained object function. The method was named after Joseph

Louis Lagrange, and can be applied in both simple hand calculations and numerical methods. In a numerical manner the purpose is to establish the so-called Lagrange function by the use of Lagrange multipliers from which the optimum solution can be found afterwards. However, in order to understand the Lagrange function, the Lagrange multipliers is firstly presented.

The method of Lagrange multipliers relies on the intuition that the objective function has reached maximum when its gradient vector is parallel to the gradient vector of an equality constraint function. Thus, the method is based on the insight of gradient vectors, which in multivariable calculus always provide a direction and magnitude of a vector perpendicular to a given function at the considered point. The directions must be the same when reaching the optimum solution. In a simple case with a function  $f(x, y)$  constrained by another function  $g(x, y)$  this would lead to

$$\nabla f(x, y) = \begin{bmatrix} f'_x(x, y) \\ f'_y(x, y) \end{bmatrix} \parallel \nabla g(x, y) = \begin{bmatrix} g'_x(x, y) \\ g'_y(x, y) \end{bmatrix}.$$

The principle is illustrated in Figure 5.3.

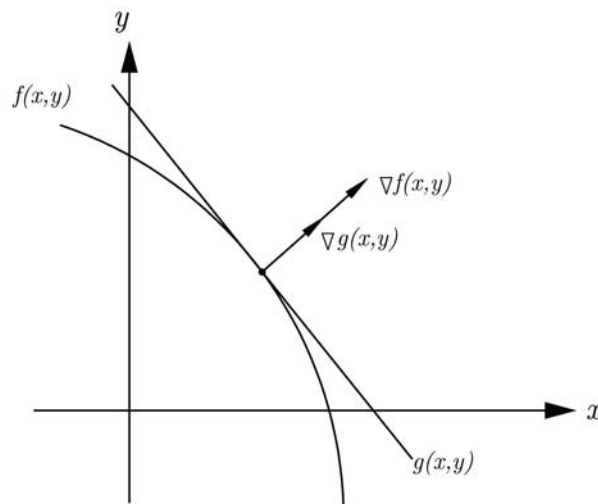


**Figure 5.3.** Parallel gradient vectors  $\nabla f(\mathbf{x})$  and  $\nabla g(\mathbf{x})$ .

In order to verify that the vectors are parallel, a new variable is introduced; namely, the Lagrange multiplier,  $\lambda$ . Lagrange multipliers are needed due to the obvious issue that a gradient vector for an objective function and the gradient vector for a constraint function might be parallel, but have different magnitudes. However, if the vectors are parallel it is possible to find a scalar, which multiplied with one of the vectors equals the other vector. This implies that if considering the above example once again, the following expression must be satisfied when having reaching optimum

$$\begin{bmatrix} f'_x(x, y) \\ f'_y(x, y) \end{bmatrix} - \lambda \begin{bmatrix} g'_x(x, y) \\ g'_y(x, y) \end{bmatrix} = \begin{bmatrix} 0 \\ 0 \end{bmatrix},$$

where  $\lambda$  is the Lagrange multiplier that verifies whether the vectors are parallel. The physical aspect of the multipliers has already been explained in section Appendix B: and thus, the Lagrange function can now be established.

### 5.2.3 Lagrangian Function

The idea of the Lagrange function or Lagrangian is to define a single function describing the entire problem. Thus, an incorporation of the constraint functions into the objective function is achieved by multiplying a Lagrange multiplier,  $\lambda$ , with each constraint equation. The Lagrangian is established as follows

$$\mathcal{L}(\mathbf{y}, \mathbf{s}, \boldsymbol{\lambda}, \mathbf{v}) = \mathbf{b}^T \mathbf{y} + \mu \sum_{i=1}^k \log(s_i) - \boldsymbol{\lambda}^T (\mathbf{f}(\mathbf{y}) + \mathbf{s}) - \mathbf{v}^T (\mathbf{c} - \mathbf{A}\mathbf{y}), \quad (5.7)$$

where  $\lambda$  and  $v$  denotes the earlier mentioned Lagrange multipliers. More specific,  $\lambda$ , can be seen as the magnitude of the plastic strains in the upper bound solution formulated in section Appendix B:. Likewise,  $v$ , can be seen as the magnitude of the plastic displacements in the upper bound solution.

The Lagrangian in Eq. (5.8) is differentiated with respect to all the variables to obtain the first order optimality conditions elaborated in section Appendix B:

$$\nabla \mathcal{L}(\mathbf{y}, \mathbf{s}, \boldsymbol{\lambda}, \mathbf{v}) = \begin{bmatrix} \frac{\partial \mathcal{L}}{\partial \mathbf{y}} \\ \frac{\partial \mathcal{L}}{\partial \mathbf{s}} \\ \frac{\partial \mathcal{L}}{\partial \boldsymbol{\lambda}} \\ \frac{\partial \mathcal{L}}{\partial \mathbf{v}} \end{bmatrix} = \begin{bmatrix} \nabla_{\mathbf{y}} \mathbf{f}(\mathbf{y}) \boldsymbol{\lambda} - \mathbf{A}^T \mathbf{v} - \mathbf{b} \\ \mathbf{S} \boldsymbol{\lambda} - \mu \mathbf{e} \\ \mathbf{f}(\mathbf{y}) + \mathbf{s} \\ \mathbf{c} - \mathbf{A}\mathbf{y} \end{bmatrix} = \begin{bmatrix} \mathbf{0} \\ \mathbf{0} \\ \mathbf{0} \\ \mathbf{0} \end{bmatrix}, \quad (5.8)$$

where  $\mathbf{e}$  is a vector of ones. The optimum solution is reached when the equations equal a zero vector. An iteration process is therefore needed in order to find the variables providing this solution.

### 5.2.4 Newton's Method

Newton's method is often used within mathematical optimization for numerically solving nonlinear expressions. The iterations in the method end when a proper solution is obtained. The solution is achieved by using first order Taylor series expansion from which an inverse operation is used to find new increments that updates the variables as each iteration proceeds. For the sake of convenience, a simple case with a single variable problem is firstly considered, where the task is to satisfy the following equation

$$f(y) = 0$$

The function has to be once continuously differentiable in order to use Newton's method. Newton's method uses first order Taylor series expansion to approximate the increment that is required to fulfil the above expression

$$f(y^k) \approx f(y^{k-1}) + \Delta d \cdot f'(y^{k-1}) ,$$

where  $k$  denotes the iteration number,  $f(y^{k-1})$  is a known solution, and  $\Delta d$  denotes the increments required to obtain a zero solution, that is,  $y^k - y^{k-1}$ . This process is illustrated in the figure below.

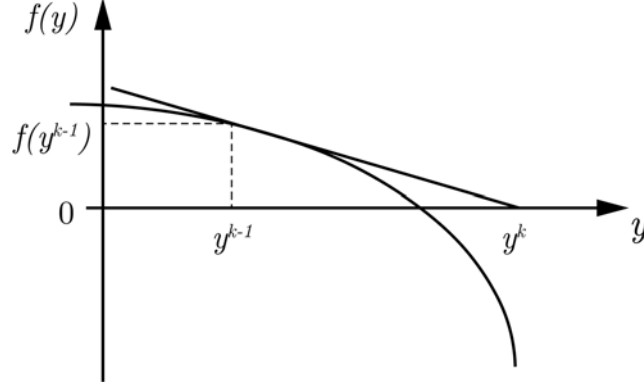


**Figure 5.4.** Principle of Newton's Method with one variable.

The  $f(y^k)$  is set to zero since the optimum solution must converge against that. The increment  $d\Delta$  is solved by the following expression for each iteration

$$0 = f(y^{k-1}) + \Delta d \cdot f'(y^{k-1}) \rightarrow \Delta d = -\frac{f(y^{k-1})}{f'(y^{k-1})} .$$

Each iteration provides a new increment, which in simple case is added to the previous variable value

$$y^k = y^{k-1} + \Delta d .$$

With this clarified it is possible to convert this iteration principle into the Lagrange problem given in Eq. (5.7)

$$\mathbf{0} = \nabla \mathcal{L}(\mathbf{y}, \mathbf{s}, \boldsymbol{\lambda}, \mathbf{v}) + \Delta \mathbf{d} \cdot \nabla^2 \mathcal{L}(\mathbf{y}, \mathbf{s}, \boldsymbol{\lambda}, \mathbf{v}), \quad (5.9)$$

which can be rewritten as

$$\Delta \mathbf{d} = \frac{-\nabla \mathcal{L}(\mathbf{y}, \mathbf{s}, \boldsymbol{\lambda}, \mathbf{v})}{\nabla^2 \mathcal{L}(\mathbf{y}, \mathbf{s}, \boldsymbol{\lambda}, \mathbf{v})}, \quad (5.10)$$

where the partial derivatives of the Lagrange function form the Hessian matrix in Eq. (5.11) and thus, Eq. (5.10) is actually an inverse operation.

$$\nabla^2 \mathcal{L}(\mathbf{y}, \mathbf{s}, \boldsymbol{\lambda}, \mathbf{v}) = \begin{bmatrix} \mathbf{H} & \mathbf{0} & \nabla_{\mathbf{y}} \mathbf{f}(\mathbf{y}) & -\mathbf{A}^T \\ \mathbf{0} & \mathbf{z} & \mathbf{S} & \mathbf{0} \\ \nabla_{\mathbf{y}} \mathbf{f}(\mathbf{y})^T & \mathbf{I} & \mathbf{0} & \mathbf{0} \\ -\mathbf{A} & \mathbf{0} & \mathbf{0} & \mathbf{0} \end{bmatrix} \quad (5.11)$$

$\mathbf{z}$  is a diagonal matrix of  $\lambda$ , and  $\mathbf{I}$  provides an unit matrix. The  $\mathbf{H}$ -matrix is given as

$$\mathbf{H} = \sum \lambda \nabla_{\mathbf{y}\mathbf{y}}^2 \mathbf{f}(\mathbf{y}) . \quad (5.12)$$

The equilibrium equations play no role in this matrix because the second derivatives are all zeros. When conducting the inverse operation, a direction vector  $\Delta \mathbf{d}$  containing increments of all the variables and the Lagrange multipliers is found to

$$\Delta \mathbf{d} = [\Delta \mathbf{y} \quad \Delta \mathbf{s}^T \quad \Delta \boldsymbol{\lambda}^T \quad \Delta \mathbf{v}^T]^T. \quad (5.13)$$

From this the new variables are updated by the following expressions

$$\begin{aligned} \mathbf{y}^k &= \mathbf{y}^{k-1} + \Delta \mathbf{y} \cdot \eta \\ \mathbf{s}^k &= \mathbf{s}^{k-1} + \Delta \mathbf{s} \cdot \eta \\ \boldsymbol{\lambda}^k &= \boldsymbol{\lambda}^{k-1} + \Delta \boldsymbol{\lambda} \cdot \eta \\ \mathbf{v}^k &= \mathbf{v}^{k-1} + \Delta \mathbf{v} \cdot \eta, \end{aligned} \quad (5.14)$$

where the iteration number is denoted by  $k$ , and  $\eta$  is an appropriate step length ensuring that  $\mathbf{s}$  and  $\boldsymbol{\lambda}$  stay positive.

### 5.3 Numerical implementation in MATLAB – `fmincon`

The formulated lower bound problem in Eq. (2.6) is to be implemented numerically into MATLAB and Mosek since the optimization algorithms in these two software programs are based on the interior point method.

MATLAB offers an optimization toolbox that provides functions capable of solving linear, quadratic, integer and nonlinear problems. [19] The functions can be used to obtain parameters that minimize or maximize objective functions. Both discrete and continuous problems can be solved for finding optimal solutions.

The `fmincon` function in MATLAB is used for optimizing the lower bound problems in section 2.4. `fmincon` is a function that is capable of finding minimum and maximum of constrained nonlinear multivariable functions. By default, the minimization problem in MATLAB has to be specified by

$$\min_x f(x) \text{ such that } \begin{cases} c(x) \leq 0 \\ ceq(x) = 0 \\ A \cdot x \leq b \\ Aeq \cdot x = beq \\ lb \leq x \leq ub \end{cases} \quad (5.15)$$

where  $f(x)$  is a scalar objective function,  $c(x)$  and  $ceq(x)$  are nonlinear inequality and equality constraints, respectively.  $A$  and  $Aeq$  are linear inequality and equality constraints, and  $lb$  and  $ub$  are the bounds. The objective function  $f(x)$  can either be linear or nonlinear.

In `fmincon` it is possible to use four different solvers and among these is the interior point algorithm. The interior point algorithm is the default solver, and it is the one used for solving the lower bound formulation. The algorithm is capable of handling both large<sup>1</sup>, sparse problems and small dense problems, and that is why it is preferable compared to the other solvers. [20] One of the benefits of using the interior point algorithm is that it can recover from NaN (Not a Number) or Inf (Infinite numbers). By using the interior point algorithm in MATLAB, the user is not demanded to formulate key concepts in the method, such as the Lagrange function, hessian matrices nor establishing Newton's method as iteration process to secure first order optimality since it is already implemented in the function. Thus, the user is only required to provide input to the function.

---

<sup>1</sup> Large scale problems are based on linear algebra that doesn't need to use full matrices.

### 5.3.1 Barrier Function and Solving Methods

The original problem that has to be solved by the *fmincon* interior point algorithm is expressed by

$$\begin{aligned}
 & \text{minimize} && -\mathbf{f}(\mathbf{x}) \\
 & \text{subjected to} && \mathbf{h}(\mathbf{x}) = \mathbf{0} && \text{(Equilibrium)} \\
 & && \mathbf{g}(\mathbf{x}) \leq \mathbf{0}, && \text{(Yield Criterion)}
 \end{aligned} \tag{5.16}$$

where  $\mathbf{h}(\mathbf{x})$  are the equality constraints and  $\mathbf{g}(\mathbf{x})$  are inequality constraints. The problem in Eq. (5.16) is reformulated by introducing a logarithmic term, also called a barrier function

$$\begin{aligned}
 & \text{minimize} && -(\mathbf{f}_\mu(\mathbf{x}, \mathbf{s}) - \mu \sum_i \ln(s_i)), \quad \mathbf{s}_i \geq \mathbf{0} \\
 & \text{subjected to} && \mathbf{h}(\mathbf{x}) = \mathbf{0} && \text{(Equilibrium)} \\
 & && \mathbf{g}(\mathbf{x}) + \mathbf{s}, && \text{(Yield Criterion)}
 \end{aligned} \tag{5.17}$$

where  $\mu$  is a barrier parameter that has to be greater than zero ( $\mu > 0$ ). For each inequality constraint  $g$  there is a slack variable  $s$ . Each slack variable has to be greater than zero ( $s > 0$ ). When  $\mu$  decreases, the objective function  $f_\mu$  approaches  $f$ . By reformulating the problem in Eq. (5.16) to the problem in Eq. (5.17) only equality constraints are considered which are much easier to solve than the original inequality constraints.

*fmincon* uses one of two types of step at each iteration to solve the minimization problem in Eq. (5.17)

- Newton's step
- CG (conjugate gradient) step

By default, *fmincon* uses Newton's step, but if it is not possible then a conjugate gradients (CG) step is used instead. Newton's step solves the first order optimality conditions (KKT-conditions) as described in section Appendix B: by a linear approximation.

### 5.3.2 Including Gradient and Hessian

In the *fmincon* algorithm in MATLAB it is possible to include the gradient and hessian of for objective function and for the nonlinear constraints. By default, the gradient and hessian are calculated numerically by approximated methods. The disadvantage is that the solvers return an approximated hessian that in some cases is far from the true hessian. As an alternative to the approximated methods it is possible for the user to provide a function that is able to calculate the partial derivatives analytically [21]. The analytical approach to the gradient and hessian typically leads to a faster, robust and more accurate solution to the problem.

### fmincon Hessian

The Hessian of the nonlinear constraints can be calculated by selecting one of the following algorithms in the interior point algorithm in fmincon

- 'bfgs' (Broyden–Fletcher–Goldfarb–Shanno algorithm)
- 'lbfgs' (Limited-memory Broyden–Fletcher–Goldfarb–Shanno algorithm)
- 'fin-diff grads'
- 'HessianFcn'

'bfgs', 'lbfgs' and 'fin-diff-grads' are three different ways of calculating an approximated Hessian matrix, whereas 'HessianFcn' is a user-defined approach. The default way of calculating the Hessian to the nonlinear constraints in fmincon is by 'bfgs', which calculates the Hessian by a dense quasi-Newton approximation. The second approach, 'lbfgs', is also a quasi-Newton approach but it is more suited for limited-memory, large-scale problems as is the case with the lower bound formulation. By choosing the 'fin-diff-grads', the Hessian matrix is calculated by a Hessian-times-vector product by finite differences of the gradients.

The 'HessianFcn' is the only non-approximated way of calculating the Hessian matrix, but the user has to define the Gradient and Hessian analytically [22]. Fewer iterations are typically needed to solve the problem when the analytical approach is implemented. In the interior point algorithm, the Hessian of Lagrangian includes the Lagrange multipliers and the Hessian corresponding to the nonlinear constraints. The Hessian for the nonlinear constraint functions has to be developed as a separate function but it still has to be able to include the Lagrange multipliers.

The relative memory usage compared to the relative efficiency for each Hessian approach is seen in Table 5.1.

**Table 5.1.** Different Hessian approaches for 'interior point' in fmincon [23]

Hessian	Relative Memory Usage	Relative Efficiency
'bfgs' (default)	High (for large problems)	High
'lbfgs'	Low to Moderate	Moderate
'fin-diff-grads'	Low	Moderate
'HessianFcn'	(depends on user-defined code)	High (depends on your code)

The memory usage of the user provided partial derivatives depends on the programmed code. For the lower bound problem, the 'bfgs' isn't recommended since it is not suitable for large-scale problems. Generally, the 'lbfgs' and user-defined approaches are the most efficient when calculation time and accuracy is considered in combination.

## 5.4 Numerical implementation in Mosek (SOCP)

The lower bound load formulation for steel plates and reinforced concrete plates can also be optimized by means of the interior point optimizer in Mosek as an alternative to fmincon. Mosek is an efficient software for solving large-scale sparse problems, especially when it comes to second-order cone programming. Therefore, the lower bound formulation has to be expressed in terms of constraints describing second-order cones.

### 5.4.1 Second-Order Cone Programming (SOCP)

During the history it has been shown that the interior point method was effective in solving problems with convex constraints. The discovery gave rise to that the method could be extended to new algorithms, and among these is the *second-order cone programming* (SOCP) [7]. The constraints in SOCP are defined by a number of cones.

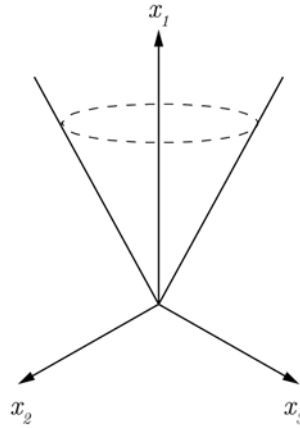


**Figure 5.5.** Second-order cone with three variables ( $x_1 \geq \sqrt{x_2^2 + x_3^2}$ )

The most general constraints in SOCP are the *Quadratic Cone* (QC)

$$x_1 \geq \sqrt{\sum_{j=2}^n x_j^2}, \quad (5.18)$$

and the *Rotated Quadratic Cone* (RQC)

$$2x_1x_2 \geq \sum_{j=3}^n x_j^2 ; x_1, x_2 \geq 0 . \quad (5.19)$$

When considering limit state analysis of reinforced concrete plates, M.P. Nielsen's yield criterion is effective since the formulation is already expressed as two cones. In this study, von Mises yield criterion is formulated such that it corresponds to the quadratic cone (QC) in Eq. (5.18), whereas M.P. Nielsen's yield criterion and the MN-relation for reinforcement is formulated such that it corresponds to the rotated quadratic cone in Eq. (5.19). By reformulating von Mises, Nielsen's yield criterion and the MN-relation, it gives rise that Mosek can be implemented to solve the lower bound problem. The reformulation of the yield criterions is derived in Appendix E.

### 5.4.2 Mosek Optimization Procedure

Mosek is a software package capable of efficiently optimizing linear and nonlinear problems. The optimization is in this case based on second-order programming and the well-known primal-dual formulation as described in section 5.2. Besides optimization, Mosek is capable of utilizing some pre-steps that makes the algorithm faster and numerically more stable. A general procedure for conducting an optimization in Mosek is as follows [24]

- Presolve (reduces the problem size)
- Dualizer (choosing whether to run primal or dual solution)
- Scaling (scales the unknown variables)
- Optimize (solves the problem)

In the presolve stage, Mosek reduces the problem size by e.g. removing redundant equations before optimizing. This is because some constraint equations may be linearly dependent, and by removing those, a more efficient and stable optimization can be obtained. This issue has also been treated in [25].

Another relevant feature that is included in Mosek is the possibility to scale different variables. If the value of a variable is large or small, say  $1.0e + 11$  or  $1.0e - 9$ , some optimization algorithms struggle to converge and inaccurate results may be obtained. This is because computers are based on finite precision and some important digits may be truncated [24]. A well-scaled problem is preferable, which means that the variables should have more or less the same magnitude. The scaling issue can be circumvented in Mosek and a better numerical stability is obtained. The scaling possibility feature isn't implemented in e.g. `fmincon`.

Different examples on optimizing steel and reinforced concrete plates in Mosek is presented later in the report.

## 6. Program for Verification of Critical Stress Spots

In the finite element method, numerical errors induce critical stress spots that can make it a challenge to fulfill the ultimate limit state when designing static loaded steel plates by the theory of elasticity. More specific, stress concentrations and stress singularity spots often induce stresses exceeding the elastic load bearing capacity. Critical stress spots are common in finite element analyses as a result of concentrated loads, concentrated supports, poor mesh discretization, and concave geometrical corners. As a consequence, the stress spots often lead to oversized designs due to high local stresses that in fact don't appear in reality. The stresses can be verified in terms of conducting a nonlinear analysis of the entire structure, but this is time-demanding, in terms of both iterations and model size, and furthermore it is unsafe.

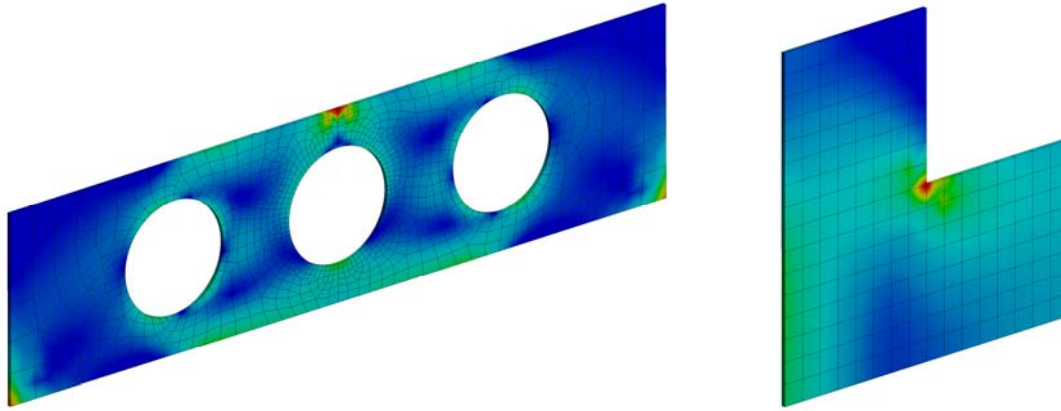


**Figure 6.1.** *Examples of critical stress spots in plates.*

To accommodate this problem, an efficient program for verifying the influence of critical stress spots in two-dimensional plates has successfully been developed. The same approach could have been made in the three-dimensional case. Furthermore, a paper regarding the submodelling program has been elaborated, which is presented in Appendix I.

The developed program relies on the intuition that a subarea enclosing the critical stress spot is examined based on perfect plastic material behaviour. The assumption of the material behaviour is needed as the subarea is investigated by a lower bound limit state analysis. The limit analysis provides a load bearing capacity for the enclosed region by allowing a redistribution of the stresses. The capacity is defined by a scalar load multiplier,  $\alpha$ , that is optimized by different optimization approaches in this thesis. The scalar load multiplier is an indicator of the load bearing capacity of the structure in comparison to the originally applied load. A scalar value greater than 1.0 implies that yielding will not occur in the considered region. Thus, a verification of the problem size is found by considering only a small domain of the entire structure. Besides dealing with submodels, the program is also capable of optimizing global models in order to obtain the load bearing capacity, see Appendix F.1 Full Plate Model Optimization.

The advantage of using our submodeling approach is that the load multiplier is always on the safe side since the capacity is only verified in a restricted part of the model. By only considering a subarea, yielding can be specified to only involve a defined part of the structure. This is of great advantage in comparison to nonlinear analyses of global models, where the capacity is defined as the point when yielding in the entire cross section is obtained. Another advantage of our approach in comparison to numerical analyses based on a nonlinear material behaviour, is the convergence path as illustrated in Figure 6.2.

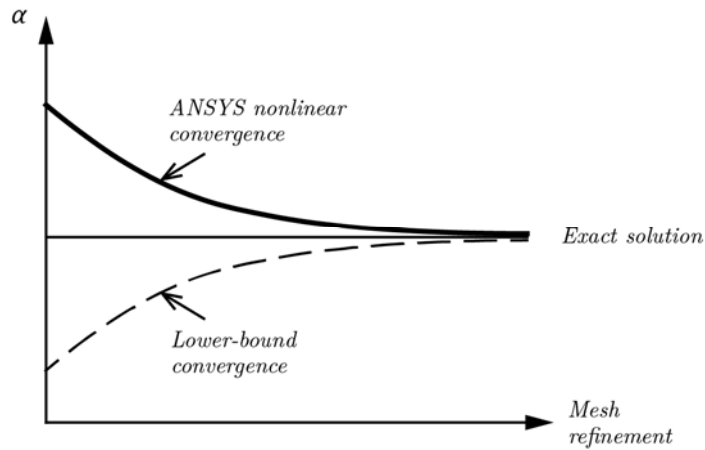


**Figure 6.2.** Convergence path for nonlinear and lower bound convergence.

Nonlinear analyses produce an exact solution in the plasticity analysis based on the given mesh of the considered model. This can lead to a load multiplier that is on the unsafe side and thereby an overestimation of the load bearing capacity if a proper mesh is not assigned. The load bearing capacity in our approach will always be located on the safe side as the lower bound theorem is utilized.

## 6.1 Procedure for Stress Verification

In this study the approach for verification of critical stress spots in static loaded plates is based on an interaction between ANSYS Workbench and MATLAB. Instead of ANSYS Workbench an arbitrary finite element software could have been used.

The overall process of the program, from creating a global model to obtaining a submodel solution, is exemplified in Figure 6.3.

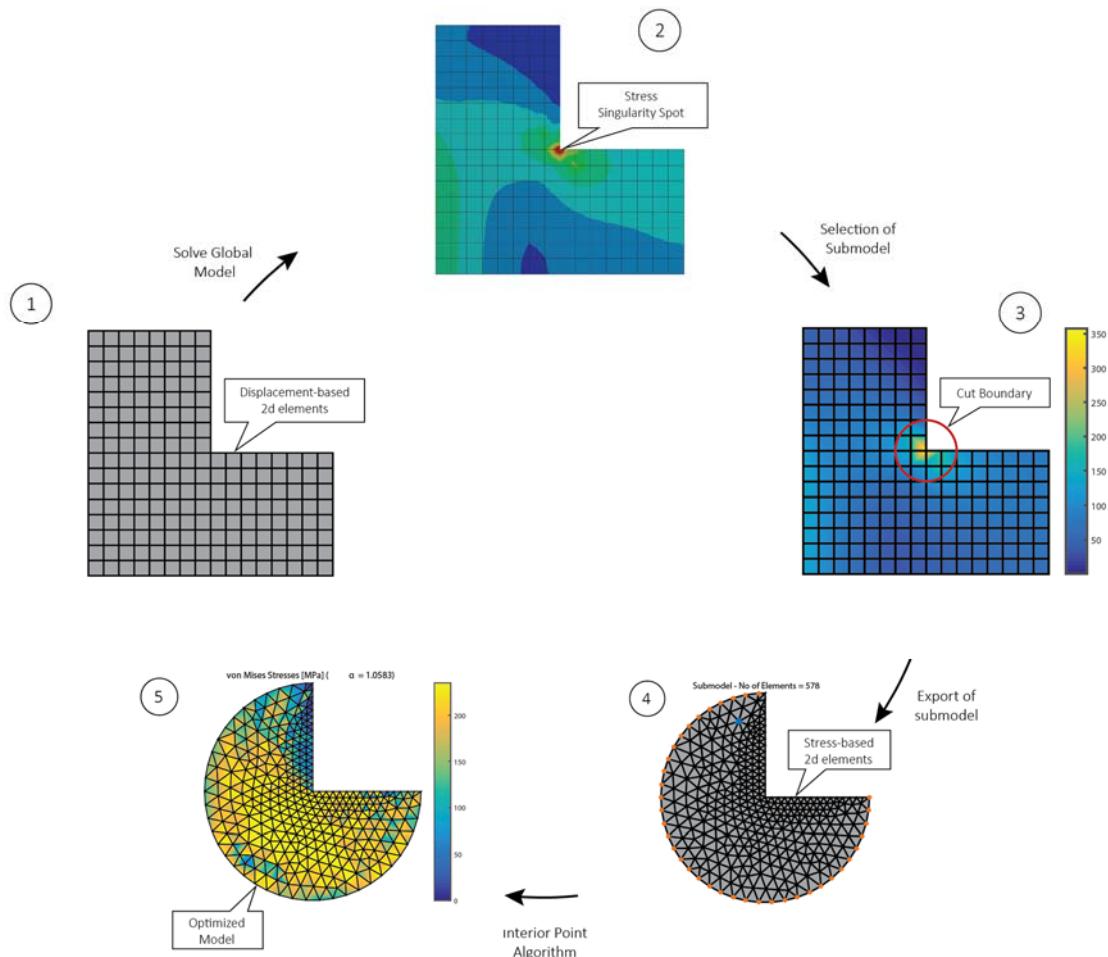


**Figure 6.3.** Overall process of the program.

In the first steps, ANSYS Workbench is used to solve a global user-defined model by means of a displacement-based finite element method. By solving the global model, it is possible to conclude whether critical stress spots appear. A submodel area is defined by only considering a specific region of the domain. In this region the problematic stress spots are solely located, why the problem is significantly reduced regarding calculation time and numerical errors. The submodel is exported to MATLAB by an interaction with ANSYS Workbench that includes a direct transformation from a displacement-based mesh utilized in ANSYS to a stress-based mesh generated in MATLAB. The problem is solved in MATLAB where a nonlinear load optimization is conducted based on the interior point method. The optimization results in a scalar load multiplier  $\alpha$  verifying the problem size.

## 6.2 Submodeling Technique

In order to verify critical stress spots, the user has to discretize a global problem to a submodel that encloses the critical region. The submodeling technique is well known within finite element analysis where the aim is to obtain more accurate stress results in specific regions. In order to conduct a submodel analysis a global model is needed and the corresponding solution. The global model has a coarse mesh, whereas the mesh of the submodel is fine to obtain accuracy. By making a coarse global model, the computational cost is minimal.

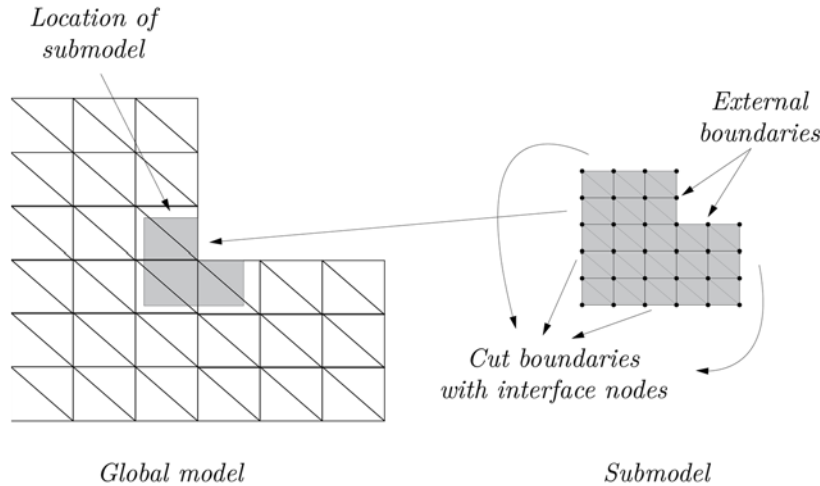


**Figure 6.4.** Technical terms within the field of submodeling.

The solution from the global model is used as boundary conditions for the defined submodel. All the boundary conditions are imported to a separate defined finite element submodel with a refined mesh as illustrated in Figure 6.4.

For the submodeling approach in this study, the stresses from the global model are interpolated and applied on the cut boundary of the submodel. There is no need for the cut boundary to coincide with the element boundaries in the global model, which is of great advantage. Another advantage is the ability to assign arbitrary mesh types and elements for the global model in the submodel approach.

## 6.3 Submodeling in ANSYS Workbench

ANSYS Workbench is used for two purposes in this study. Firstly, ANSYS is used to solve a global plate model and secondly to create a submodel for the upcoming limit analysis in MATLAB. The global model in ANSYS is solved by using displacement-based elements (see Figure 6.5) where the structural stresses are related to the nodal displacements.

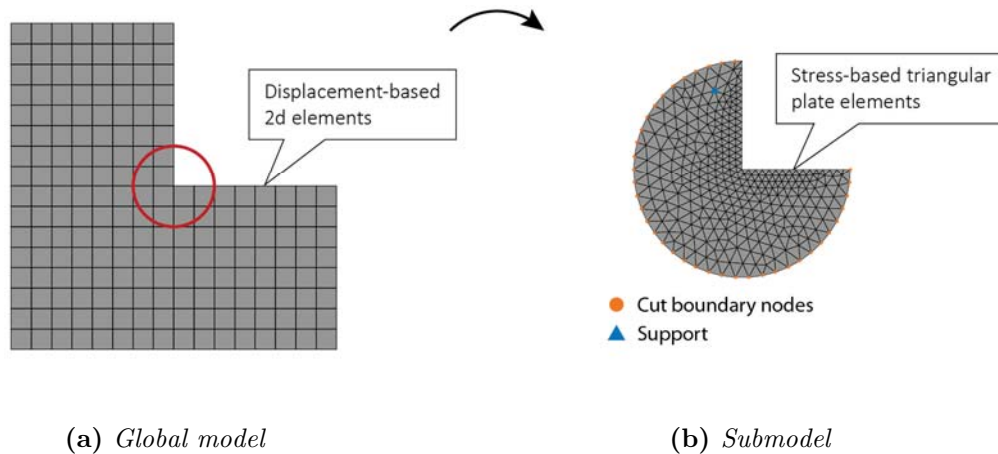


**Figure 6.5.** Example of the submodeling principle in this study.

After solving the global model, a custom made APDL-script is implemented in ANSYS Workbench in order to create a submodel and to export the submodel topology and boundary conditions for the 2D stress-based element formulated in MATLAB.

```

!--- INPUT -----
Geometry = 2      ! 1 = Circle,
                  ! 2 = Rectangle

! Center coordinates of submodel
x = 100.0        ! x-coordinate of center of radius
y = 25.0         ! y-coordinate of center of radius

! Number of division of external boundary of submodel
nodiv = 16       ! 16 Recommended for rectangular submodel
                  ! 70 Recommended for circular submodel

! Only if the submodel is a circle
r = 10           ! Radius of circle

! Only if the submodel is a rectangle
w = 25           ! Width of rectangle
l = 25           ! Length of rectangle

```

**Figure 6.6.** Input windows in the APDL-script.

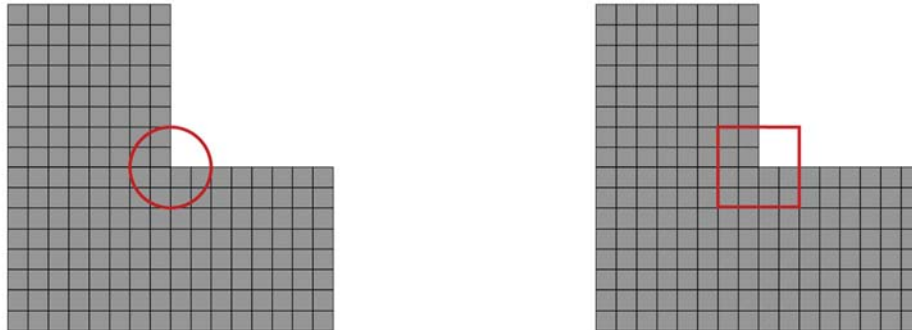
The submodel is made by a user-defined stress path in ANSYS. An APDL-script is necessary to implement since ANSYS Workbench isn't able to export boundary stresses and the topology for a submodel by default.

In order to conduct a lower bound limit analysis in the developed program, the following parameters need to be exported from ANSYS Workbench:

- node coordinates
- element topology
- plate thickness
- stress components at cut boundary
- density
- gravitational acceleration and direction

### 6.3.1 Submodel Geometries

In the developed program, the submodel can either be defined from a *circular* or a *square* cut boundary, see Figure 6.6 and Figure 6.7.



(a) Global model with circular submodel selection

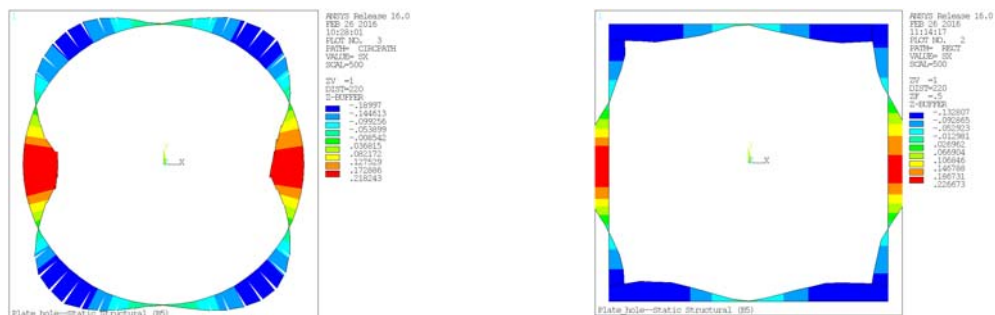
(b) Global model with rectangular submodel selection

**Figure 6.7.** Example of different submodel geometries.

The size and mesh of the two submodel geometries are user-defined, which is done by typing the specifications in the imported APDL-script in ANSYS Workbench. The rectangular submodel is defined based on the coordinates of the center in global Cartesian coordinates and the length and width, whereas the circular submodel is defined by the circle radius and coordinates to the center, see Figure 6.6.

### 6.3.2 Export of Cut Boundary Stresses

The submodel is based on a stress path that can be placed anywhere in the model independent of the global node and element position as earlier described.



(a) Circular submodel

(b) Rectangular submodel

**Figure 6.8.** Example of normal stress distribution along a stress path on the submodel boundary.

A linear elastic analysis is conducted in ANSYS Workbench for a global model and from the analysis it is possible to obtain the stress state for the global model. After conducting

the linear analysis, the three stress components at each node on the cut boundary are interpolated to perform the lower bound limit analysis in MATLAB. The stresses from the stress path are used as boundary conditions in the limit state analysis in MATLAB.

### 6.3.3 Mesh Generation for the Submodel

The principle of making submodels is that the global model has to be meshed coarsely, whereas the mesh of the submodel has to be fine. The mesh of the submodel is assigned based on a user defined edge sizing of the cut boundary. The edge sizing is based on the number of divisions chosen for the path operation, see Figure 6.6. This makes it possible to directly apply the shear and normal stresses calculated from the displacement -based elements into the boundary nodes in the stress-based model. This is due to that the stresses are assumed to vary linearly over the element edges and that the stress-based elements are located at the same position as the displacement -calculated path stresses.

The fine submodel mesh is created with ANSYS Workbench by means of the input in the APDL-script where the mesh is assembled from CST-elements since triangular stress-based elements use the same topology. By having the same element geometry and number of nodes on the displacement -based CST-elements as the stress-based elements, it is possible to directly import node coordinates and element topology from ANSYS to the program in MATLAB.

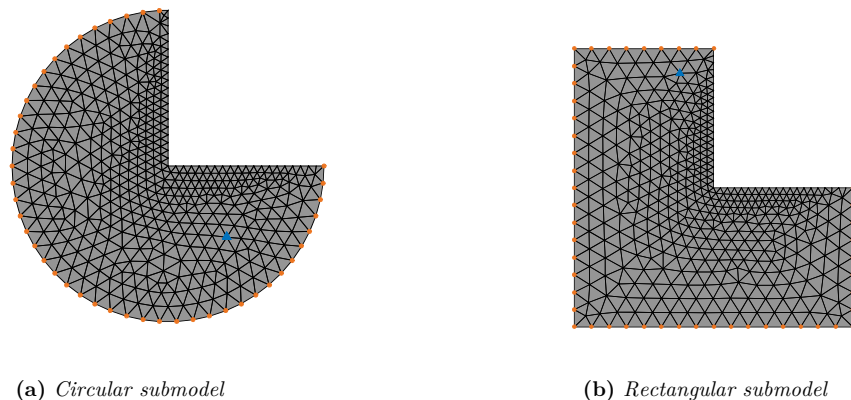


**Figure 6.9.** Examples of submodel mesh.

In the APDL-script, the mesh of the submodel is set to be free, but a mapped mesh can also be assigned if the submodel geometry allows it.

## 6.4 Parameters Influencing the Load Multiplier

When conducting the submodel analysis, the user has to be aware of the parameters that influence the scalar load multiplier  $\alpha$  in the limit analysis

- *mesh* of the global model
- *size* of the submodel
- *mesh* of the submodel.

The mesh of the global model has a large influence on the load multiplier since the imported stresses depend on the mesh of the global model. A study of the global mesh influence on the load multiplier is seen in Appendix G.4 Study of Cut Boundary Stresses. In order to obtain the most accurate value for the load multiplier, the global model mesh should consist of higher order elements as concluded in the appendix. A study of the submodel size is shown in Appendix G.1 Study of Submodel Size. From the appendix it is concluded that a larger subarea results in a higher load multiplier. Thereby, the load multiplier is always on the safe side when the optimization is conducted for a submodel rather than a global model.

If a fine mesh is assigned a more accurate scalar load multiplier is obtained, but it also increases the problem size and thereby the calculation time, see Appendix G.2 Study of Submodel Mesh Refinement. The influence of refining the submodel mesh is not as significant factor as applying an appropriate global model mesh and choosing a proper size of the submodel. Thereby, when conducting a submodel optimization the load multiplier is an interaction between the size and mesh of the submodel, and the mesh of the global model.

## 6.5 Example of Application – Plate with Stress Singularity

A plate with a hole is evaluated to exemplify the application of the submodeling program, see Figure 6.10. Stress singularities appears as a result of the concave corner in the structure. The plate is subjected to a transverse force of 5 kN at the right side, and a fixed support is defined for the left edge. The plate has a thickness of 10 mm.

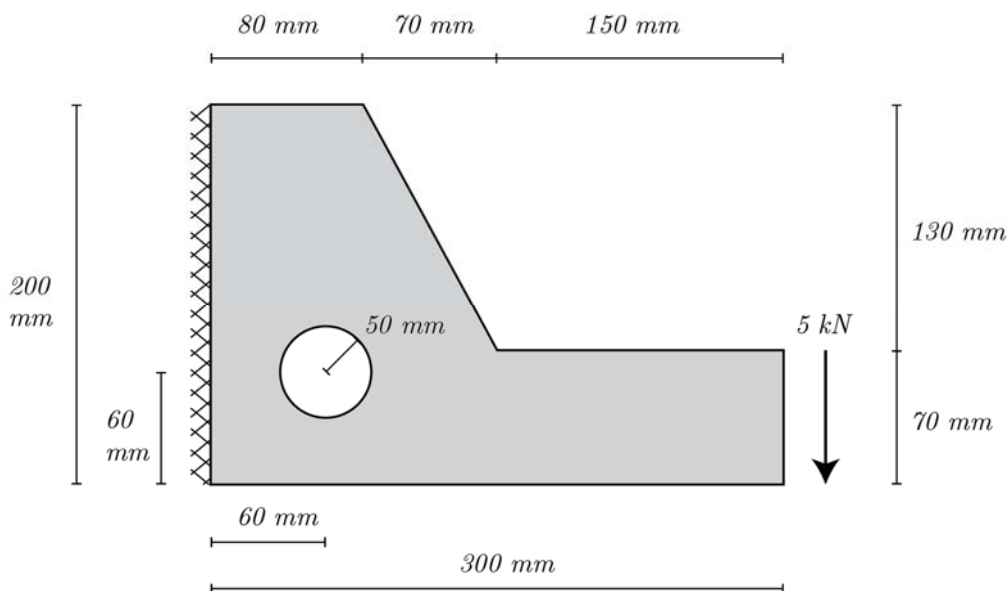


**Figure 6.10.** Free body diagram of the considered plate structure.

The plate is made of steel and the yield strength is assigned to 235 MPa.

### 6.5.1 Linear Elastic Stress Analysis in ANSYS Workbench

A linear elastic stress analysis has been conducted in ANSYS Workbench based on the boundary conditions shown in Figure 6.10. The mesh of the model consists of Q8-elements as seen in Figure 6.11.

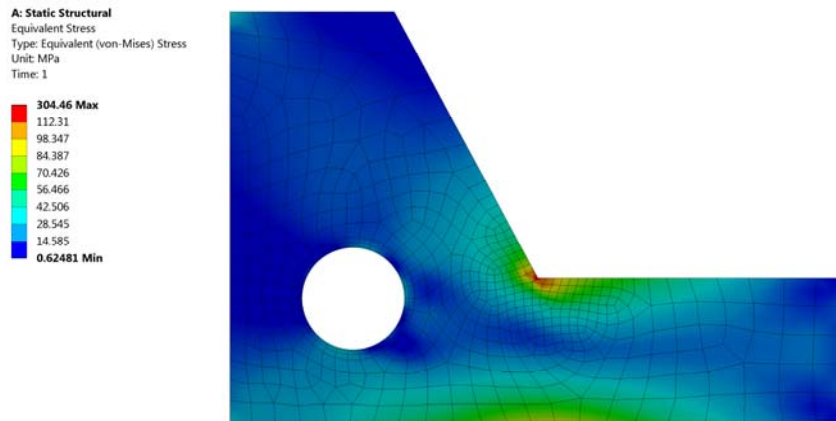
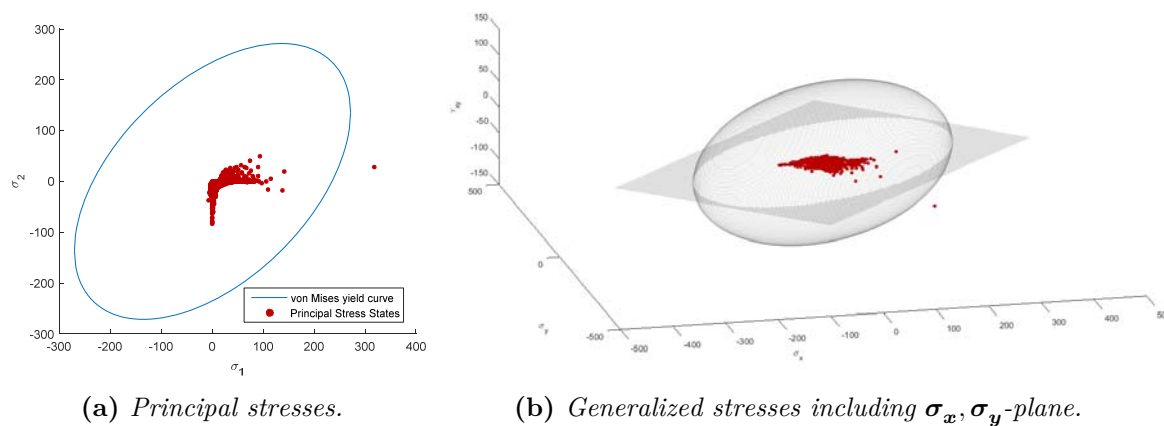


**Figure 6.11.** Plot of mesh and resulting von Mises stresses.

From the linear elastic stress analysis in ANSYS Workbench it is seen that the highest von Mises stresses are obtained in the region of the sharp corner, whereas the stresses are much lower in the remaining part of the plate.



(a) Principal stresses.

(b) Generalized stresses including  $\sigma_x, \sigma_y$ -plane.

**Figure 6.12.** Plot of von Mises yield criterion and stress states for the global model.

By plotting the stresses of each node of the global model, as seen in Figure 6.12, it is seen that only a single stress state is critical as it is located outside the yield criterion. Since the structure has a lot of capacity, the stresses at the critical areas can be redistributed such that an optimized stress state is obtained.

### 6.5.2 Submodeling

In order to redistribute the stresses, a circular subregion with a radius of 20 mm is sliced, in which the redistribution of stresses has to be conducted. By choosing a radius of 20 mm it means that the upcoming load multiplier corresponds to that yielding is only allowable

up to 20 mm from the singularity spot. This is advantageous in comparison to a nonlinear analysis in ANSYS, as the entire structure needs to be considered.

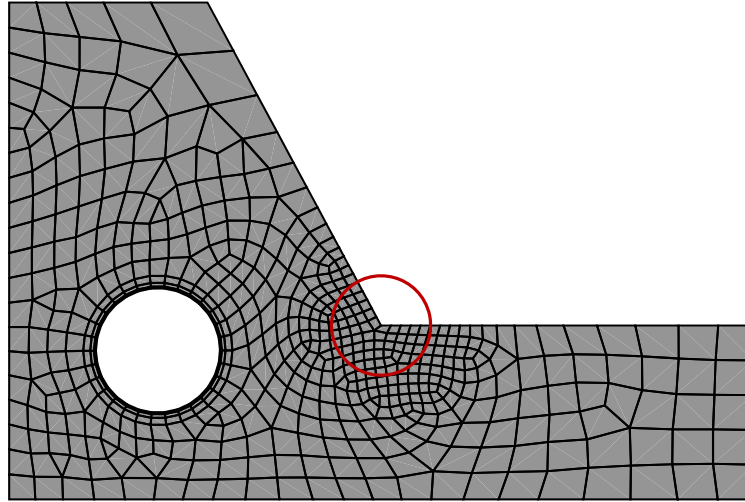


**Figure 6.13.** *Global model with selected subregion.*

For the submodel area a mesh is generated in ANSYS Workbench by means of the APDL-script. The external force is applied in the submodel at the nodes located on the cut boundary, see Figure 6.14.

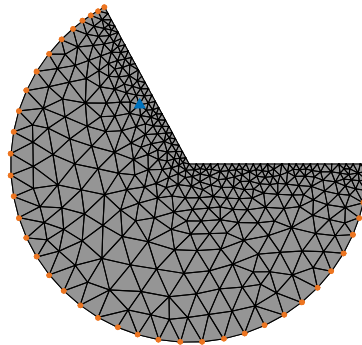


**Figure 6.14.** *Submodel mesh.*

The model consists of 630 elements, and a refinement is performed at the edges near the singularity spot. The submodel is statically indeterminate, which gives rise to stress redistributions.

### 6.5.3 Verification of Critical Stress Spots

The scalar load multiplier  $\alpha$  is to be calculated for the submodel in order to clarify whether the given stress state results in structural collapse.

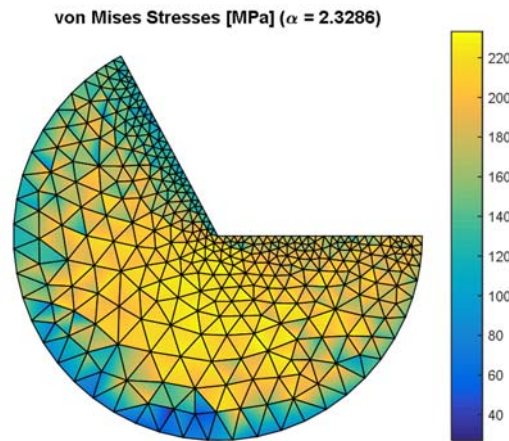
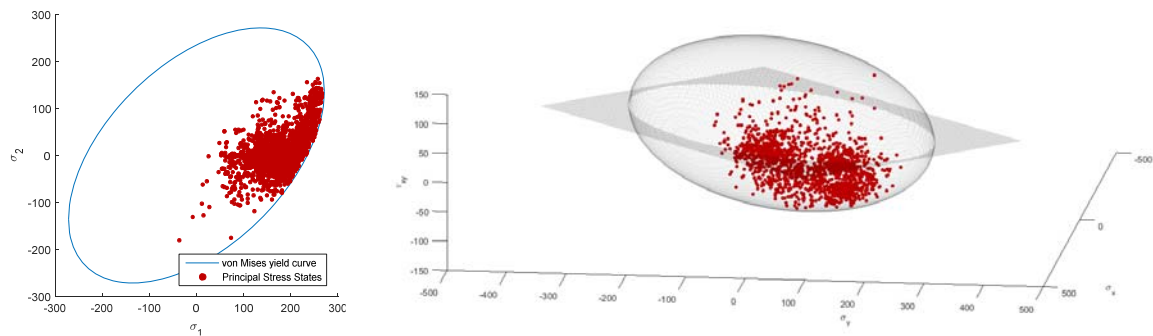


**Figure 6.15.** *von Mises stress of optimized submodel.*

The scalar load multiplier  $\alpha$  is calculated to 2.32. As the load multiplier is above 1.0, it can be concluded that the applied force doesn't result in collapse, even though the elastic analysis shows critical stresses for the global model.

By plotting the stress states and von Mises yield criterion, as seen in Figure 6.16, it is seen that an allowable stress field is obtained.



**(a)** *Principal Stresses.*

**(b)** *Generalized stresses with  $\sigma_x, \sigma_y$ -plane.*

**Figure 6.16.** *von Mises yield criterion and principal and generalized stress states of optimized submodel.*

The developed submodel program can also be used for structures with stress concentrations and singularities regarding concentrated supports and forces, and not only geometrical singularities as it is the case in this example.



# 7. Load Optimization of Reinforced Concrete Plates

A program concerning load and material optimization of reinforced concrete plates has been developed. The elaboration of the load optimization part is presented in this chapter, while the material optimization is examined in the subsequent chapter. The intention with the following chapter is to compare the numerical approach presented in this thesis with well-known design approaches, such as the stringer method. Furthermore, the capability of the numerical approach is explained and demonstrated by examples.

The numerical method employed in this thesis is a modification of an earlier presented approach that is based on the lower bound formulation, see section 2.4. The formulation is based on a statically admissible solution and a non-violated yield criterion. The formulation of the elements and the yield criterions, in this approach, can be recalled from chapter 3 and chapter 4. As the optimization involves different element types, a proper interaction between the elements is validated, and it is presented by examples in Appendix H:. The approach in this thesis contributes to a nonlinear yield criterion, and likewise, a nonlinear relation between the moment and normal force in a rebar element, in comparison to the method presented in [1]. Furthermore, the lower bound problem is solved by second order cone optimization in Mosek, which is found as a rather unexplored approach regarding optimization of reinforced concrete plates.

## 7.1 Problem Formulation

The problem formulation in this chapter is similar to the formulation for steel plates as the task is to maximize the scalar load multiplier by the restriction of a statically admissible solution, and a yield criterion. However, the problem is more complex in a numerical point of view as different element types are considered, and additional constraint equations are introduced. The lower bound formulation for optimizing reinforced concrete plates is stated as a summary of the derivation in the previous chapters

maximize

$$\alpha \tag{7.1}$$

subjected to

$$H\beta - \alpha R = R_c \tag{7.2}$$

$$-(f_t^x - \sigma_x)(f_t^y - \sigma_y) + \tau_{xy}^2 \leq 0 \tag{7.3}$$

$$-(f_c + \sigma_x)(f_c + \sigma_y) + \tau_{xy}^2 \leq 0 \quad (7.4)$$

$$\frac{M}{M_p} + \left(\frac{N}{N_p}\right)^2 - 1 \leq 0 \quad (7.5)$$

$$\frac{M}{M_p} - \left(\frac{N}{N_p}\right)^2 + 1 \geq 0 \quad (7.6)$$

$$-f_c \leq \sigma_x \leq f_t^x \quad (7.7)$$

$$-f_c \leq \sigma_y \leq f_t^y \quad (7.8)$$

$$-1 \leq \frac{M}{M_p} \wedge \frac{N}{N_p} \leq 1. \quad (7.9)$$

In case of higher reinforcement degrees ( $\Phi \geq 0,3$ ) a limit is added to the shear stresses at

$$|\tau_{xy}| \leq 0.5\nu f_c. \quad (7.10)$$

As the problem is solved by cone optimization a reformulation of the yield criterions in Eq. (7.3), (7.4), (7.5) and (7.6) has been necessary, see Appendix E:.

## 7.2 Example – End Wall Exposed to Wind Load

In the following example, a load optimization is conducted for an end wall exposed to wind load, see Figure 7.1. The structure has previously been examined by the stringer method, see [1], [6] and [25], where a load multiplier of  $\alpha = 72.25$  was obtained. The aim is to compare previously obtained results with the numerical solution presented in this thesis.

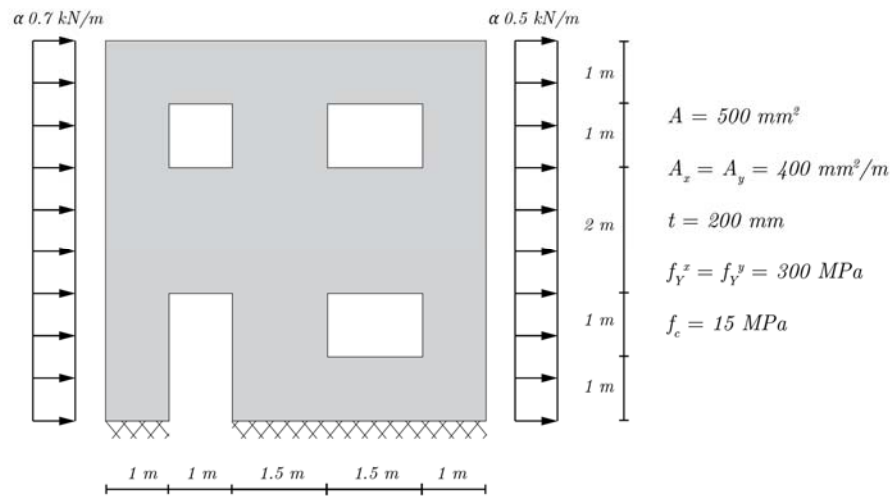
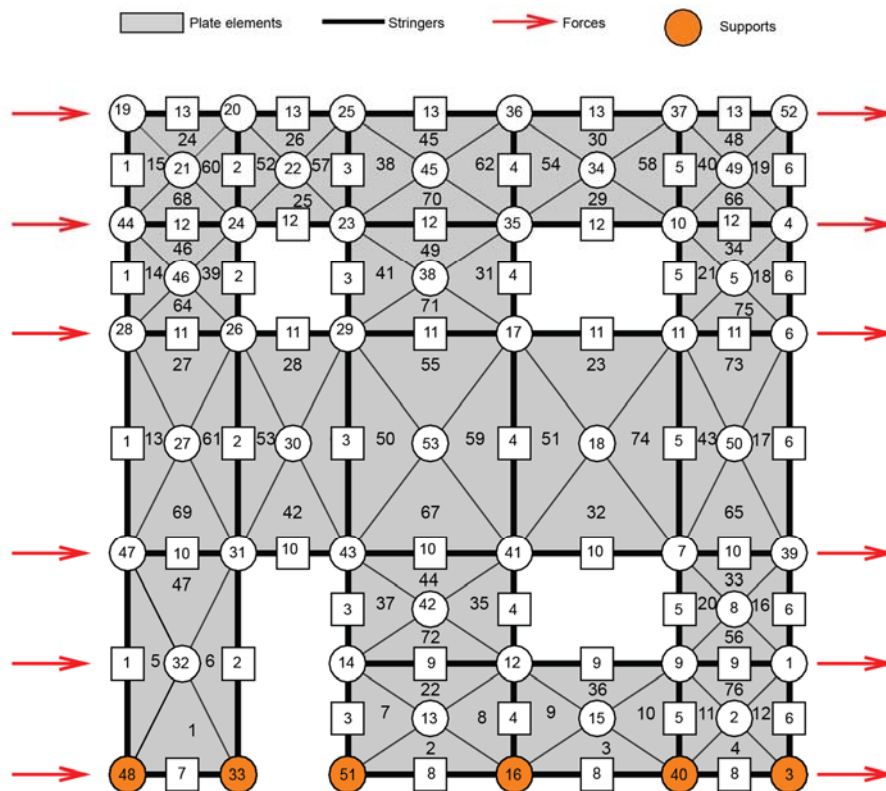


Figure 7.1. End wall exposed to wind from left.

The base of the end wall is considered rigid, and a compressive force is applied at the left side, while a tensile force acts at the right side of the wall. The thickness of the structure is 200 mm, which is relatively small compared to the width and height. Thus, the wall can be analysed as a plane structure. The material properties of the reinforced concrete and concentrated reinforcement appear in Figure 7.1.

The model is implemented in MATLAB by a discretization as seen in the figure below. The finite element discretization of the end wall is made by dividing each shear field from the study in [6] into four triangular elements. This provides a total of 76 triangular elements and 13 rebar elements. In order to compare with the stringer method, the load is distributed into the horizontal rebar elements as illustrated in Figure 7.2.



**Figure 7.2.** Finite element discretization of plate model in MATLAB.

Two load cases are considered in this example. In the first load case, the forces are applied in the rebar elements at each side of the structure, while the second load case investigates the structural response when the forces are applied in the concrete.

### 7.2.1 Application of Forces in Rebars

By performing a load optimization in the developed program, a load multiplier of  $\alpha = 107.14$  is obtained when the load is applied in the rebar elements. The stress distribution corresponding to the load multiplier is illustrated in Figure 7.3.

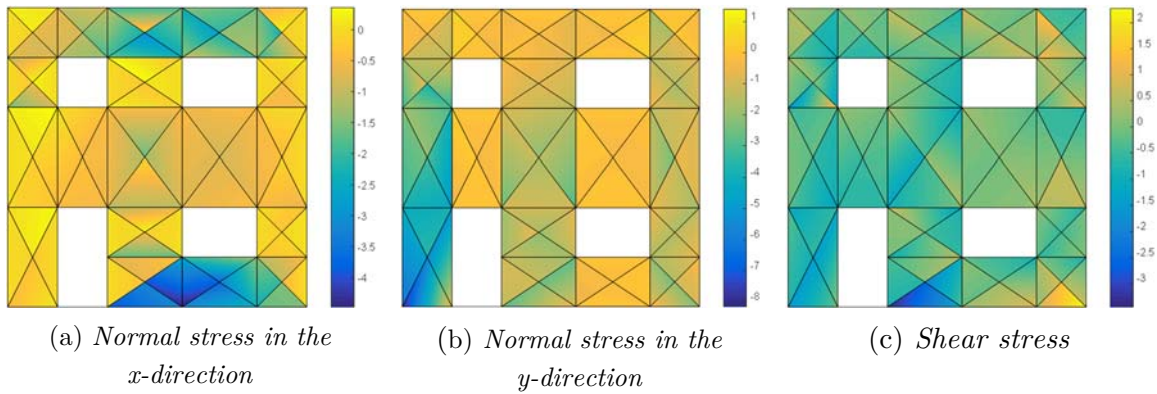


**Figure 7.3.** Stress distribution of the optimized structure.

From the figures above it is clear, that normal stresses are introduced in the concrete plates, which is not possible in the stringer method. Furthermore, it can be noticed that the stress capacity is still available in the concrete when considering all three generalized stresses. This implies that collapse has occurred as a result of failure in a concentrated reinforcement bar. Both observations are seen in the figures below.

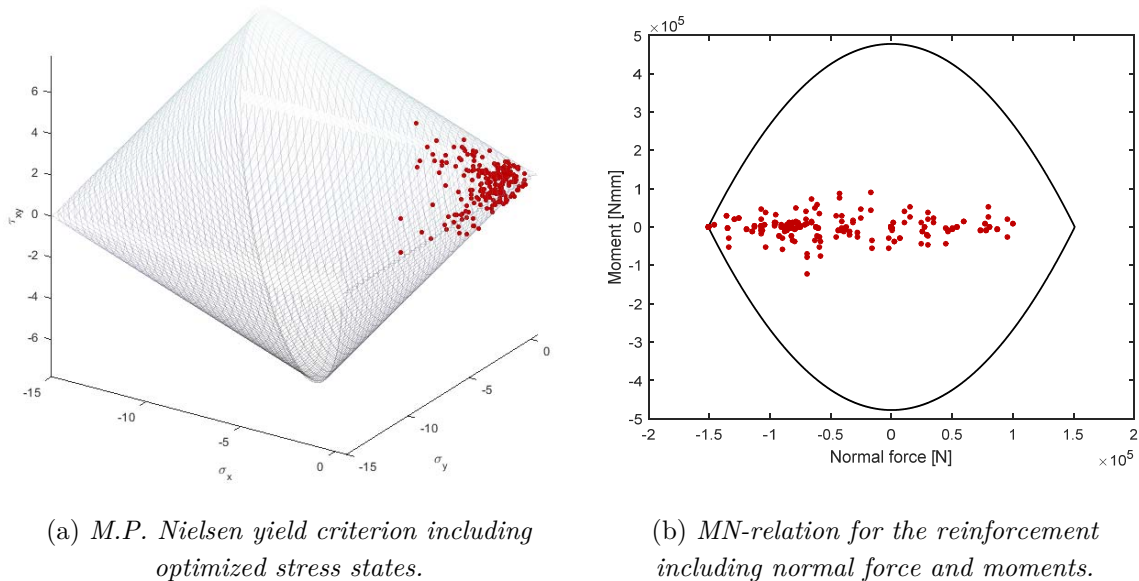


**Figure 7.4.** Yield criteria for reinforced concrete plates and rebars.

The influence of the nonlinearity in M.P. Nielsen yield criterion is not significant in this case as the concentrated reinforcements are critical. However, for structures where the concrete is having more influence on the load multiplier, the nonlinear yield surface could provide a larger load multiplier in comparison to the use of a linear yield criterion.

It can be concluded that the presented method provides a load multiplier that is 32.5 % higher than the obtained by the stringer method.

### 7.2.2 Application of Forces in the Concrete

By performing a load optimization in the developed program, a load multiplier of  $\alpha = 123.8$  is obtained when the load is applied in the concrete elements. The stress distribution corresponding to the load multiplier is illustrated in Figure 7.7.

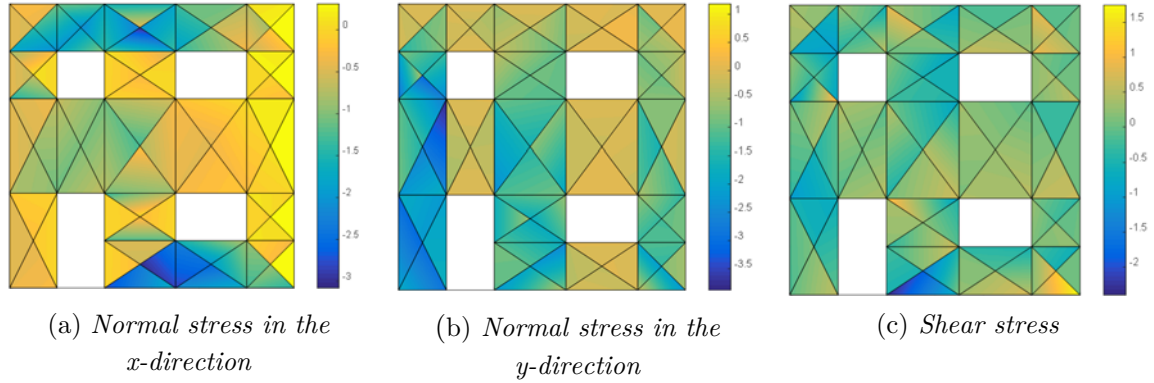


**Figure 7.5.** Stress distribution of the optimized structure.

The corresponding stress states, normal forces, and moments are illustrated in the figure below.

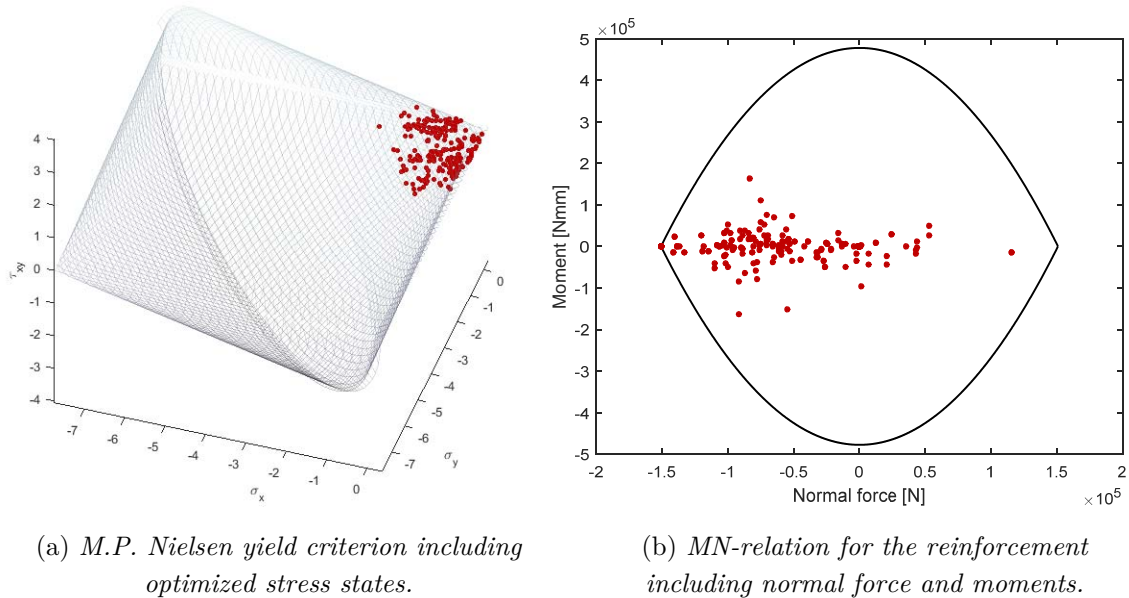


**Figure 7.6.** Yield criteria for reinforced concrete plates and rebars.

By applying the external force in the concrete it is seen that the obtained load multiplier is 15.9 % higher in comparison to the approach presented in [1]. The value of the load multiplier seems reasonable as nonlinear yield criteria are implemented for both the reinforced concrete and rebar elements, which is not the case in [1].

### 7.3 Example – Plate with Curved Reinforcement

In the following example a u-stirrup casted into a concrete plate is considered, see Figure 7.7. The main purpose is to show the importance and capabilities by giving the concentrated reinforcement beam properties. The transverse beam forces in the u-stirrup (or rebar element) has to be transferred to the neighboring plate elements, which results in compression in the concrete. It has to be pointed out that the analysis only serves the purpose of showing the capability by the numerical method as u-stirrups can cause local stresses exceeding the compressive strength in the concrete. Uncritical analyses of such cases can lead to collapse, which is described at the end of the example.

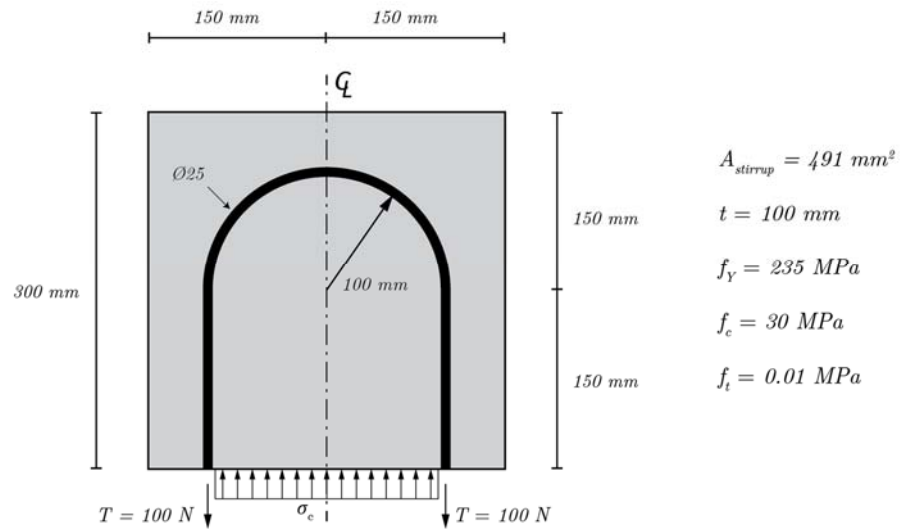


**Figure 7.7.** Plate system with U-stirrups.

The finite element model is established by applying a load of  $T = 100\text{ N}$  at the two ends of the u-stirrup, while the plate elements between the stirrup are supported in the vertical direction, see Figure 7.7. Furthermore, the tensile strength in the concrete is defined as  $f_t = 0.01\text{ MPa}$  due to convergence issues.

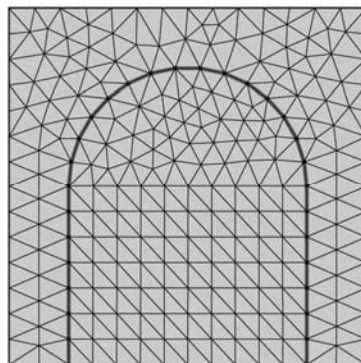


**Figure 7.8.** Finite element discretization of plate model in MATLAB.

The model is implemented in MATLAB by discretizing the model as seen in Figure 7.8. The discretized mode consists of 430 reinforced concrete elements and 29 rebar element describing the u-stirrups.

By performing a load optimization in the developed program, a load multiplier of  $\alpha = 1152$  is obtained. The principal stress distribution corresponding to the load multiplier is illustrated in Figure 7.9 and Figure 7.10.

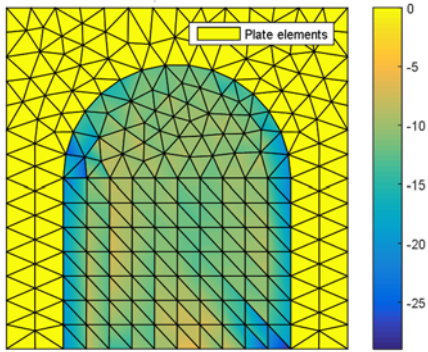


**Figure 7.9.** *Principal stresses,  $\sigma_1$ .*

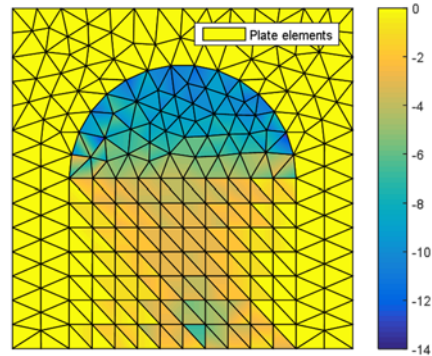


**Figure 7.10.** *Principal stresses,  $\sigma_2$ .*

The corresponding principal directions are illustrated in Figure 7.11.

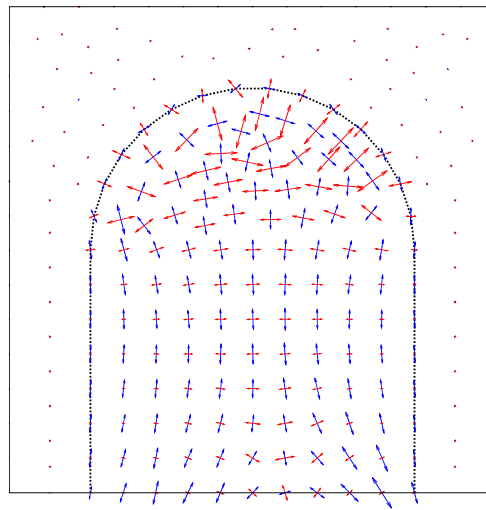
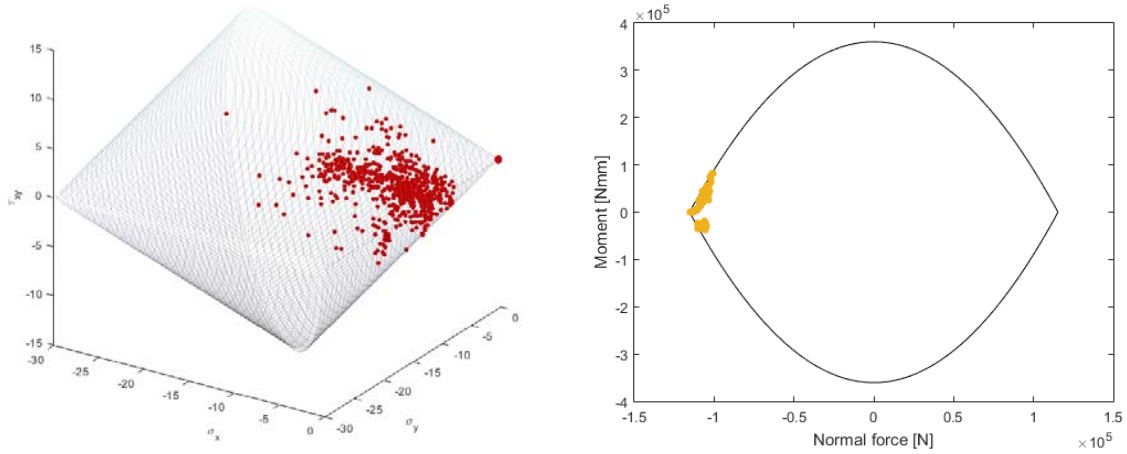


**Figure 7.11.** *Principal directions.*

In Figure 7.9 and Figure 7.10 it can be seen that no stresses occur outside the u-stirrup, which means that the applied tensile forces are carried as pressure in the concrete, solely. Furthermore, it can be seen that the compressive stresses in the concrete is growing towards the stirrup ends, and that the principal direction is pointing slightly towards the top of the stirrup. This is as expected since the concrete can carry higher shear stresses under compression, and thereby transfer higher tangential forces from stirrup to the plate element.



(a) *M.P. Nielsen yield criterion including optimized stress states.*

(b) *MN-relation for the reinforcement including normal force and moments.*

**Figure 7.12.** Yield criteria for reinforced concrete plates and rebars.

The load multiplier corresponds to yielding in the u-stirrup, which is also seen in the figure above.

$$\frac{T \cdot \alpha}{A_{stirrup}} = \frac{100 \text{ N} \cdot 1152}{491 \text{ mm}^2} = 235 \text{ MPa} = f_y.$$

Thus, yielding occurs in the stirrup when the tensile force is 115 kN. Additionally, the moment capacity is reached at multiple points along the u-stirrup due to the transverse loading of the rebar element.

### 7.3.1 Analytical Concrete Pressure

The internal concrete pressure can be calculated analytically according to [8] if the projection perpendicular to the rebar element is assumed equal to the tensile stress in the u-stirrup element

$$f_c = \frac{2T}{dD} = \frac{2 \cdot 115 \cdot 10^3 \text{ N}}{25 \text{ mm} \cdot 200 \text{ mm}} = 46 \text{ MPa},$$

where  $d$  is the cross-sectional diameter of the u-stirrup, and  $D$  is the diameter of the curved reinforcement. Thus, the concrete pressure is actually higher than the uniaxial compressive strength in the concrete, which was described in the beginning of this example. More specific, the limit analysis distributes the pressure along the entire area of the plate instead of the area acting over the u-stirrup, solely. This can lead to high local stresses and potential collapse, see Figure 7.13.

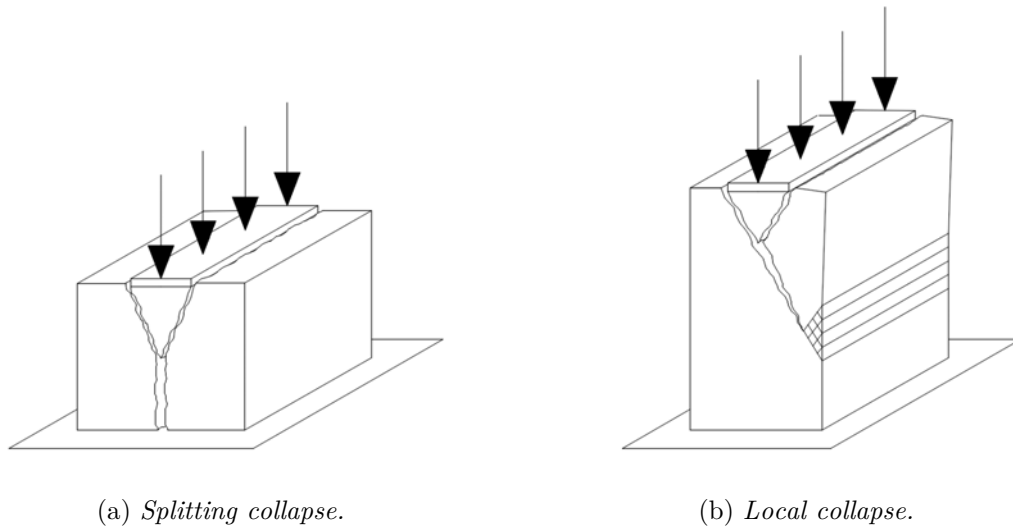


**Figure 7.13.** *Different collapse forms.*



## 8. Reinforced Concrete Plates – Material Optimization

The optimal cost of structures is found as a combination of several factors that are all weighted in a total cost function. The purpose of performing material optimization of reinforced concrete plates is to reduce the material amount as this cost is overriding. A major component in this regard is the material costs, which is treated in this chapter. Yet, material optimization has become quite important in other fields, such as production, where the time costs are highly related to the material design at various fronts. As an example, a growing problem in the industry is the tendency to oversize reinforcement, which often causes space and production problems as the reinforced concrete elements are not well-proportioned in terms of plate thickness and the amount of reinforcement.

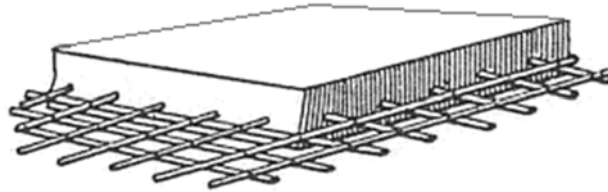


**Figure 8.1.** *Distributed reinforcement in a concrete plate.*

The fundamental difference between load and material optimization is that the material strength is fixed at load optimization, whereas the material strengths are defined variables in the material optimization. The material optimization is performed by the lower bound approach and in overall the aim is to reduce different material variables, e.g.

- minimize the reinforcement in the plate elements
- minimize the concentrated reinforcement
- proportion of concrete mixture to meet the applied load configuration and thereby minimizing the cost of mixture (w/c) ratio

In this thesis it is chosen to demonstrate the main principle of conducting material optimization. Thus, the optimization solely concerns minimization of the reinforcement.

### 8.1 Problem Formulation

In order to conduct material optimization of reinforced concrete plates, the problem needs to be defined by a formulation that satisfies the lower bound approach. The general formulation can be recalled as (see section 2.4)

minimize:

$$w^T d . \tag{8.1}$$

where  $d$  is a vector containing the design variables. The objective function is restricted by a statically admissible stress field and a yield criterion, respectively. The constraints are expressed as equality constraints

$$\mathbf{H}\boldsymbol{\beta} = \mathbf{R} \quad (8.2)$$

$$-(\Phi_x f_c - \sigma_x)(\Phi_y f_c - \sigma_y) + \tau_{xy}^2 + s = 0, \quad (8.3)$$

$$-(f_c + \sigma_x)(f_c + \sigma_y) + \tau_{xy}^2 + s = 0, \quad (8.4)$$

where  $s$  is a non-negative slack variable. Similarly, the  $d$ -vector in Eq. (8.1) consists of non-negative variables since a geometrical parameter by nature can't be negative. The stress variables in the yield criterion needs to be located within the following bounds

$$-f_c \leq \sigma_x \leq f_t^x \quad (8.5)$$

$$-f_c \leq \sigma_y \leq f_t^y \quad (8.6)$$

The concentrated reinforcement is restricted by a linear MN-relation, which is expressed in Eq. (8.7) and Eq. (8.8).

$$-1 < \frac{N_i}{A f_y} < 1 \quad (8.7)$$

$$-1 < \frac{M_i}{W_{pl} f_y} < 1 \quad (8.8)$$

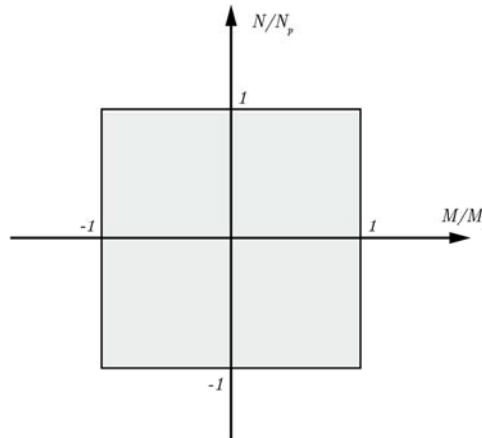


**Figure 8.2.** Linearized MN-relation.

Hence, the objective is to minimize the  $d$ -vector containing the material parameters. It can be noticed that the material parameters are multiplied with a scalar weight,  $w$ , that is further elaborated with the objective function in the following section.

## 8.2 Weighted Object Function

As explained in the introduction to this chapter, a cost function is normally used when conducting material optimization. The principle of a cost function is that each material

variable can be multiplied with a weighting factor. In that way many aspects can be included, and certain variables can be preferred over others by assigning a higher weighting in comparison to the remaining variables. Thus, the weighting system can be chosen in many different configurations in order to control the design variables. The price and volume are one of many factors that are typically taken into account.

In this thesis, the aim is to reduce the total reinforcement volume of a given concrete structure. The total reinforcement volume is a sum of the contribution from the equally spaced reinforcement in the plate, and the contribution from the concentrated reinforcement. Any difference in construction cost with regards to the two types of reinforcement isn't taken into account. The two types of reinforcement casted into the concrete plate is described in the object function by the following expression

$$d = [\Phi \quad A_1 \dots A_n]^T, \quad (8.9)$$

where the equally space reinforcement is described in terms of the reinforcement degree,  $\Phi$ , and the remaining variables  $A_n$  are related to the concentrated reinforcement. The reinforcement degree is assumed to be isotropically distributed in both directions,  $\Phi_x = \Phi_y$ . The weighting part is formulated so that the object function expresses the total steel volume in the plate

$$w = \left[ \frac{f_c \cdot t}{f_y} \cdot A_{plate} \quad L_1 \dots L_n \right]. \quad (8.10)$$

Thereby, the total volume of the plate is expressed as

$$w^T d = V_{total}. \quad (8.11)$$

The weighting system can in fact be chosen by many different configurations in order to optimize the design variables.

### 8.3 Example – End Wall Exposed to Wind Load

In this section an example of a material optimization is presented by considering the same structure as it was the case for the load optimization in section 7.2. The considered material is divided into two different groups, including the rebar elements and the equally spaced reinforcement in the plate elements. The reinforcement in the plate is considered to be isotropic, where the reinforcement degree is optimized in the vertical and horizontal direction in terms of the same reinforcement degree,  $\Phi$ . The rebars are constrained by a linear MN-relation, which in this example has shown to be a good approximation since the moments are small, see section 7.2. The load and the initial stress configuration are equal to the ultimate load bearing capacity from section 7.2. This means that the applied load in the upcoming example is a product of the optimized load multiplier,  $\alpha = 107$ , and the actual wind load. The loads are applied as concentrated forces in the rebars.

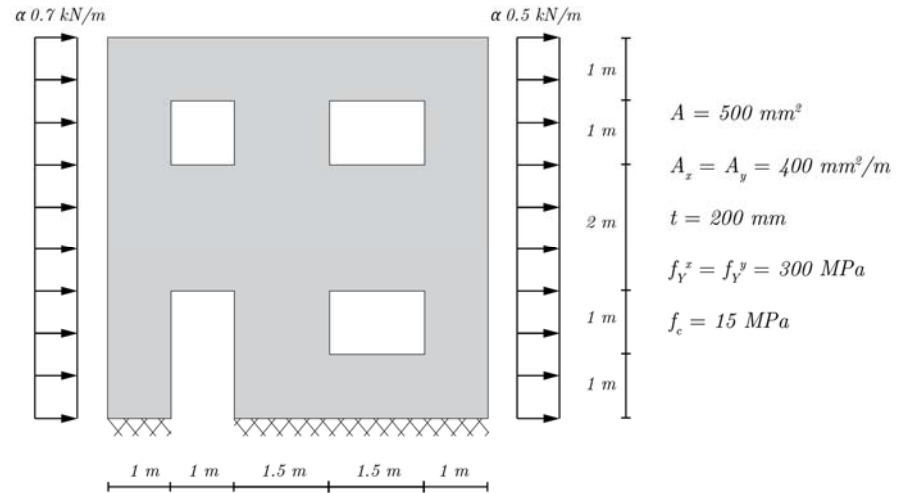


**Figure 8.3.** Illustration of end wall exposed to wind from left.

The structure is discretized as seen in Figure 7.2 by having 76 triangular plate elements and 13 rebar elements.

In order to weight the two different material groups properly, a scalar value is multiplied with the different material parameters to define the total volume of reinforcement in the plate. The object function can be formulated by

$$w^T d = \left[ L_1 \ L_2 \ \dots \ L_{13} \ \left( \frac{f_c \cdot t}{f_y} \cdot A_{plate} \right) \right] \begin{Bmatrix} A_1 \\ \dots \\ \dots \\ A_{13} \\ \Phi \end{Bmatrix}, \quad (8.12)$$

where  $A_i$  is the cross-sectional area of the rebars,  $L_i$  is the length of the continuous rebar elements, and  $\Phi$  is the reinforcement degree for the isotropic case. By weighting the different material parameters as shown in Eq. (8.12), the objective function can be understood as a sum of the total reinforcement volume. Due to the demand for positive material parameters, the initial values of the reinforcement degree and rebar area are as defined in Figure 8.3.

By performing a material optimization in the developed program, a cross-sectional area distribution of the rebars is obtained as seen in the figure below.

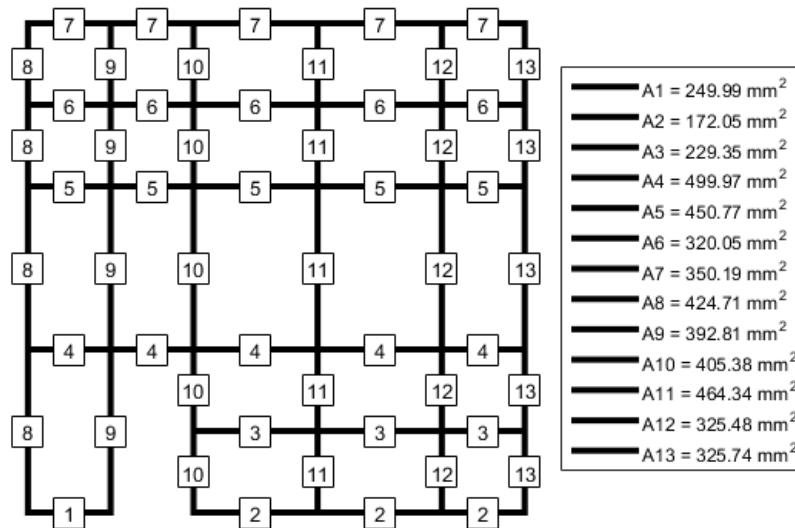


Figure 8.4. Optimized rebar cross-sectional area.

The total volume of the rebar reinforcement is  $V_r = 2.55 \cdot 10^7 \text{ mm}^3$ , which is a reduction of 36% in comparison to the original concentrated reinforcement. The optimized isotropic reinforcement degree is found to  $\Phi = 0.033$ , which gives a tensile strength for the reinforced concrete plate of  $f_t = 0.49 \text{ MPa}$ , and a total reinforcement volume in the plate of  $V_p = 1,96 \cdot 10^7 \text{ mm}^3$ . The isotropic reinforcement is reduced by 22%, and summarized with the reduction of the rebar volume, a total reinforcement reduction of 30% is achieved. The resulting normal stress distribution in the rebar is as seen in Figure 8.5.

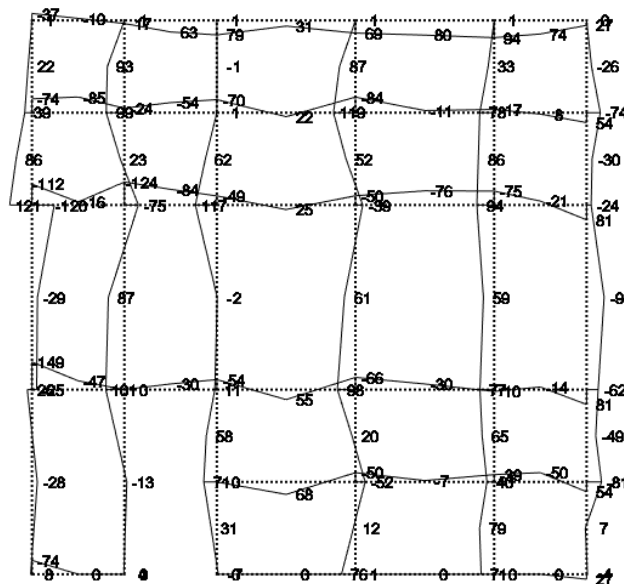


Figure 8.5. Normal stress variation in the rebars.

If a more representative material optimization should be performed, multiple load cases should be included in the algorithm. In order to achieve a further reinforcement reduction, the model could be divided into subareas with inclusion of anisotropic reinforcement.



## 9. Conclusion

An efficient program for verification of critical stress spots in steel plates has successfully been developed. The program is based on a submodeling principle and the lower bound limit analysis. In the lower bound limit analysis, stress-based elements are used to calculate the scalar load multiplier  $\alpha$  in order to specify whether a stress state leads to structural collapse. The program appears to be very efficient since only a submodel is considered and only few steps are needed in the overall process. Furthermore, the results are always on the safe side as the lower bound method is implemented, and only a submodel is considered.

By implementing the efficient self-developed script in ANSYS, it is possible to export all the needed finite element information to set up the lower bound problem for the submodel. The maximization of the lower bound problem is solved by means of nonlinear programming theory using interior point solvers in MATLAB and Mosek. Especially the second order cone programming in Mosek has proven to be very efficient in optimizing large scale problems.

The efficiency of the program has been presented by an example of a plate subjected to a geometrical stress singularity. The developed submodel program is versatile since it can be used for structures subjected to both stress concentrations, and stress singularities regarding concentrated supports and forces, and not only geometrical singularities as it is the case in the example.

A finite element program capable of conducting limit state analyses of reinforced concrete plates is likewise developed. The program is based on the lower bound theorem where bar and beam elements have been introduced. A load optimization example has been presented in terms of an end wall, and the efficiency of the load optimization program has been shown as the method provides a load multiplier that is 32.5 % higher in comparison to the stringer method when the force is applied in the rebar elements. When the load is applied in the concrete a 15.9 % higher load multiplier is obtained in comparison to the approach presented in [1], which is seen as a result of the implementation of nonlinear yield criterions.

Furthermore, the beam properties of a rebar element are demonstrated by means of an example where a u-stirrup is considered. The example shows the transfer of beam forces in the u-stirrup to the neighbouring plate elements. It is also seen that the moments aren't violating the nonlinear MN-relation.

The material optimization in the developed program is based on a weighting system with the purpose of reducing the total amount of reinforcement when considering both the distributed reinforcement and concentrated reinforcement, respectively. Finally, the program is used to conduct a material optimization of the end wall, which resulted in a total reinforcement reduction of 30 %. The material reduction was obtained on behalves of the limit load from the previous, structure, which illustrates principle and potential of the numerical approach.

## Appendix A: Upper and Lower Bound Solution of a Statically Indeterminate Beam

In this appendix a one-time indeterminate beam system is considered. The purpose is to show how a coincided solution can be found regarding the upper and lower bound theorem. The considered system is clamped in the left end and simple supported in the right end. The system is exposed to two vertical forces  $P$ , each acting  $\frac{1}{6}L$  from the middle of the span. As seen in the figure, the system is discretized by four nodes.

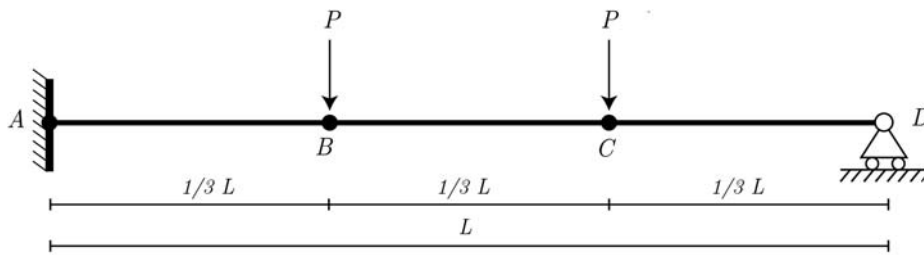


Figure 9.1. one-time indeterminate beam system.

### Upper Bound solution

The upper bound solutions are found by considering all possible collapse mechanisms between the nodes  $A$ ,  $B$ ,  $C$ , and  $D$ . The collapse mechanisms are sketched in the figure below.

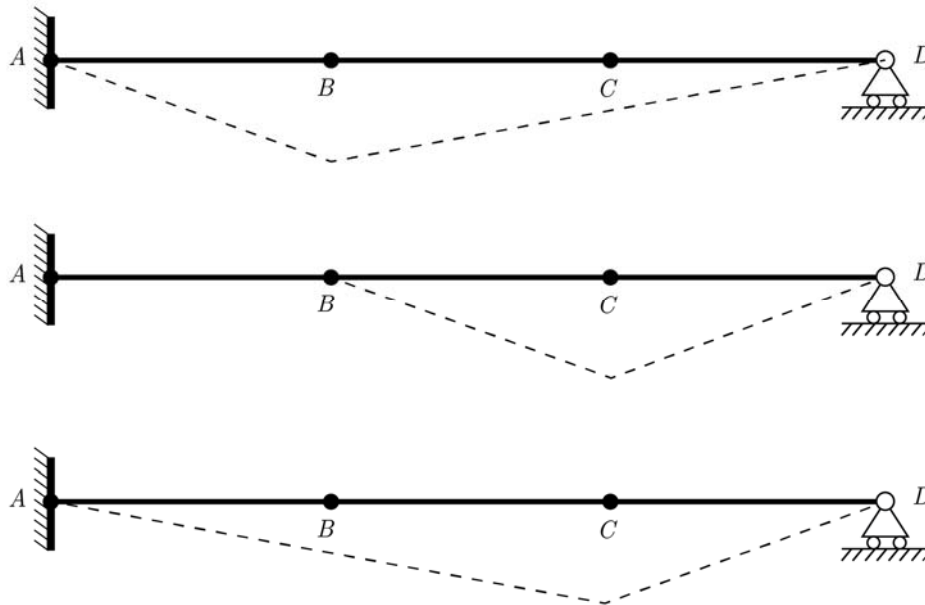


Figure 9.2. Collapse mechanisms for the indeterminate beam.

From this simple discretized system three collapse mechanisms must be investigated, and the most critical collapse mode is to be compared with the optimum solution in the lower bound solution. The upper bound solution is based on the following consideration from which the critical load can be found by solving.

$$W_{internal} = W_{outer}$$

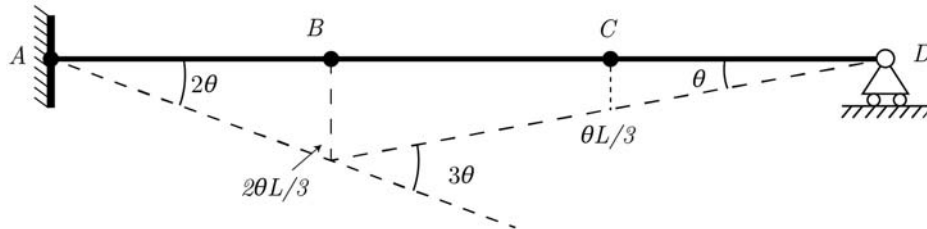


Figure 9.3. Collapse mechanism.

Collapse between node A and B.

$$2\theta \cdot M_P + 3\theta \cdot M_P = \frac{1}{3}pl \cdot 2\theta + \frac{1}{3}pl \cdot \theta \rightarrow P = 5 \frac{M_P}{L}$$

Collapse between node B and C.

$$\theta \cdot M_P + 2\theta \cdot M_P = \frac{1}{3}pl \cdot \theta \rightarrow 9 \frac{M_P}{L}$$

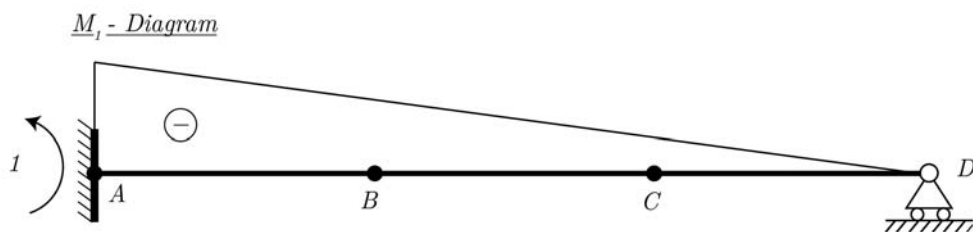
Collapse between node A and C.

$$\theta \cdot M_P + 3\theta \cdot M_P = \frac{1}{3}pl \cdot \theta + \frac{1}{3}pl \cdot 2\theta \rightarrow P = 4 \frac{M_P}{L}$$

The most critical collapse form is therefore between node A and C, which will be compared with the optimal lower bound solution.

### Lower Bound Solution

The optimum lower bound solution is found by the force method. Thus the so-called  $M_0$  and  $M_1$  moment diagram are found and used to find the optimal stress field.



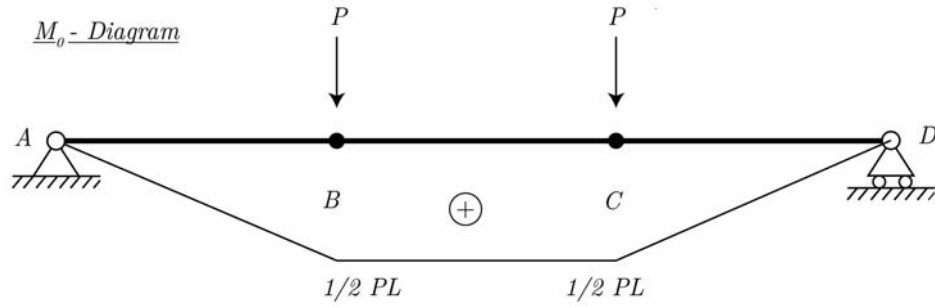


Figure 9.4.  $M_0$  and  $M_1$  diagram.

Moment equations

$$M_A = 0 + x_1 \cdot 1 = \pm M_P$$

$$M_B = \frac{1}{3}pl + x_1 \cdot \frac{2}{3} = \pm M_P$$

$$M_C = \frac{1}{3}pl + x_1 \cdot \frac{1}{3} = \pm M_P$$

$$M_D = 0 + 0 = \pm M_P$$

Isolate  $p$  when  $x_1 = 0$

$$p = 0$$

$$p = \pm \frac{3M_P}{L}$$

$$p = \pm \frac{3M_P}{L}$$

$$p = 0$$

Isolate  $x_1$  when  $p = 0$

$$x_1 = \pm M_P$$

$$x_1 = \pm \frac{3}{2}M_P$$

$$x_1 = \pm 3M_P$$

$$x_1 = 0$$

The highest load the system can obtain by the lower bound method is now found by plotting the above  $p$  and  $x_1$  values.

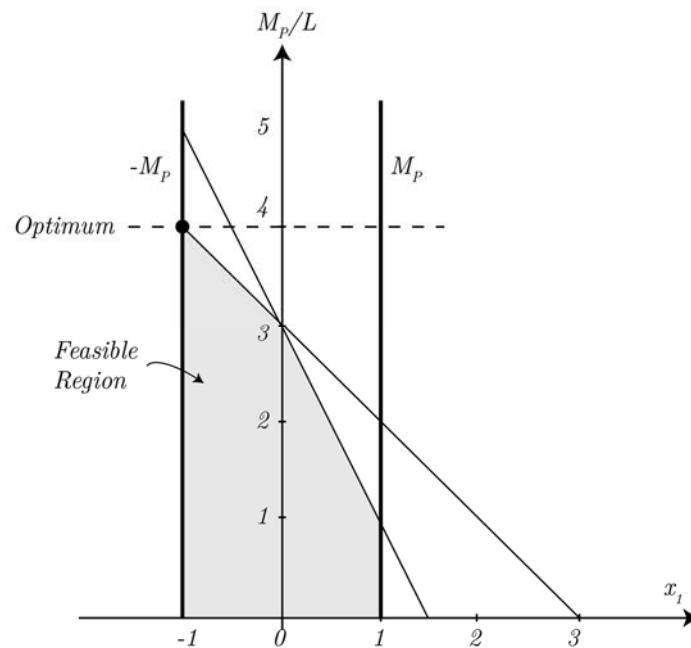


Figure 9.5. Search for lower bound optimum solution.

From Figure 9.5 it is seen that the optimum load is  $p = 4 \frac{M_P}{L}$ , which corresponds to the load of the most critical collapse mechanism found by the upper bound method.

# Appendix B: Primal-dual Formulation for Load Optimization

## Duality Theory

The duality theorem is a *mathematical* optimization theory that makes it possible to consider an optimization problem from two perspectives, either the primal problem or the dual problem. The duality theorem is useful with respect to the accuracy when calculating the scalar load multiplier. A duality theory between the lower and upper bound methods can be expressed just as it is the case with the duality in the field of linear programming.

In order to formulate the dual problem, the primal problem in Eq. (2.7) has to be linearized, which is done by use of the first-order Taylor expansion of the nonlinear yield criterion around points  $\beta^*$  lying on the yield surface

$$f(\beta) \cong f(\beta^*) + \nabla f^T(\beta - \beta^*) . \quad (\text{B.1})$$

On the yield surface  $f(\beta^*) = 0$  and hereby the linearized yield criterion can be expressed as

$$\nabla f^T \beta + s = \nabla f^T \beta^* . \quad (\text{B.2})$$

The *linearized lower bound load optimization problem* is expressed as

$$\begin{aligned} \text{maximize:} \quad & \alpha \\ \text{subject to:} \quad & \mathbf{H}\beta = \alpha R + R_c \\ & \nabla f^T \beta + s = \nabla f^T \beta^* , \\ & s \geq 0, \end{aligned} \quad (\text{B.3})$$

By performing several mathematical operations, it is possible to express the dual to the problem in Eq. (B.3) [18]

$$\begin{aligned} \text{minimize:} \quad & (\nabla f^T \beta^*)^T \lambda - R_c^T v \\ \text{subject to:} \quad & \nabla f \lambda - \mathbf{H}^T v = 0 \\ & R^T v = 1 \\ & \lambda \geq 0, \end{aligned} \quad (\text{B.4})$$

where  $\lambda$  is a vector containing the magnitude or strain rate of each plastic strain, and therefore it is associated with the yield criterion. The number of plastic strains corresponds to the number of nonlinear constraints. The plastic strain rate is expressed by the normality rule

$$\varepsilon_{ij}^p = \lambda \frac{\partial f}{\partial \beta_{ij}} \quad (\text{B.5})$$

In the dual problem in Eq. (B.4)  $v$  denotes the displacements, or velocities, when the structure collapses. The displacements,  $v$ , are i.e. associated with the upper bound formulation of the load optimization for the discrete problem.

The external and internal work have to be in equilibrium and each of these are given by

$$W^e = (\alpha R^T + R_c^T)v, \quad W^i = (\nabla f^T \beta^*)^T \lambda \quad (\text{B.6})$$

By setting the internal work equal to the external work and solving with respect to  $\alpha$ , it is possible to obtain the scalar collapse load factor  $\alpha$

$$\alpha = \min_{v, \lambda} \left( \frac{(\nabla f^T \beta^*)^T \lambda - R_c^T v}{R^T v} \right). \quad (\text{B.7})$$

The displacements  $v$ , that are calculated based on the dual formulation, can have different interpretations depending on the finite element discretization. In the mixed finite element formulation, the interpretation of the displacements  $v$  is straightforward as they define the displacements in the nodes of the assembled mesh [18]. In this project a finite element discretization with rigorous equilibrium elements is formulated such that stress discontinuities are permitted as long as normal and tangential stresses across element interfaces are continuous in the lower bound solution. The permission of stress discontinuities in the lower bound solution means that velocity discontinuities are kinematically admissible in the upper bound method [18]. In the mixed finite element formulation, the stresses and displacements are therefore obtained directly in each node of the assembled mesh, whereas in the rigorous finite element formulation the allowance of stress discontinuity is compensated by a set of inter-element conditions and a number of overall equilibrium conditions. This means that the displacement field should be made with certain reservations.

### Optimality Conditions

The optimality conditions for the lower bound formulation are explained in the following section. It includes a derivation and a physical interpretation of the optimization problem. The optimality conditions are expressed by the duality theorem by considering both the upper and lower bound formulation.

From mechanics of constitutive modelling it is known that an exact solution to the limit analysis is reached when the kinematical solution is equal to the statically solution.

Recalling that the dual feasibility conditions for the linearized lower bound problem are given by

$$H\beta = \alpha R + R_c, \quad (\text{B.8})$$

$$\nabla f^T \beta + s = \nabla f^T \beta^*, \quad (\text{B.9})$$

$$s \geq \mathbf{0}. \quad (\text{B.10})$$

The corresponding primal feasibilities are

$$\nabla f \lambda - H^T v = \mathbf{0} \quad (\text{B.11})$$

$$R^T v = 1 \quad (\text{B.12})$$

$$\lambda \geq \mathbf{0}, \quad (\text{B.13})$$

The difference between the primal and dual solution is expressed by a duality gap,  $\gamma$

$$\gamma = (\nabla f \beta^*)^T \lambda - \mathbf{R}_c^T \mathbf{v} - \alpha = 0 \quad (\text{B.14})$$

The zero duality gap from Eq. (B.14) is rewritten by the feasibility conditions in Eq. (B.8) and (B.9)

$$\begin{aligned} \gamma &= (\nabla f \beta^* + \mathbf{s})^T \lambda - (\mathbf{H}\beta - \alpha \mathbf{R})^T \mathbf{v} - \alpha \\ &= \mathbf{s}^T \lambda + \beta^T (\nabla f \lambda - \mathbf{H}^T \mathbf{v}) + \alpha (\mathbf{R}^T \mathbf{v} - \mathbf{1}) \\ &= \mathbf{s}^T \lambda \end{aligned} \quad (\text{B.15})$$

The last expression in Eq. (B.15) has to be equal to zero, which leads to

$$\mathbf{s}_j \lambda_j = \mathbf{0}, \quad j = 1, 2, \dots, p \quad (\text{B.16})$$

where  $\lambda$  and  $s$  both have to be greater than or equal to zero. The condition in Eq. (B.16) is also known as the *complementary slackness*. If a stress state on the yield surface is considered, the value for the slackness  $s$  will be equal to zero ( $s_j = 0$ ), whereas the strain rate  $\lambda$  is positive ( $\lambda > 0$ ) and Eq. (B.16) is thereby fulfilled. An opposite effect is seen when a stress state within the yield surface is considered.

In matrix notation Eq. (B.16) is stated as

$$\mathbf{S}\lambda = \mathbf{0}, \quad (\text{B.17})$$

where  $\mathbf{S} = \text{diag}(\mathbf{s})$ .

Thus, the full set of optimality constraints is expressed as

$$\mathbf{H}\beta = \alpha \mathbf{R} + \mathbf{R}_c \quad (\text{B.18})$$

$$\mathbf{f}(\beta) + \mathbf{s} = \mathbf{0} \quad (\text{B.19})$$

$$\nabla f \lambda - \mathbf{H}^T \mathbf{v} = \mathbf{0} \quad (\text{B.20})$$

$$\mathbf{R}^T \mathbf{v} = \mathbf{1} \quad (\text{B.21})$$

$$\mathbf{S}\lambda = \mathbf{0} \quad (\text{B.22})$$

From the optimality conditions it is seen that Eq. (B.18) and (B.19) correspond to the constraints from the original optimization problem in Eq. (2.7) with a nonlinear yield criterion. The optimality conditions in Eq. (B.20) and (B.21) correspond to the constraints in the dual problem for the linearized lower bound formulation in Eq. (B.4). The constraints in the optimality conditions are supplemented with the condition that the product of  $s$  and  $\lambda$  has to be equal to zero as seen in Eq. (B.22). When considered in a mathematical perspective, the optimality conditions are known as the first-order Kuhn-Tucker optimality conditions.

## Appendix C: Example of Path Following Interior Point Method

In this appendix, an example of the path following interior point method is to be shown in order to illustrate the principles behind the method. The path following method is based on the primal and dual linear programming formulation. [15]

An example of a primal dual problem is formulated in Table C.1 where  $z_j$  denotes the slack variables for the dual problem.  $x_j$  are the variables for the primal solution and  $\pi_j$  are the variables for the dual solution.

**Table C.1.** Primal dual formulation.

Primal model		Dual model	
Maximize	$z_p = 2x_1 + 3x_2$	Minimize	$z_D = 8\pi_1 + 6\pi_2$
Subject to	$2x_1 + x_2 + x_3 = 8$	Subject to	$2\pi_1 + \pi_2 - z_1 = 2$
	$x_1 + 2x_2 + x_4 = 6$		$\pi_1 + 2\pi_2 - z_2 = 3$
	$x_j \geq 0, j = 1, \dots, 4$		$\pi_1 - z_3 = 0$
			$\pi_2 - z_4 = 0$
			$z_j \geq 0, j = 1, \dots, 4$

The primal formulation from Table C.1 is rewritten to a dual formulation based on the principle in Table C.2.

**Table C.2.** Formulas for rewriting a primal formulation to a dual formulation.

Primal		Dual	
Maximize	$z_p = cx$	Minimize	$z_D = \pi b$
Subject to	$Ax = b$	Subject to	$\pi A - z = c$
	$x \geq 0$		$\pi_1 + 2\pi_2 - z_2 = 3$

The primal formulation consists of  $m$  equations and  $n$  variables, which are all expressed as equality constraints. Since the problem is an equality problem, there is no restriction in the sign of the dual variables  $\pi$ .

The iterations of the primal and dual solutions are shown in Figure 9.6, where #1 denotes the first iteration step that lies within the feasible region. The solution converges towards the extremum point for each iteration as seen in the figure. This is due to that the primal and dual solution variables ( $x_j$  and  $z_j$ ) are modified for each iteration until primal feasibility, dual feasibility and complementary slackness are satisfied to a certain degree [15]. It is possible to determine the degree of satisfaction by a gap that expresses the difference in the object function for the primal and dual solution, respectively.

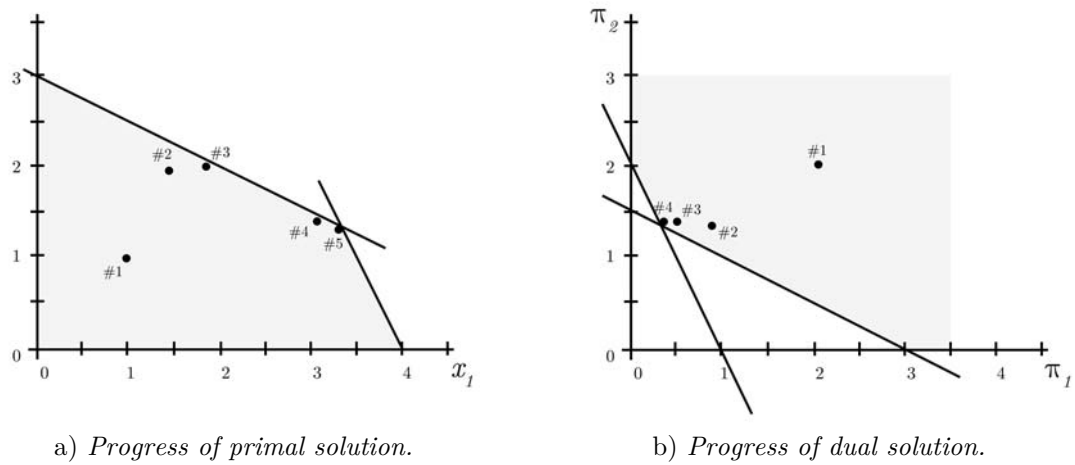


**Figure 9.6.** Progress of primal and dual solutions.

From the figure it can be seen that the primal solution corresponds to a maximization problem, whereas the dual problem corresponds to a minimization problem.

## Appendix D: Steel Plate Optimization – *fmincon* Study

The appendix investigates the different *fmincon* options in order to conclude at which setting the interior point algorithm optimizes most efficiently.

The study is based on a global plate model as seen in Figure 9.7. The plate is subjected to a tensional force of 4 kN at both the left and the right edge. The plate is constrained from moving in both the vertical and horizontal direction at the bottom edge. The plate has a thickness of 1 mm and is made of steel with a yield strength of 235 MPa.

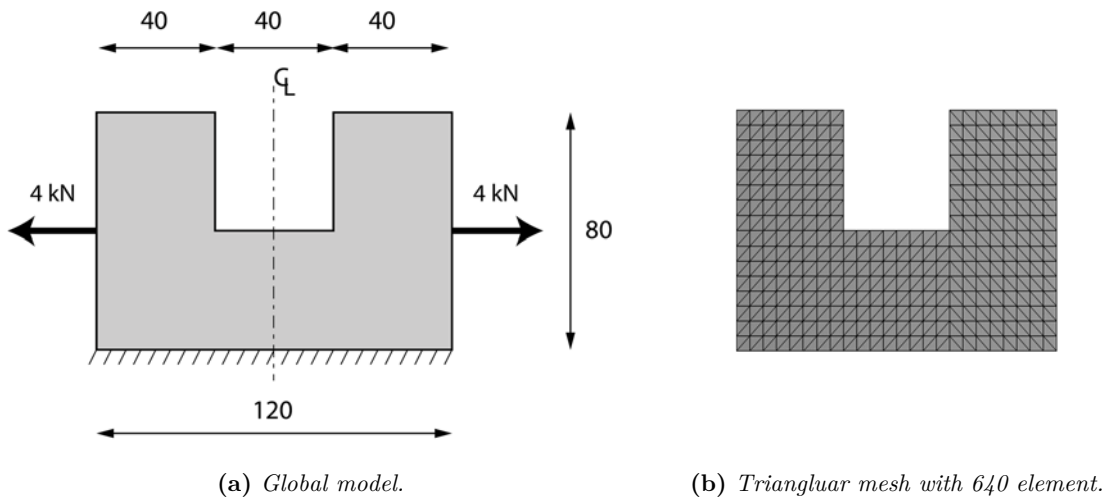


**Figure 9.7.** Free body diagram and mesh of considered plate model.

In all of the analyses, the mesh is assigned as seen in Figure 9.7 with 640 elements and the load multiplier  $\alpha$  is used as the representative value for comparison.

For all the upcoming comparisons the interior point algorithm is chosen in *fmincon* since large scale problems are considered. In the interior point algorithm, it is possible to choose between different Hessian approximations or to implement a user-supplied. The following five different ways of optimizing are investigated in *fmincon* when the interior point algorithm is chosen:

<b>Hessian approach</b>	<b>Subalgorithm</b>
1. lfbgs (large-scale),	ldl-factorization
2. lfbgs (large-scale),	cg (conjugate-gradient-dense hessian)
3. Fin-diff-grads	cg (conjugate-gradient-dense hessian)
4. User-supplied	ldl-factorization
5. User-supplied	cg (conjugate-gradient-dense hessian)

For each of the Hessian approaches a subalgorithm has to be chosen, which has the function of determining how the iteration step is calculated. In *fmincon* two different subalgorithms can be chosen; namely, ldl and cg. Both of the algorithms are to be investigated for the hessian approximations and the user-supplied hessian matrix.

It also has to be mentioned that the Hessian user-supplied approaches highly depend on the self-developed script, and it can be optimized more than how it is now. This could make the approach faster.

In the following analyses, the stopping criteria is chosen to 100 iterations, which means that the iterations stop when the 100<sup>th</sup> iteration is reached. The gradients are also user-supplied, both for the hessian approximation methods and for the user-supplied hessian.

Both the number of iterations to reach the converged value and the calculation time is considered in the analyses. This is because some methods may use a lower number of iterations to converge, but the calculation time may be higher. All of the analyses are calculated on a laptop with the following operating system and hardware specifications:

MacBookPro8,1  
 Windows 7 Ultimate 64-bit  
 Intel® Core™ i5-2415M CPU @2.30 GHz  
 4.00 GB RAM  
 Intel(R) HD Graphics 3000

The convergence of the object function  $\alpha$  for each of the five approaches is seen in Figure

9.8.

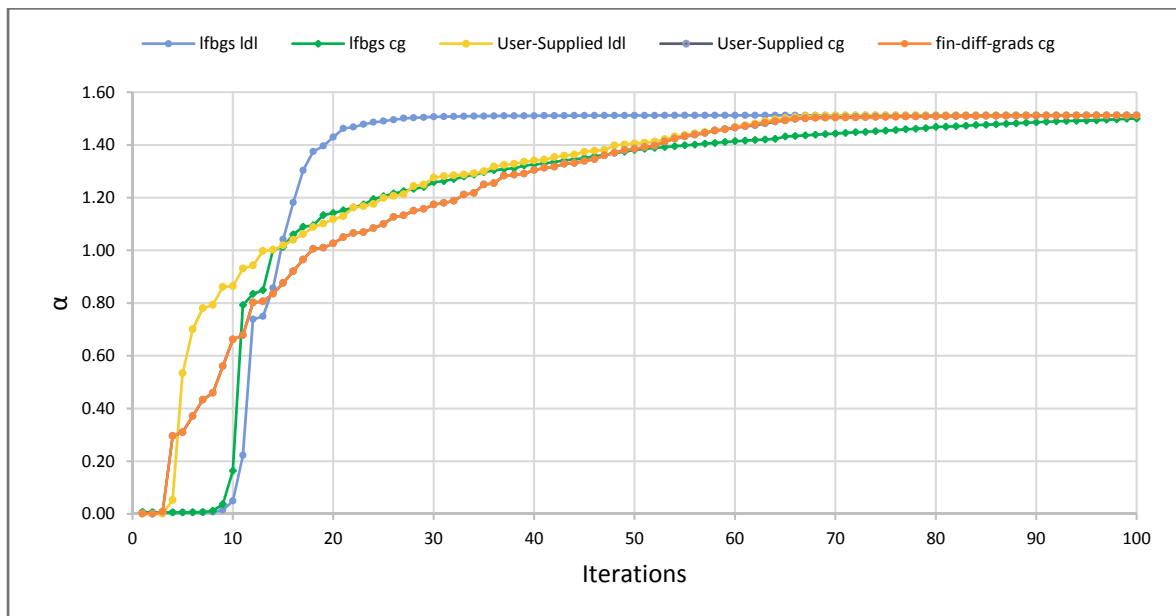


**Figure 9.8** Convergence of the object function.

All of the five methods converges towards the proper  $\alpha$ -value. The lfbgs (ldl) method uses the fewest number of iterations to obtain the converged  $\alpha$ -value, but this doesn't necessarily make it the fastest approach. It can also be seen that the fin-diff-grad (cg) method converges

slowly in the beginning but it obtains the optimized value at a lower iteration value than the lfbgs (cg) method.

The first study investigates the elapsed time to complete 100 iterations of each approach. This study only says something about the elapsed time and not the accuracy.

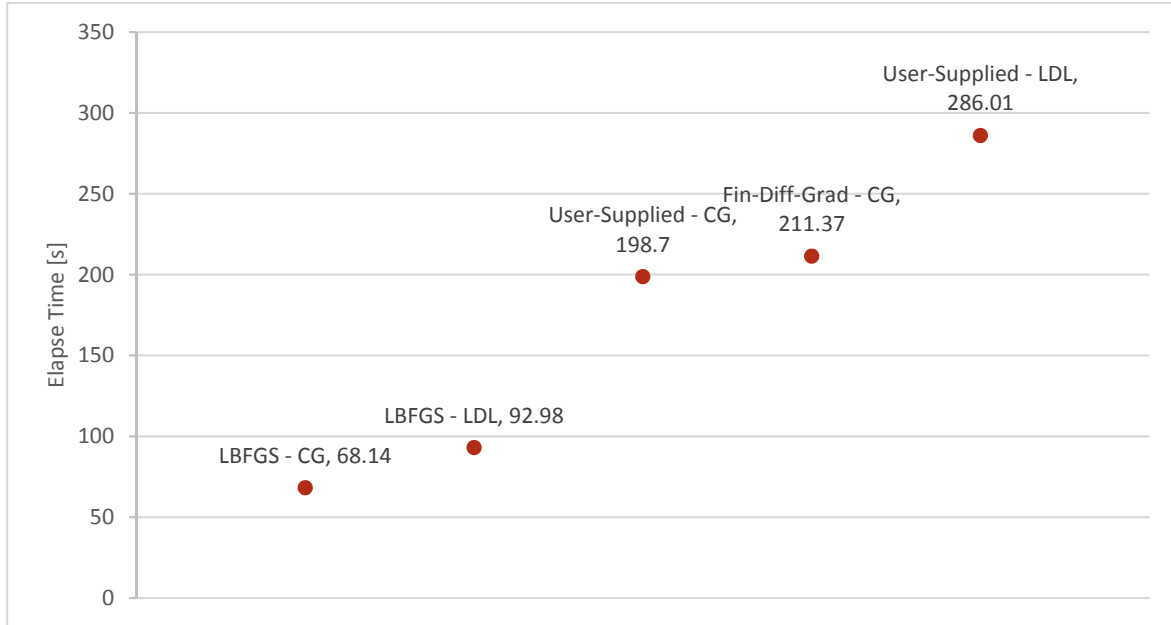


**Figure 9.9.** Study of elapsed time.

From the study it can be seen that the lfbgs (cg) method is the fastest to reach 100 iterations followed by the lfbgs (ldl). Even though lfbgs (cg) is fastest it isn't the most accurate method as seen in Figure 9.10 and Figure 9.8. However, lfbgs (ldl) is very effective since it doesn't take long time and since the accuracy is very high as seen in the following graph.

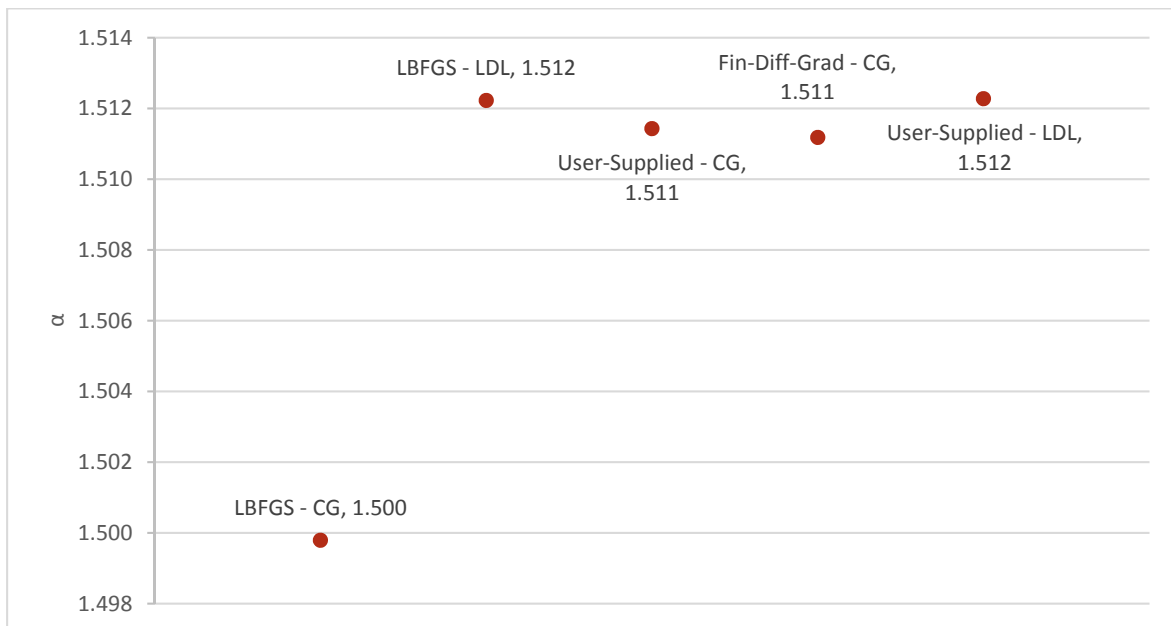


**Figure 9.10.** Accuracy Study.

The lfbgs (cg) method should be used with precaution since an accurate result takes many iterations. An explanation of the efficiency of lfbgs (ldl) is seen in Figure 9.11 and Figure 9.12.

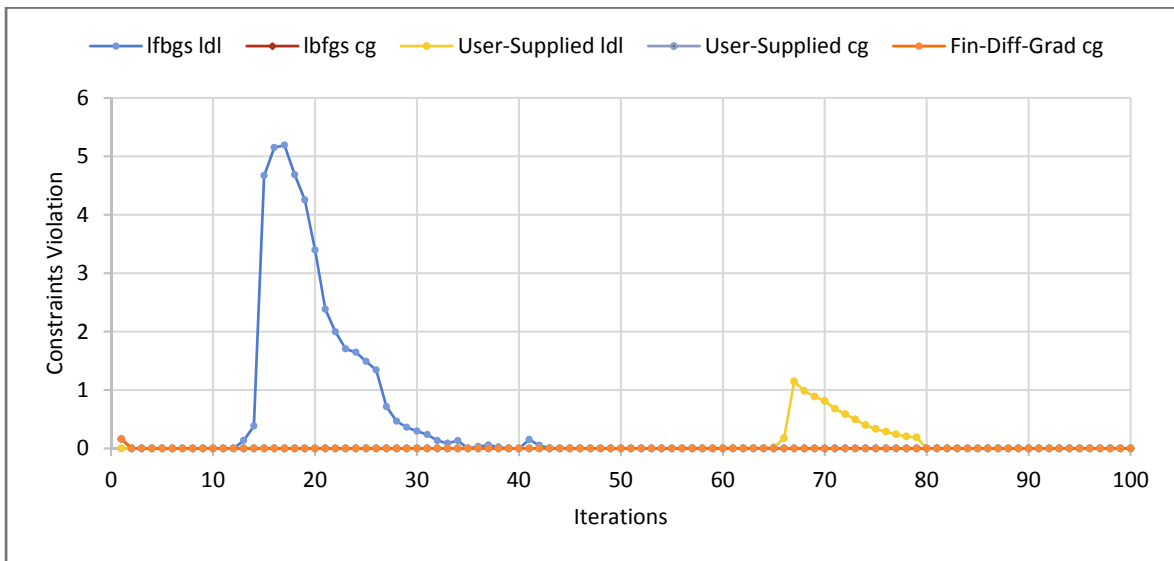


Figure 9.11. Maximum constraint violation at different iterations.

The ldl-method violates the constraints the most and that is why it is so effective. The largest violation takes place in the preliminary iterations for lfbgs and the violation is often negligible since the violation at the last step of the iteration is almost zero.

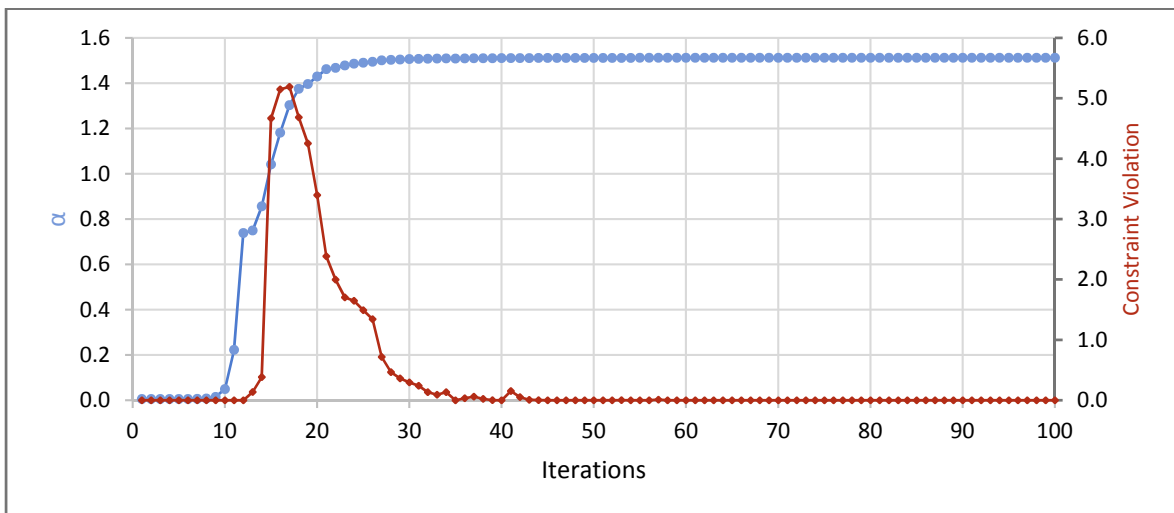
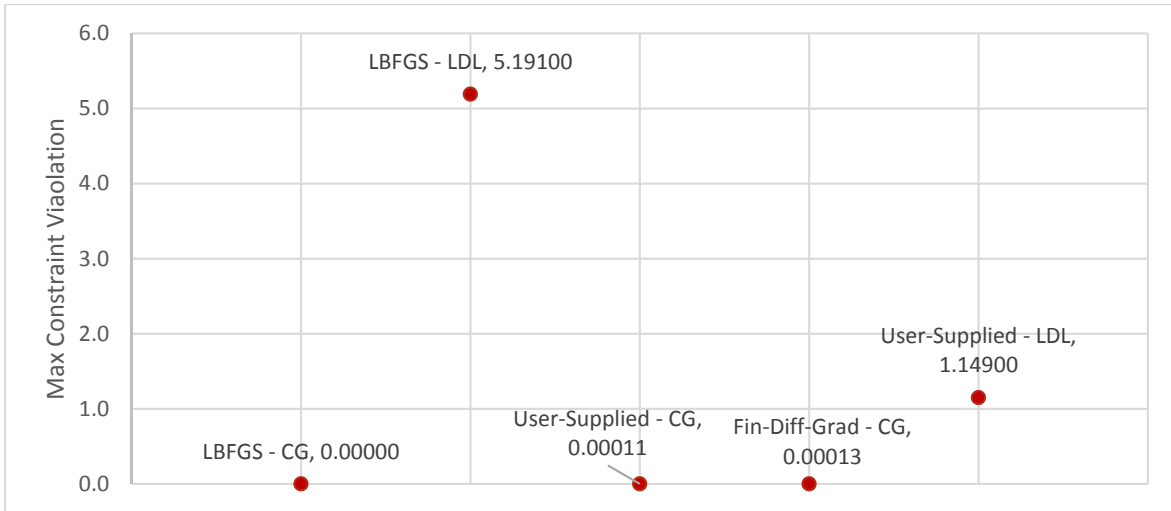


Figure 9.12. Maximum Constraint Violation and  $\alpha$ -value for iteration with lfbgs and ldl-solver.

It is also seen in Figure 9.12 that the increment in the object function  $\alpha$  is largest at the iterations where the violation is highest.



**Figure 9.13.** *Maximum Constraint Violation for each solver.*

As illustrated in Figure 9.13, the LDL-factorization method should be used with precaution and the constraint violation should be checked at the last iteration step.

Another measure of convergence is the first-order optimality conditions (KKT-Conditions). The optimality conditions should be fulfilled such that it equals to zero when the result has converged.

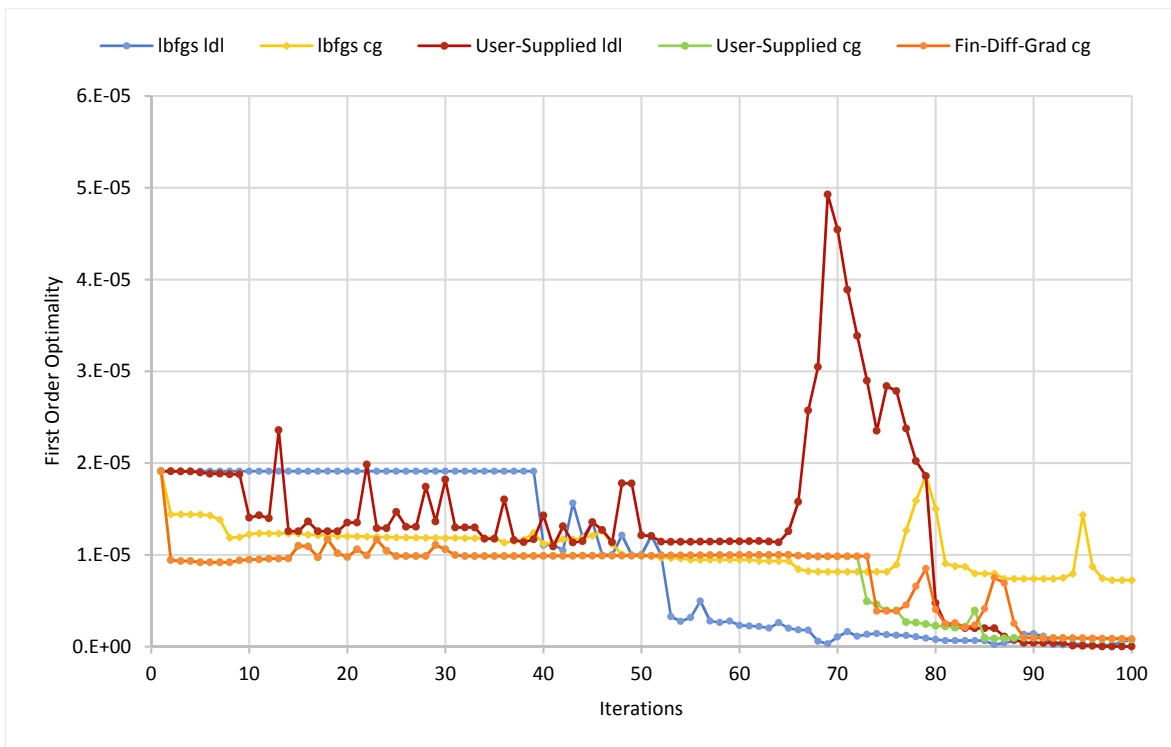


**Figure 9.14.** *First Order Optimality Constraint.*

From Figure 9.14 it can be seen that once again the lbfgs (ldl)-solver is the most effective, and it should also be noted that a relatively high first order optimality value is obtained for the user-supplied (ldl) method at the iteration where the constraint is violated the most.

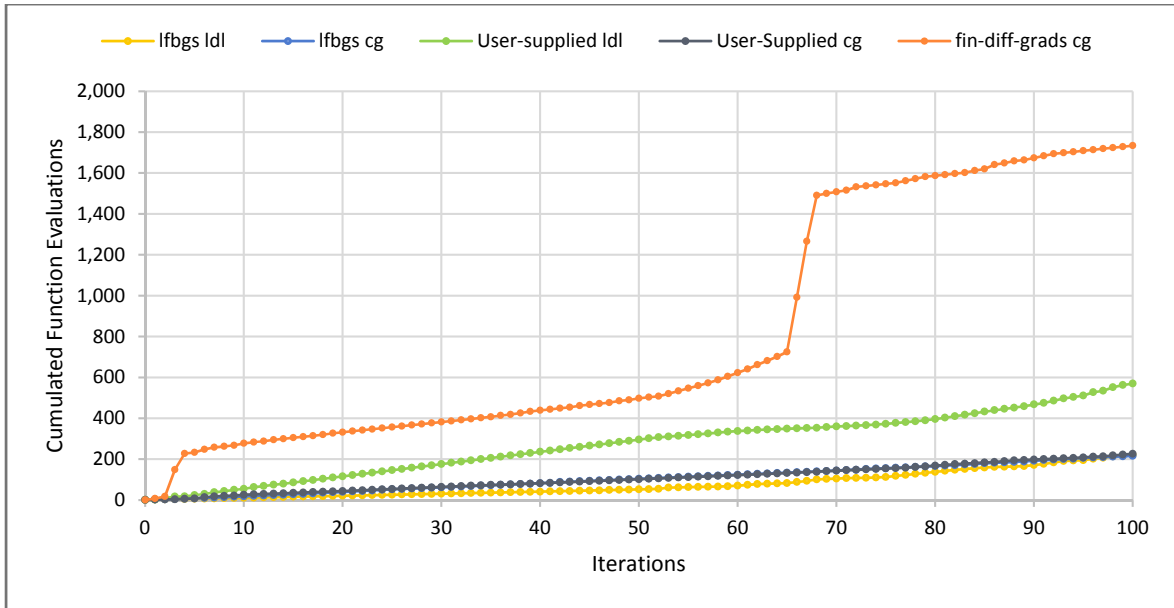


Figure 9.15. Cumulated Function Evaluations.

At each iteration the objective function has to be evaluated at least once. From the figure above it can be seen that the fin-diff-grads (cg) method takes many function evaluation, but it doesn't necessarily make it a slow approach. It can also be seen from Figure 9.15 that the number of function evaluations is lower for the lfbgs method than for the user-supplied hessian approach.

### Conclusion

Based on the study it can be concluded that the lfbgs is the fastest method. From the study it can also be concluded that the most effective method is the lfbgs method with ldl-factorization, even though it should be used with precaution since it can violate the constraint by a relatively high value. The ldl-factorization is effective since it violates the constraints and thereby reaches the optimal result fastest.

# Appendix E: Reformulation of Yield Criteria to Second-Order Cones

This appendix concerns reformulation of yield criteria to second-order cones with the purpose of implementing the constraints in Mosek. von Mises yield criterion has to be expressed in terms of a quadratic cone (QC), whereas M.P. Nielsen's yield criterion and the MN-relation for reinforcement has to be expressed as rotated quadratic cones (RQC).

## E.1 Reformulation of von Mises Yield Criterion

Von Mises yield criterion is for general plane stress defined as

$$\sqrt{\sigma_x^2 + \sigma_y^2 - \sigma_x \sigma_y + 3\tau_{xy}^2} - k \leq 0, \quad (\text{E.23})$$

where  $k$  is a strength parameter defining the yield stress.

Eq. (E.23) is rewritten such that Eq. (E.24) is obtained.

$$\sqrt{\frac{1}{2}((\sigma_x - \sigma_y)^2 + \sigma_x^2 + \sigma_y^2) + 3\tau_{xy}^2} - k \leq 0 \quad (\text{E.24})$$

It is more convenient to rename the stress parameters in Eq. (E.24) such that

$$\sigma_x = x_1, \quad \sigma_y = x_2, \quad \tau_{xy} = x_3, \quad x_4 = x_1 - x_2, \quad (\text{E.25})$$

and thereby Eq. (E.24) equals to the following expression

$$\sqrt{\frac{1}{2}(x_1^2 + x_2^2 + x_4^2) + 3x_3^2} \leq k, \quad (\text{E.26})$$

which is expanded to

$$k \geq \sqrt{\frac{1}{2}x_1^2 + \frac{1}{2}x_2^2 + \frac{1}{2}x_4^2 + 3x_3^2} \quad (\text{E.27})$$

New parameters  $x_5, x_6, x_7, x_8$  and  $x_9$  are defined by taking the square root in order to obtain the yield criterion on the form expressed in Eq. (5.18)

$$\begin{aligned} x_5 &= \frac{1}{\sqrt{2}}x_1, & x_6 &= \frac{1}{\sqrt{2}}x_2, & x_7 &= \frac{1}{\sqrt{2}}x_4 \\ x_8 &= \sqrt{3} \cdot x_3 & \rightarrow & & x_3 - \sqrt{\frac{1}{3}}x_8 &= 0 \\ x_9 &= k \end{aligned} \quad (\text{E.28})$$

Von Mises criterion is expressed by the following quadratic cone constraint

$$x_9 \geq \sqrt{x_5^2 + x_6^2 + x_7^2 + x_8^2}. \quad (\text{E.29})$$

By implementing the above formulated expression in Mosek, the lower bound problem can be solved and a scalar load multiplier can be obtained.

## E.2 Reformulation of M.P. Nielsen's Yield Criterion

M.P. Nielsen's yield criterion for reinforced concrete plates is recalled as

$$-(f_t^x - \sigma_x)(f_t^y - \sigma_y) + \tau_{xy}^2 \leq 0 \quad (\text{E.30})$$

$$-(f_c + \sigma_x)(f_c + \sigma_y) + \tau_{xy}^2 \leq 0. \quad (\text{E.31})$$

In order to reformulate the expression for Nielsen's yield criterion, four new variables  $\alpha_1, \alpha_2, \alpha_3$  and  $\alpha_4$  are introduced

$$\alpha_1 = \frac{1}{\sqrt{2}}(f_{tx} - \sigma_x) \quad (\text{E.32})$$

$$\alpha_2 = \frac{1}{\sqrt{2}}(f_{ty} - \sigma_y) \quad (\text{E.33})$$

$$\alpha_3 = \frac{1}{\sqrt{2}}(f_c + \sigma_x) \quad (\text{E.34})$$

$$\alpha_4 = \frac{1}{\sqrt{2}}(f_c + \sigma_y) \quad (\text{E.35})$$

$\alpha_1$  and  $\alpha_2$  are related to Eq. (E.30), while  $\alpha_3$  and  $\alpha_4$  describes the cone in Eq. (E.31). The expression for the rotated quadratic cone (RQC) becomes

$$2\alpha_1\alpha_2 \geq \tau_{xy}^2 \quad ; \quad \alpha_1, \alpha_2 \geq 0 \quad (\text{E.36})$$

$$2\alpha_3\alpha_4 \geq \tau_{xy}^2 \quad ; \quad \alpha_3, \alpha_4 \geq 0. \quad (\text{E.37})$$

From the above two equations it is possible to optimize the lower bound concrete formulation by the use of second-order cone programming in Mosek.

## E.3 Reformulation of the Nonlinear MN-relation

The MN-relation for reinforcement is recalled as

$$\left(\frac{M}{M_p}\right) + \left(\frac{N}{N_p}\right)^2 - 1 \leq 0 \quad (\text{E.38})$$

$$\left(\frac{M}{M_p}\right) - \left(\frac{N}{N_p}\right)^2 + 1 \leq 0. \quad (\text{E.39})$$

The expression in Eq. (E.38) is reformulated to a rotated quadratic (RQC) cone by the following procedure

$$\left(\frac{N}{N_p}\right)^2 \leq 1 - \left(\frac{M}{M_p}\right)$$

$$\begin{aligned}\frac{N^2}{N_p^2} &\leq 1 - \left(\frac{M}{M_p}\right) \\ N^2 &\leq N_p^2 - \left(\frac{MN^2}{M_p}\right) \\ N^2 &\leq \left(1 - \frac{M}{M_p}\right) N_p^2.\end{aligned}$$

Thereby the first rotated cone is derived.

The second cone is a reformulation of the expression in Eq. (E.39)

$$\begin{aligned}\left(\frac{M}{M_p}\right) - \left(\frac{N}{N_p}\right)^2 + 1 &\geq 0 \\ \left(\frac{M}{M_p}\right) + 1 &\geq \left(\frac{N}{N_p}\right)^2 \\ \left(\frac{M}{M_p}\right) + 1 &\geq \frac{N^2}{N_p^2} \\ \left(\frac{M}{M_p} + 1\right) N_p^2 &\geq N^2.\end{aligned}$$

Thereby the second cone is derived.

Four new parameters  $\alpha_1, \alpha_2, \alpha_3$  and  $\alpha_4$  have to be introduced in order to obtain the form for the second-order cone in Eq. (5.19). The first two parameters  $\alpha_1$  and  $\alpha_2$  are related to the first cone, whereas  $\alpha_3$  and  $\alpha_4$  are related to the second cone.

$$2\alpha_1\alpha_2 \geq N^2, \quad \alpha_1 = \frac{1}{\sqrt{2}} \left(1 - \frac{M}{M_p}\right), \quad \alpha_2 = \frac{1}{\sqrt{2}} N_p^2 \quad (\text{E.40})$$

$$2\alpha_3\alpha_4 \geq N^2, \quad \alpha_3 = \frac{1}{\sqrt{2}} \left(1 + \frac{M}{M_p}\right), \quad \alpha_4 = \frac{1}{\sqrt{2}} N_p^2 \quad (\text{E.41})$$

Based on the above two expressions it is possible to optimize the lower bound formulation in terms of second-order cones in Mosek.

# Appendix F: Program for Global Steel Plate Optimization

## F.1 Full Plate Model Optimization

In the developed program it is possible to optimize a full/global model as long as the global model in ANSYS is meshed with CST elements. This is because the nodal stresses can be imported directly to the MATLAB program since CST elements and the used triangular stress-based elements have the same geometry.

The procedure for optimizing a global steel plate model is illustrated in the figure below.

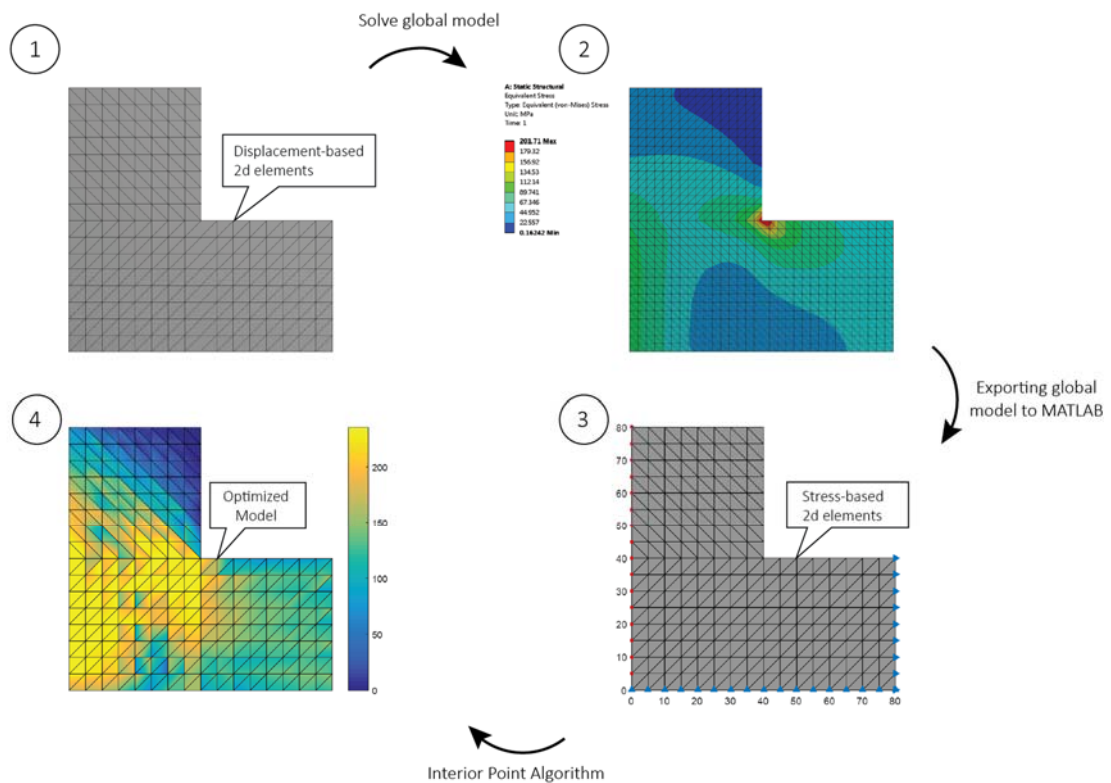


Figure 9.16. Overall process of the model approach.

## F.2 Convergence Study of a Global Model

A convergence study has been conducted for a global model in order to validate the developed MATLAB optimization program. In the study, a full plate model is investigated since the optimization algorithm is the same whether considering submodels or global models. The convergence study for the global model is based on two different approaches

- Displacement based nonlinear analysis in *ANSYS Workbench*
- Stress-based analysis in *MATLAB* based on the lower bound limit formulation

A full nonlinear displacement-based analysis in ANSYS is to be compared with a stress-based analysis in the developed MATLAB program. By comparing a displacement-based nonlinear analysis in ANSYS with the stress-based analysis in the MATLAB program, it is possible to see whether the load multiplier converges towards the same value. Thereby, it is possible to validate the developed MATLAB program.

The considered model is shown in the figure below. The plate is subjected to a tensional pressure of 30 MPa at the left edge. The plate is constrained in the vertical direction at the bottom edge, whereas the right edge is constrained in the horizontal direction. The plate has a thickness of 1 mm and is made of steel with a yield strength of 235 MPa.

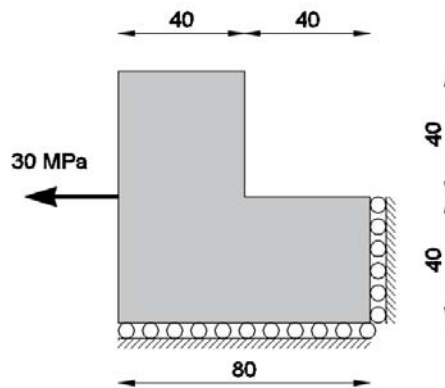


**Figure 9.17.** *Considered global model*

In the nonlinear analysis in ANSYS a perfect plastic material behaviour has been assigned by choosing a bilinear material model with a tangent modulus of zero. The nonlinear analysis in ANSYS calculates an exact solution for the critical load, corresponding to the assigned mesh.

Four different convergence studies have been conducted and has to be compared. This includes two analyses in ANSYS and two in MATLAB.

1. MATLAB with export of loads and geometry from ANSYS
2. MATLAB with export of geometry from ANSYS only
3. ANSYS nonlinear analysis with CST elements
4. ANSYS nonlinear analysis with LST elements

The first analysis in MATLAB is made by solving a global model in ANSYS and thereby exporting the boundary conditions and geometry to the MATLAB program. The second analysis in MATLAB is conducted by exporting only the topology from ANSYS, while the boundary conditions are assigned manually, and not by importing from ANSYS.

In the ANSYS studies two different elements are used; CST and LST elements, respectively. CST elements are used to directly compare with the MATLAB program since the MATLAB results are based on the exported stresses from a global CST model. A convergence study is also conducted for a global model with LST elements since it produces more accurate results. The plate model from Figure 9.17 is meshed by assigning a triangular mapped mesh that is

based on the chosen element size. Four different meshes are considered as shown in Figure 9.18. When the element size halves, the total number of elements quadruples, whereas the calculation time more than quadruples. This is why the limit in the study is 1536 elements.

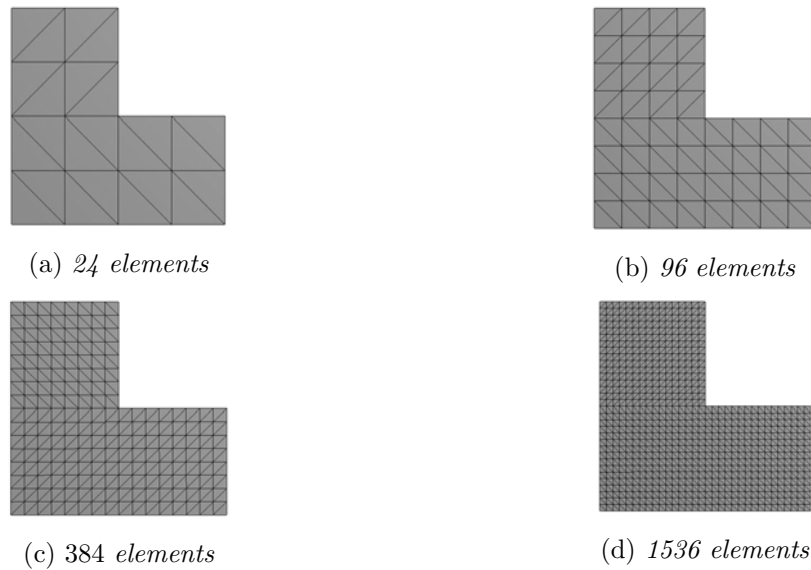


Figure 9.18. Mesh types.

Boundary conditions have been assigned in the optimization program corresponding to the model in Figure 9.17. This is done by eliminating equilibrium equations corresponding to the constrained nodes. Loads have been assigned as stresses on the boundary. The boundary conditions that are applied for the four different convergence study models are seen in the figure below, where the red nodes illustrate the loads, whereas the blue nodes show the support.

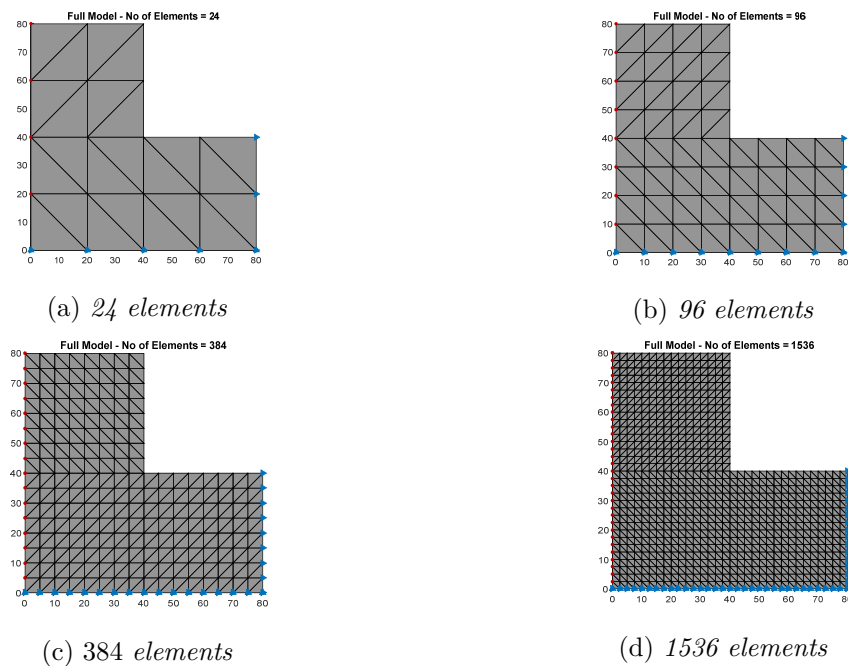


Figure 9.19. Boundary conditions as applied in the MATLAB program.

The results from the convergence studies are presented in Table F.3.

**Table F.3.** Results from the convergence study.

Element Size [mm]	No of Elements CST/LST	$\alpha$ ANSYS CST	$\alpha$ ANSYS LST	$\alpha$ MATLAB (lbfgs)	$\alpha$ MATLAB Manual
20	24	3.787	3.073	*	*
10	96	3.250	2.773	2.393	2.033
5	384	2.820	2.653	2.641	2.437
2.5	1536	2.740	2.613	2.588	2.450

\* value not possible to obtain

The critical load multipliers  $\alpha$  from the above table is shown on the graph in Figure 9.20.

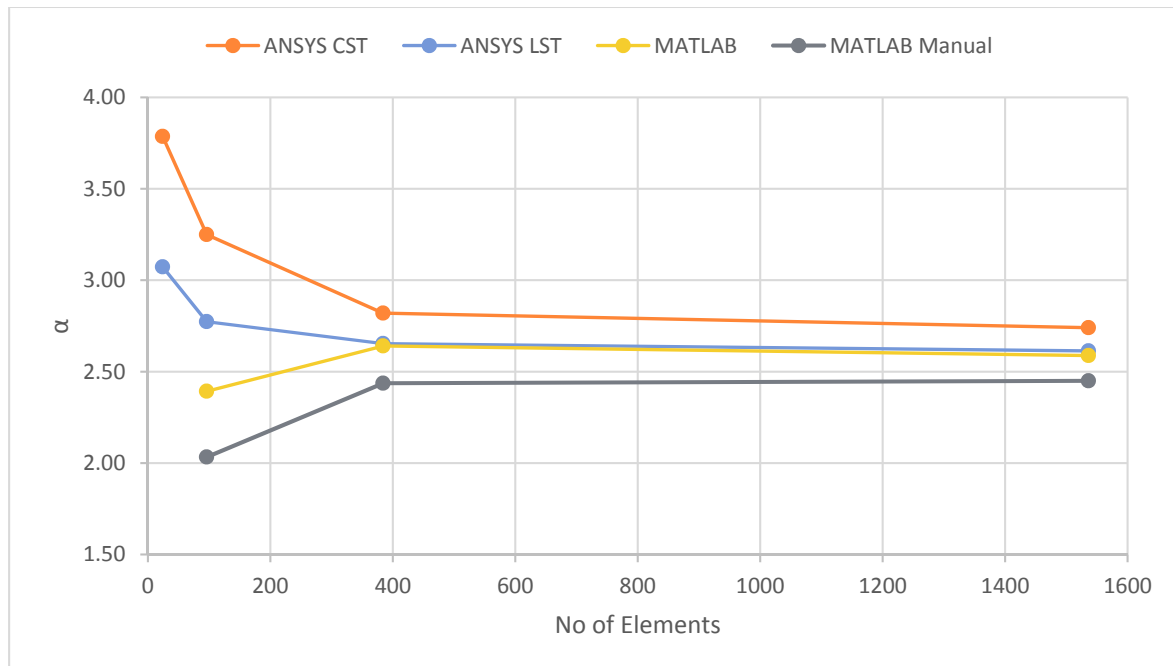


**Figure 9.20.** Convergence study results for ANSYS and MATLAB analyses.

From the study it can be seen that all four cases converge towards the same value. The MATLAB results converges by having the lowest  $\alpha$ -value for the lowest number of elements and increases as the number of elements increases. This is not the case with the nonlinear analysis in ANSYS, which makes the result on the insecure side, unless a very fine mesh is assigned. This makes the MATLAB analysis preferable compared to the nonlinear analysis in ANSYS.

From the analysis it can also be seen that the MATLAB analysis with manually selected stresses of 30 MPa gives a lower load multiplier than the MATLAB analysis with imported boundary stresses. For the particular case a global model meshed with CST elements gives a result on the insecure side.

# Appendix G: Verification of Critical Stress Spots in Steel Plates – Studies

## G.1 Study of Submodel Size

In the study, the influence of the submodel size on the load multiplier is investigated. The considered model is shown in Figure 9.21. The plate is subjected to a tensional pressure of 25 MPa at the left edge. The plate is constrained in the vertical direction at the bottom edge, whereas the right edge is constrained in the horizontal direction. The plate has a thickness of 1 mm and is made of steel with a yield strength of 235 MPa.

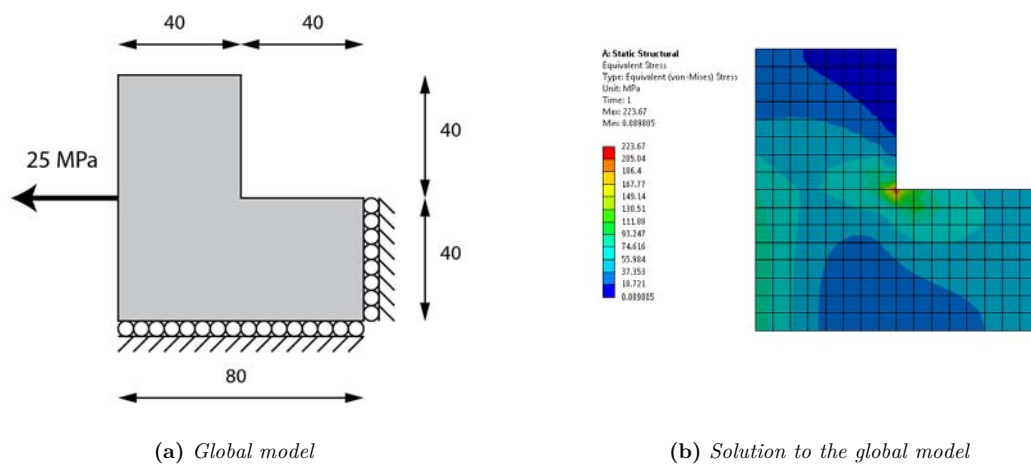


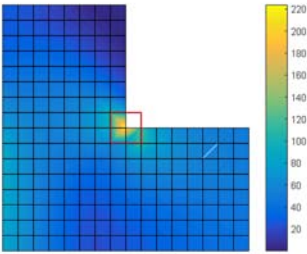
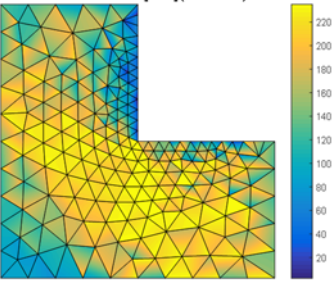
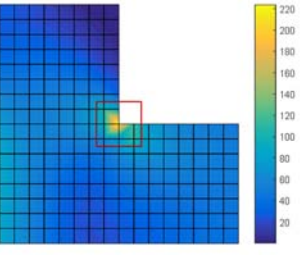
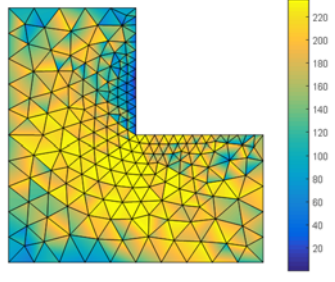
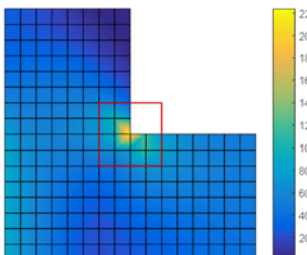
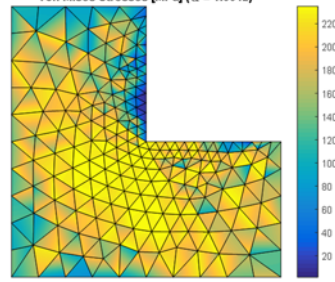
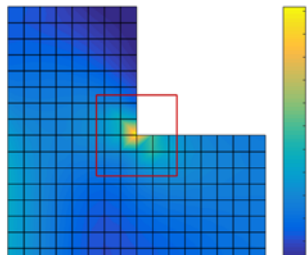
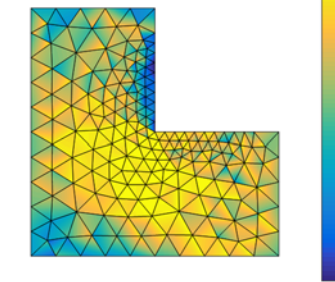
**Figure 9.21.** Considered global model

As seen in Figure 9.21 (b) the maximum von Mises stress is approximately 224 MPa.

In the investigation a square submodel is considered around the critical spot at the concave sharp edge. The global model is meshed with Q8 elements as seen in the above figure. The mesh for the upcoming submodels is more or less the same since the number of edge divisions is the same. The size of the square submodel varies in order to investigate whether a larger submodel leads to a higher load multiplier.

The study investigates submodels with lengths/widths from 10 to 35 mm.

**Table G.4.** Submodel size and optimized submodels.

Global model with submodel selection	Optimized Submodel Solution	Size of Submodel
	<p>von Mises Stresses [MPa] (<math>\alpha = 1.3524</math>)</p> 	<p>10 x 10 mm</p>
	<p>von Mises Stresses [MPa] (<math>\alpha = 1.528</math>)</p> 	<p>15 x 15 mm</p>
	<p>von Mises Stresses [MPa] (<math>\alpha = 1.8642</math>)</p> 	<p>20 x 20 mm</p>
	<p>von Mises Stresses [MPa] (<math>\alpha = 2.0502</math>)</p> 	<p>25 x 25 mm</p>

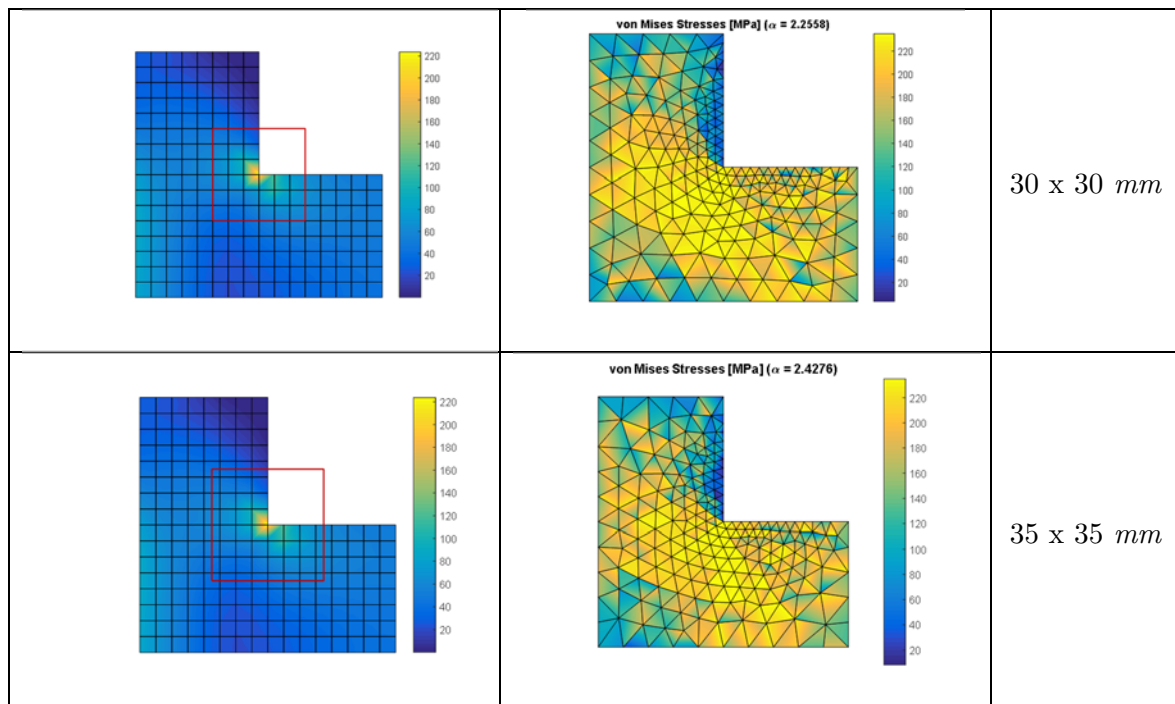


**Table G.5.** Load multipliers for different submodel sizes.

Length/Width [mm]	No of Elements	$\alpha$ MATLAB MOSEK
10	336	1.3524
15	362	1.5280
20	364	1.8642
25	316	2.0502
30	374	2.2558
35	360	2.4246

It is seen that the load multiplier  $\alpha$  increases as the submodel area increases. In order to understand the tendency, the normal stress in the  $x$ -direction on the cut boundary is plotted as illustrated in Figure 9.23. The stresses are exported by defining the same number of sample points for each submodel cut boundary and in this case 124 sample points are considered overall. The distance between two sample points for two different submodels isn't the same since the submodel size varies, but the distance between two sampling points in the same submodel is the same. Thereby, it is possible to compare stresses on the cut boundary between different submodels.

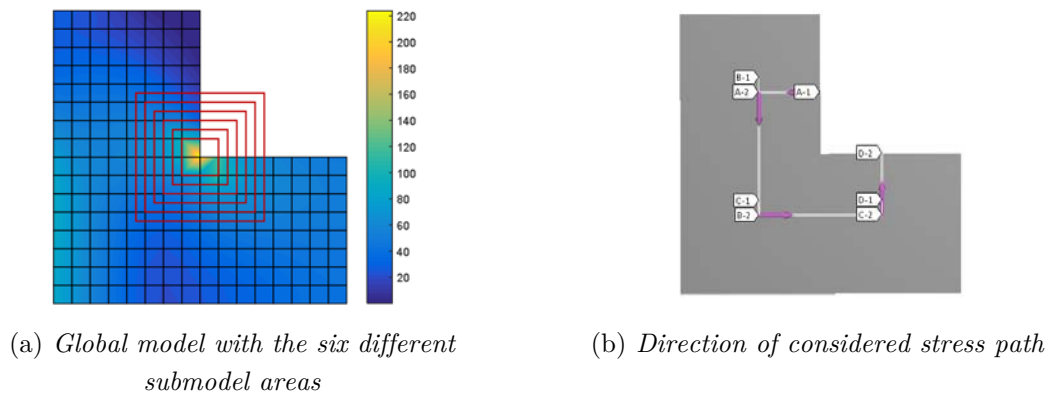


**Figure 9.22.** Submodel areas and stress path direction.

The boundary stresses for the six different models is illustrated in the figure below. It is seen that the cut boundary stresses increase as the submodel size decreases. The stress distribution also changes as the submodel boundary moves towards the singularity spot.

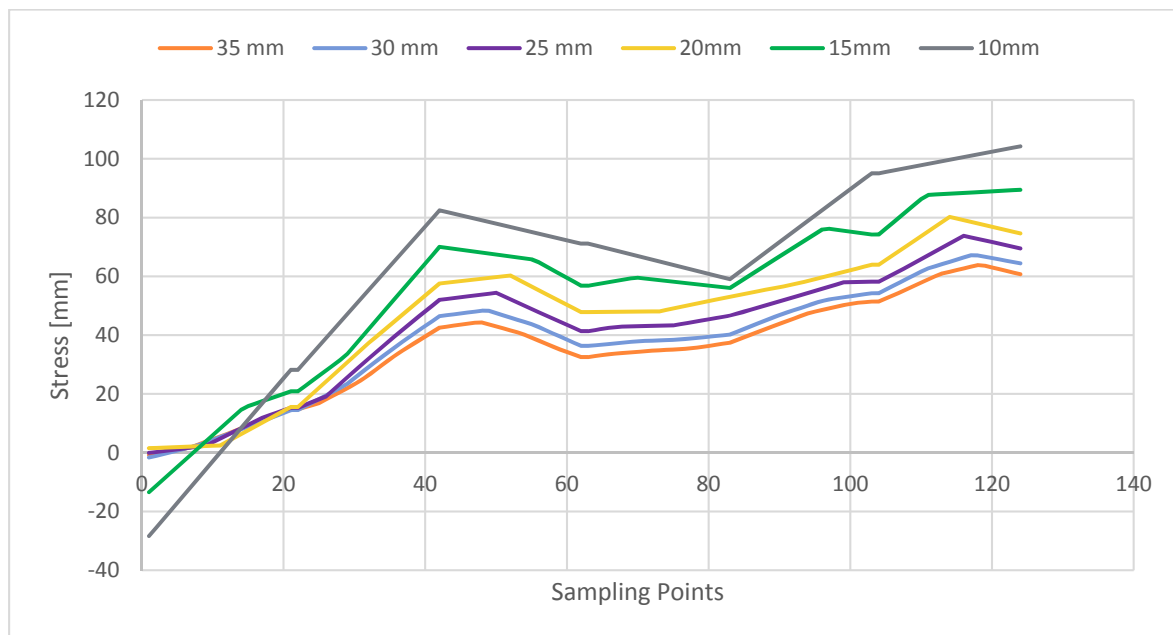


**Figure 9.23.** Normal stress distribution in the  $x$ -direction along the cut boundary.

An example of the normal stress distribution in the  $x$ -direction along the cut boundary for a submodel size of 10mm is shown in the figure below.

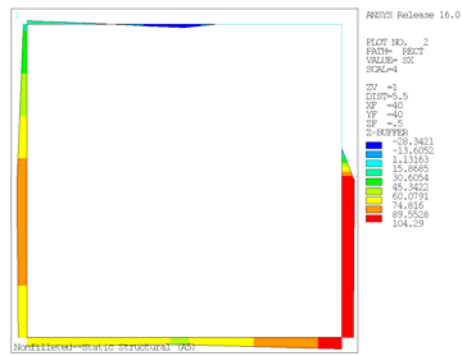


**Figure 9.24.** Normal Stress distribution in the  $x$ -direction along the cut boundary for the submodel of 10 mm.

From the study it can be concluded that a larger submodel area leads to a higher load multiplier  $\alpha$ . This is due to the fact that the boundary condition stresses changes as the submodel size increases or decreases.

## G.2 Study of Submodel Mesh Refinement

In the study, the influence of the submodel mesh on the load multiplier is investigated. The considered model is shown in Figure 9.25. The plate is subjected to a tensional pressure of 150 MPa at the right edge, whereas the left edge is constrained in both the horizontal and vertical direction. The plate has a thickness of 1 mm and is made of steel with a yield strength of 235 MPa.

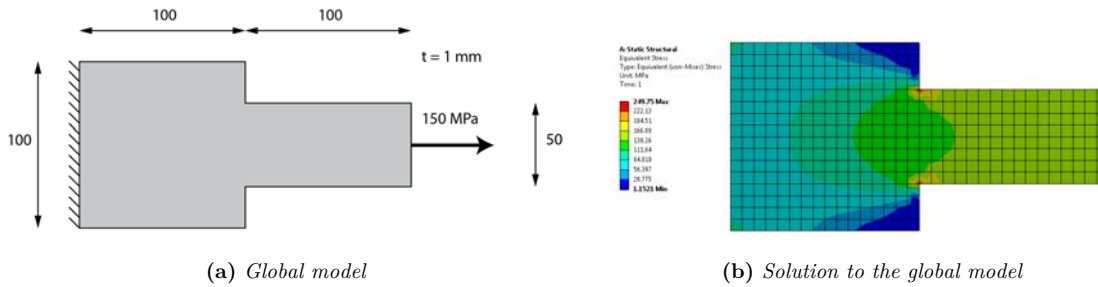


Figure 9.25. Considered global model

The global model is solved using Q8-elements and the maximum von Mises stress is approximately 250 MPa as seen in Figure 9.25 (b).

In the investigation a rectangular submodel is considered around the critical spot at the upper concave sharp edge. Different mesh refinements are investigated for the upcoming submodels. The size of the square submodel equals to 25x25 mm for all the submodels in order to investigate the mesh influence on the scalar load multiplier.

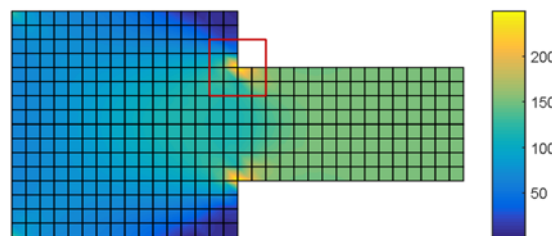
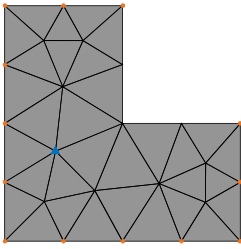
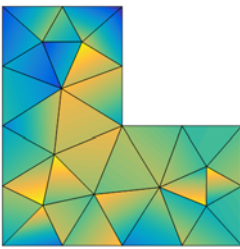
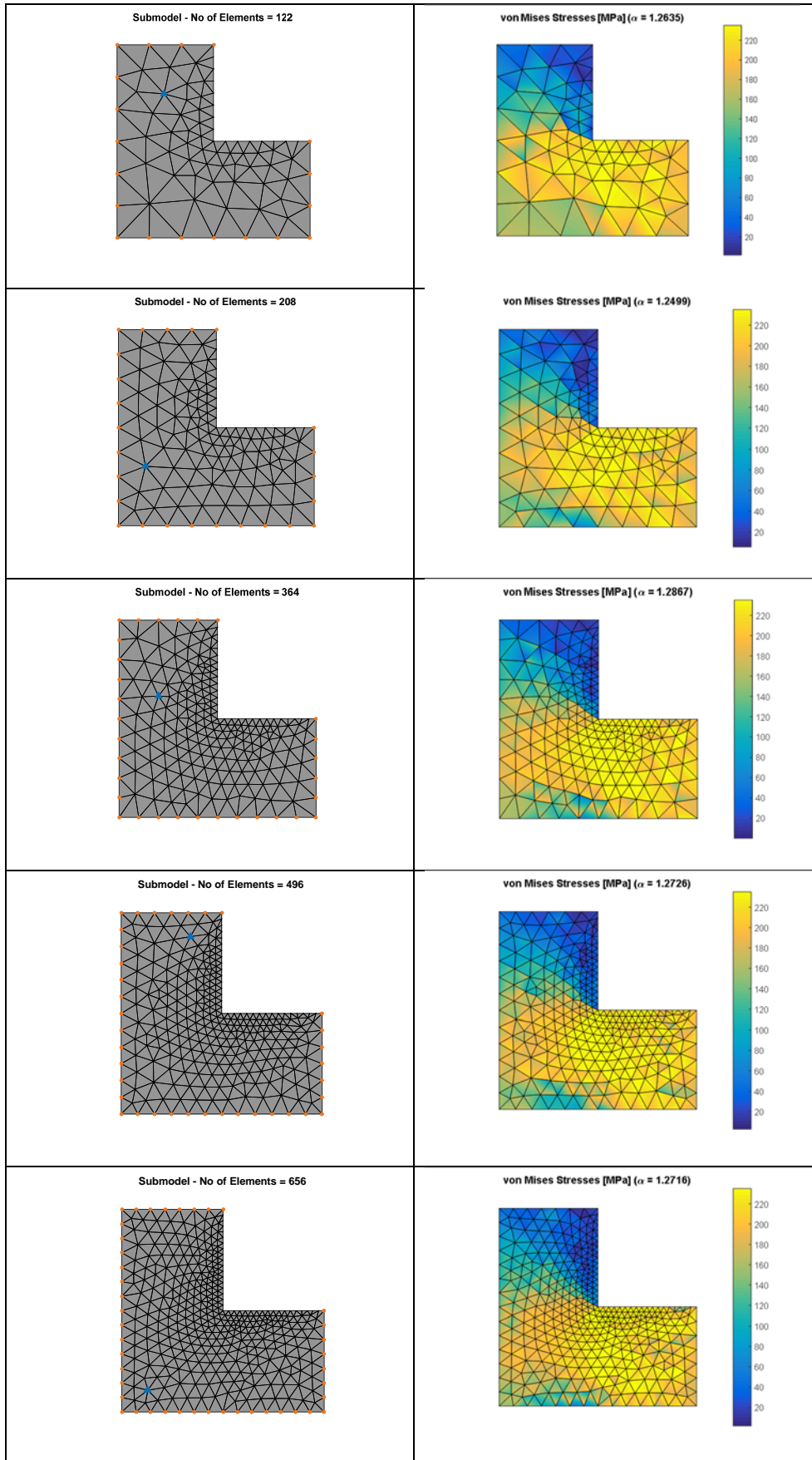
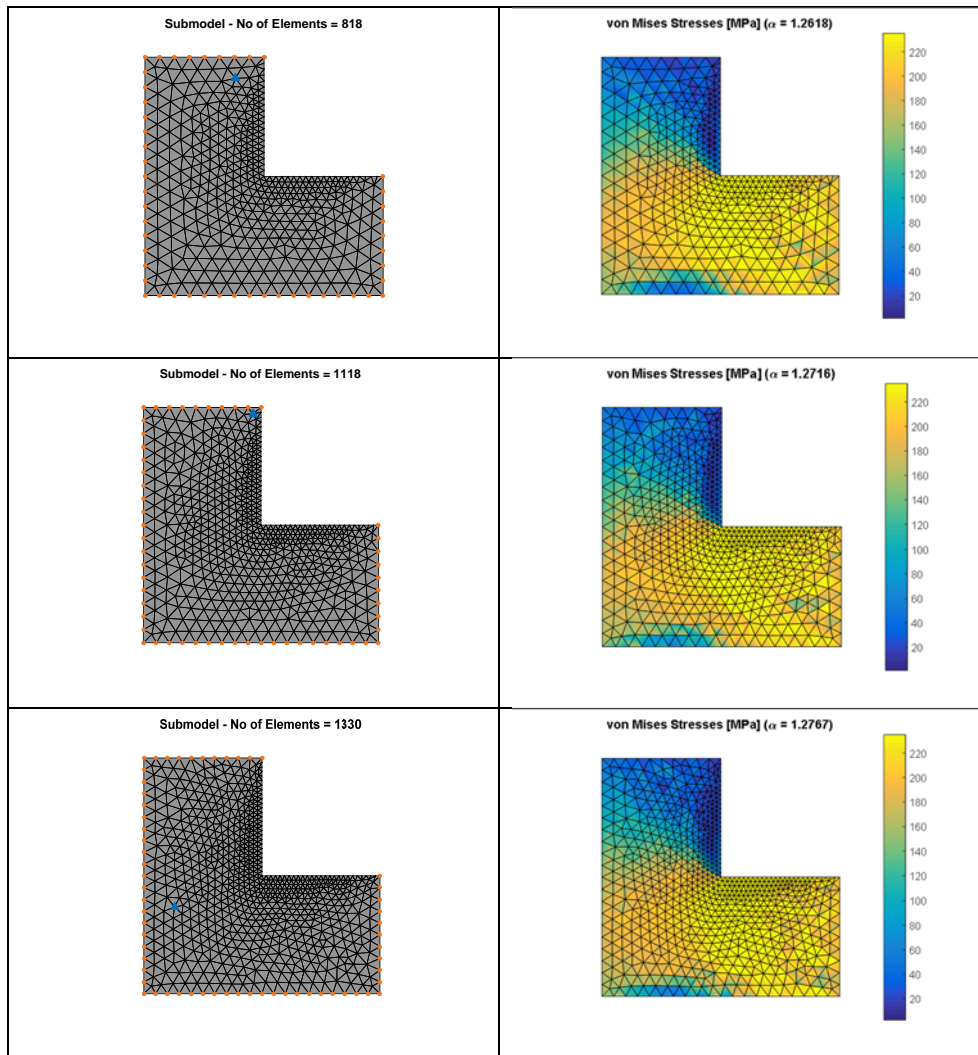


Figure 9.26. Global model with submodel selection.

The results from the different analyses are seen in the following table.

<i>Submodel Mesh</i>	<i>Optimized Submodel Solution</i>
<p data-bbox="347 1624 539 1646">Submodel - No of Elements = 32</p> 	<p data-bbox="786 1624 1026 1646">von Mises Stresses [MPa] (<math>\alpha = 0.84337</math>)</p> 





The results are scheduled in the following table

**Table G.6.** Load multipliers for different submodel mesh.

Number of Division	No of Elements	$\alpha$ MATLAB MOSEK
4	32	0.8434
6	122	1.2635
8	208	1.2499
10	364	1.2867
12	496	1.2726
14	656	1.2716
16	818	1.2618
18	1118	1.2716
20	1330	1.2767

The results from the above table is sketched in the following graph.

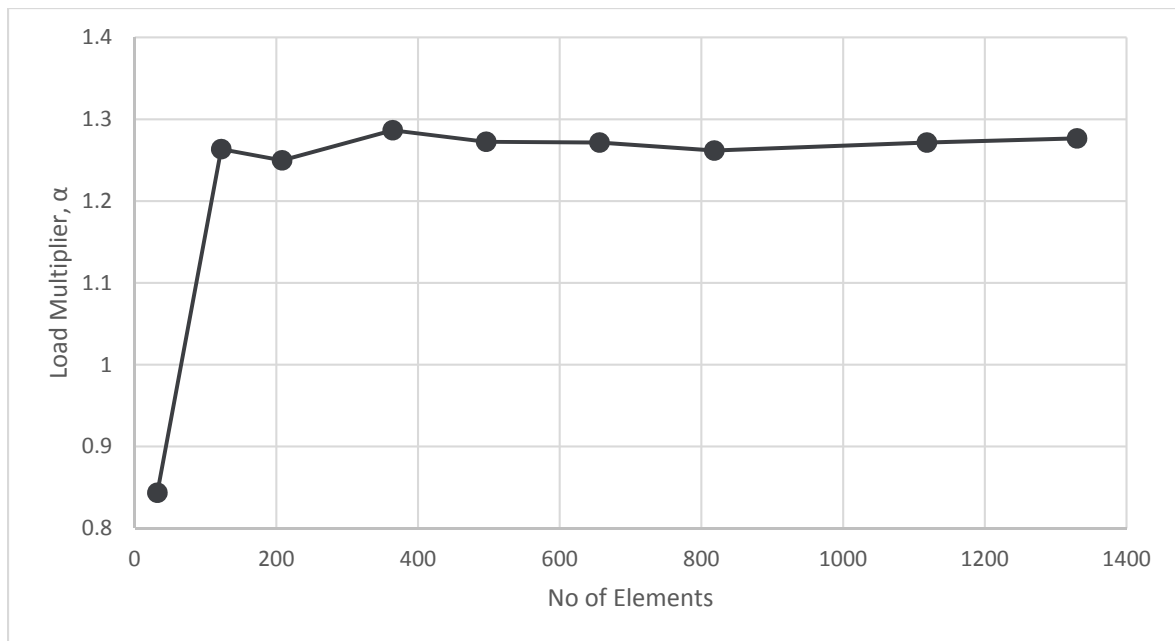


**Figure 9.27.** Load multiplier corresponding to varying number of elements of the submodel

The graph in Figure 9.27 shows that the load multiplier converges as a higher number of elements is assigned to the submodel. It should be mentioned that the analyses are associated with minimal uncertainties in the value for the load multiplier since the submodel is supported at different locations at each analysis. Another reason for the slightly variation is that the outer stresses are interpolated at different locations on the cut boundary which results in minimal deviations in the stress values and thereby the load multiplier.

From the study it can be concluded that a fine meshed submodel leads to the most accurate load multiplier, but the difference in multiplier between having a coarse submodel and fine submodel mesh isn't that significant.

### G.3 Study of Boundary Stresses in ANSYS

In the following ANSYS Workbench study, the boundary stresses are investigated when the mesh is refined. This is done in order to compare the deviation from the exact value, which in this case corresponds to the applied pressure. This study will therefore give a better understanding of the submodel cut boundary stresses.

The considered plate model is shown in Figure 9.28. The plate is subjected to a tensional pressure of 1 MPa at the left edge. The plate is constrained in the vertical direction at the bottom edge, whereas the right edge is constrained in the horizontal direction. The plate has a thickness of 1 mm and is made of steel with a yield strength of 235 MPa.

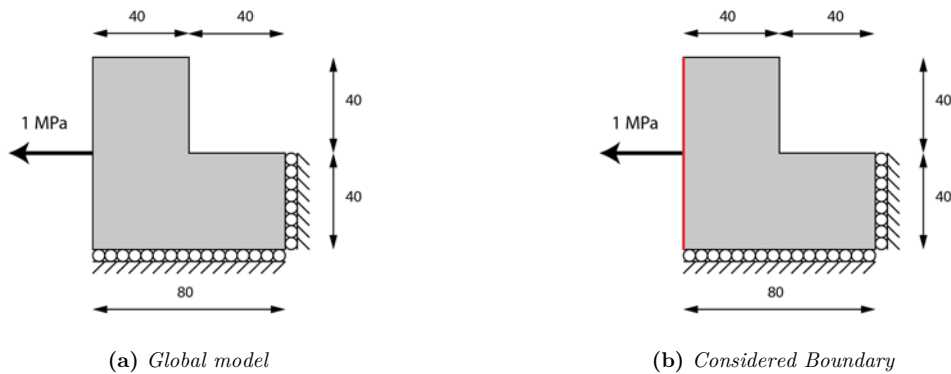


**Figure 9.28.** Free body diagram considered global model.

In the investigation, stresses at the considered boundary, illustrated in Figure 9.28 (b), are to be compared for six different Q8-based meshes. The square element size varies from 10 mm to 0.3125 mm, which corresponds to that the global model have meshes from 48 elements to 49152 elements as seen in Figure 9.29. This makes it possible to investigate the mesh importance with respect to the stresses.

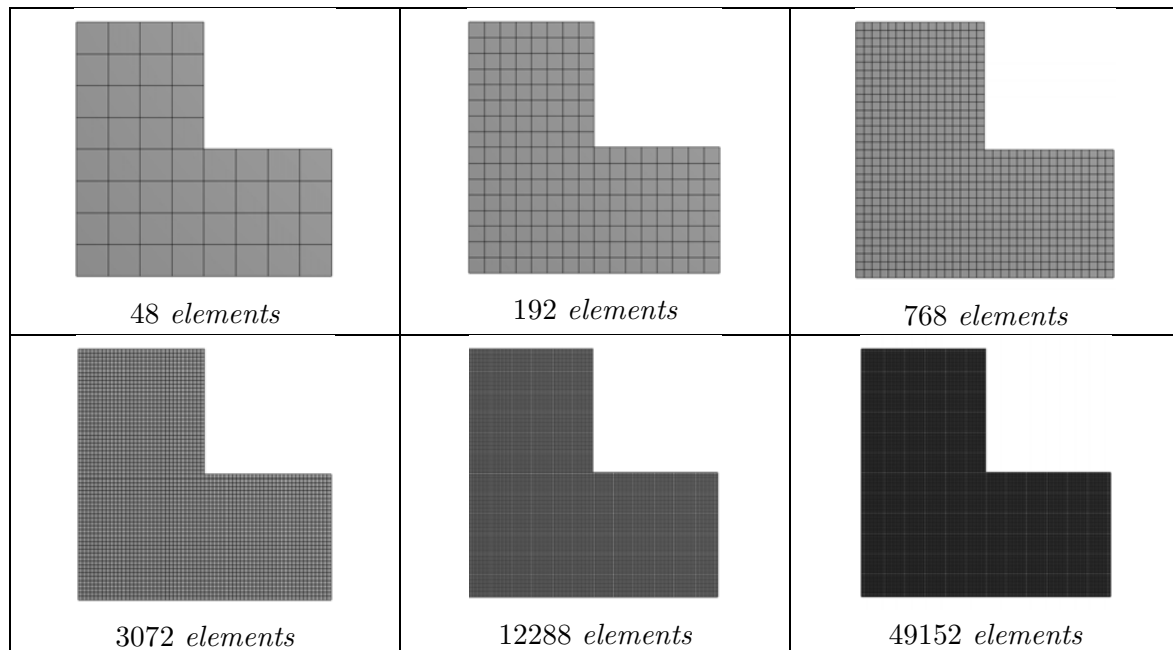


**Figure 9.29.** Six different meshes for the global model.

In the analysis, the left boundary edge is divided into 49 segments, which means that there are 50 sampling points. Both normal and shear stresses are compared. The normal stresses in the  $x$ -direction should be corresponding to the applied pressure on the considered edge. Any deviation from the applied pressure is considered as an uncertainty as a result of numerical errors.

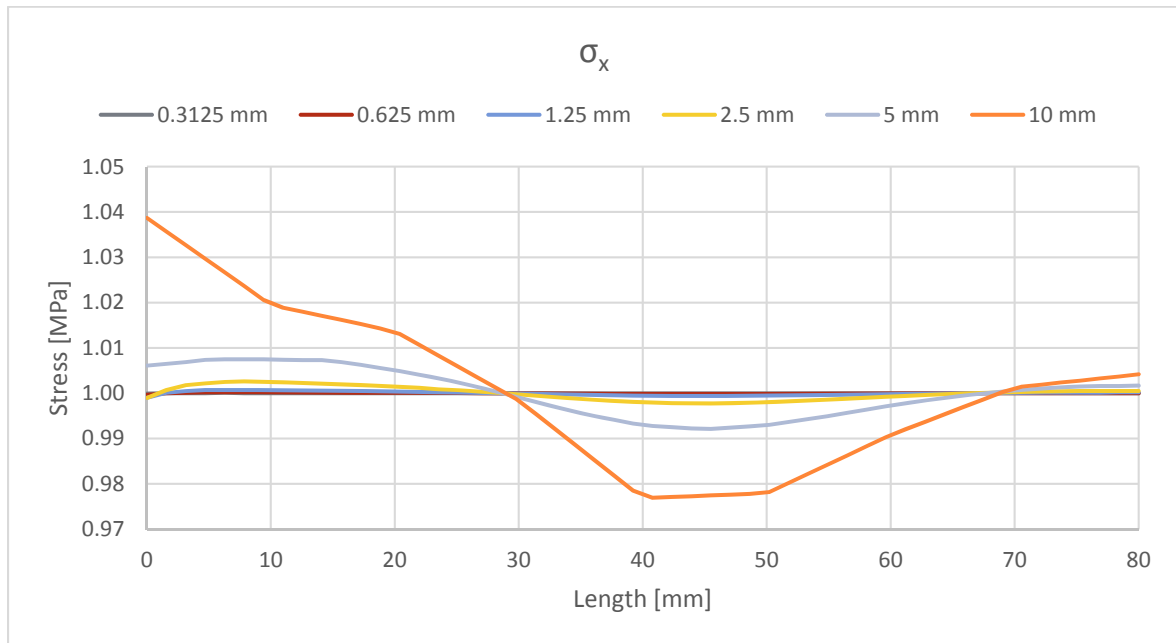


**Figure 9.30.** Normal stresses in the  $x$ -direction.

From the above graph it is seen that the results are more equally distributed towards the applied pressure of 1 MPa when the mesh becomes finer. For the global model with an element size of 10 mm, the deviation from the exact value goes up to almost 4 % at some points.

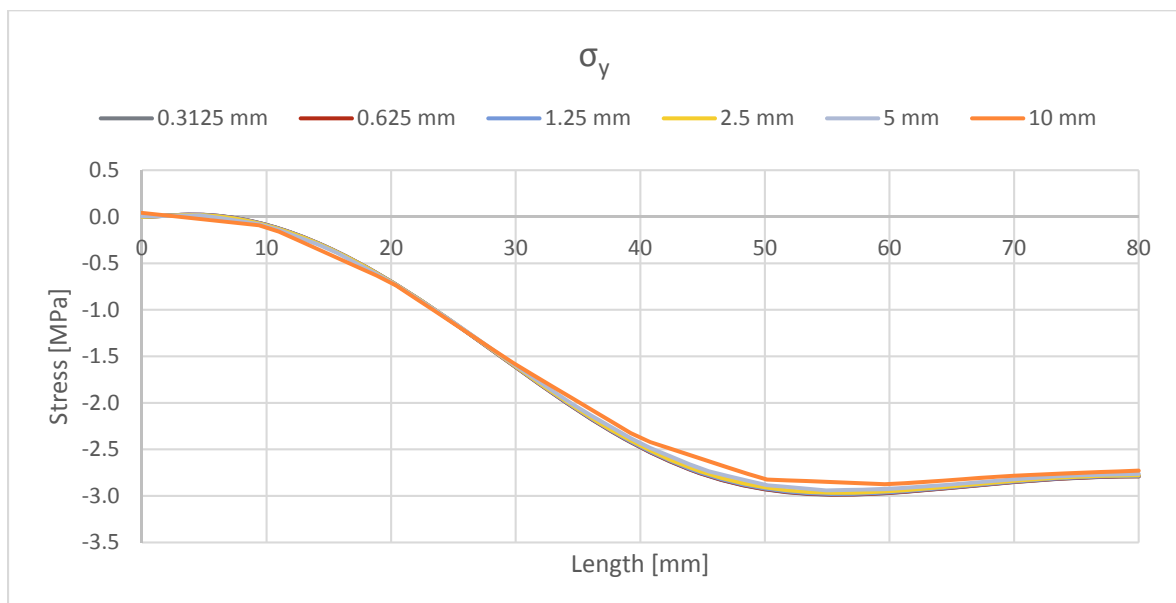


**Figure 9.31.** Normal stresses in the  $y$ -direction.

The normal stresses in the  $y$ -direction aren't deviating much when the mesh becomes finer.

The shear stress at the considered edge should be equal to zero and this is more or less the case when the mesh is really fine as illustrated in the figure below. For the mesh with an element size of 10 mm, the deviation from the exact value is more than 4 % at certain locations as seen in the graph below.

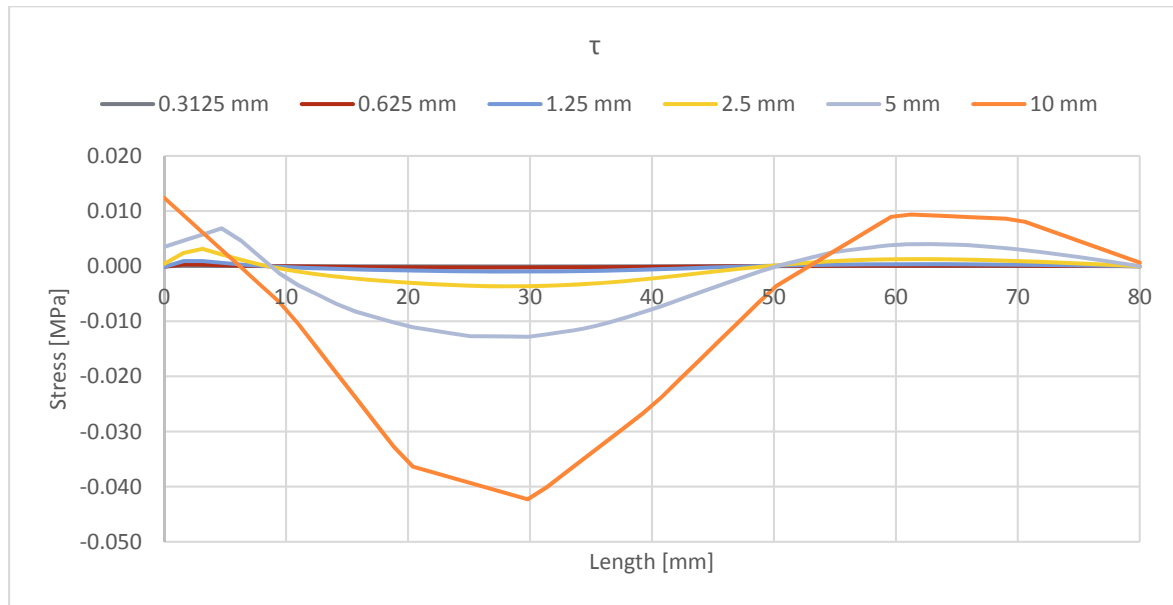


**Figure 9.32.** Shear stress distribution.

From the study it can be concluded that a finer mesh results in more accurate stress values, which can also be related to the submodeling approach in the MATLAB program. Therefore, the mesh of the global model has to be as fine as possible in the submodel approach.

## G.4 Study of Cut Boundary Stresses for different Global Meshes

In the study, the influence of the global model mesh on the submodel load multiplier  $\alpha$  is investigated. This is done by considering two different models. The first model is characterized by having a stress singularity spot, whereas the second model has a stress concentration spot.

### Non-filleted model (Stress Singularities)

The considered two-dimensional structure is shown in Figure 9.33. The plate is subjected to a tensional pressure of 25 MPa at the left edge, whereas the right edge is constrained in the horizontal direction and the bottom edge is constrained in the vertical direction. The plate has a thickness of 1 mm and is made of steel with a yield strength of 235 MPa.

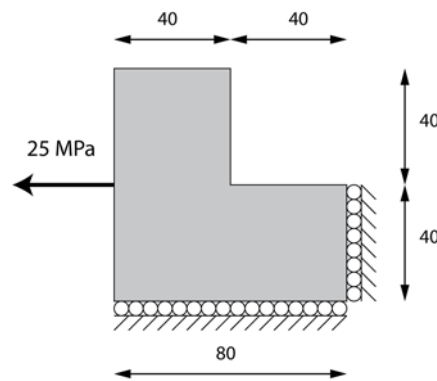
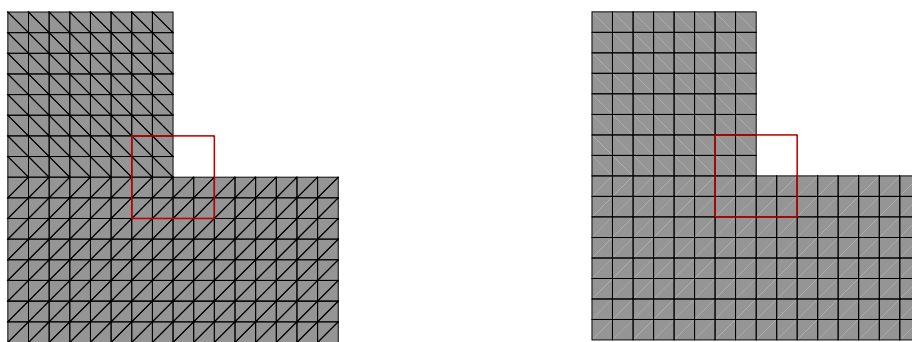


**Figure 9.33.** Free body diagram of global model.

In the investigation a rectangular submodel is considered around the critical spot at the concave corner as seen in Figure 9.34. The rectangular submodel measures 20x20mm.



(a) Global model with CST or LST elements      (b) Global model with Q4 or Q8 elements

**Figure 9.34.** Considered global model

Different element types are investigated when solving the global plate model. Q4, Q8, CST and LST elements are used respectively as indicated in Figure 9.34. This is done in order to illustrate the difference in the load multiplier when different global meshes are assigned.

The global model that is meshed with triangular elements in Figure 9.34 (a) has 384 elements, whereas the global model meshed with square elements in Figure 9.34 (b) has a total of 192 elements.

The mesh of the submodel for each analysis contains 818 triangular stress-based elements. By having the same submodel mesh a true comparison can be conducted.

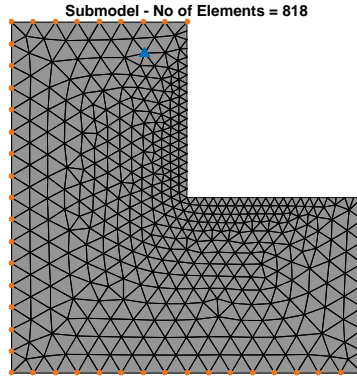
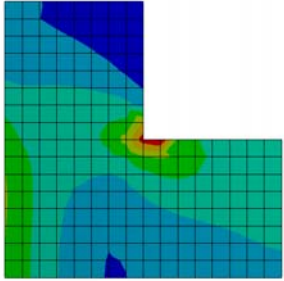
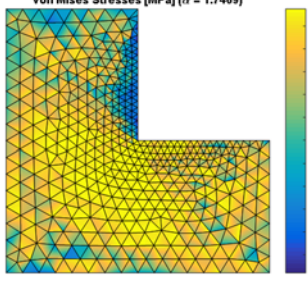
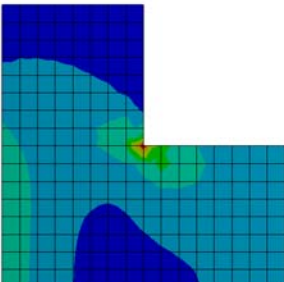
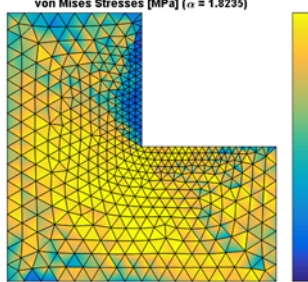
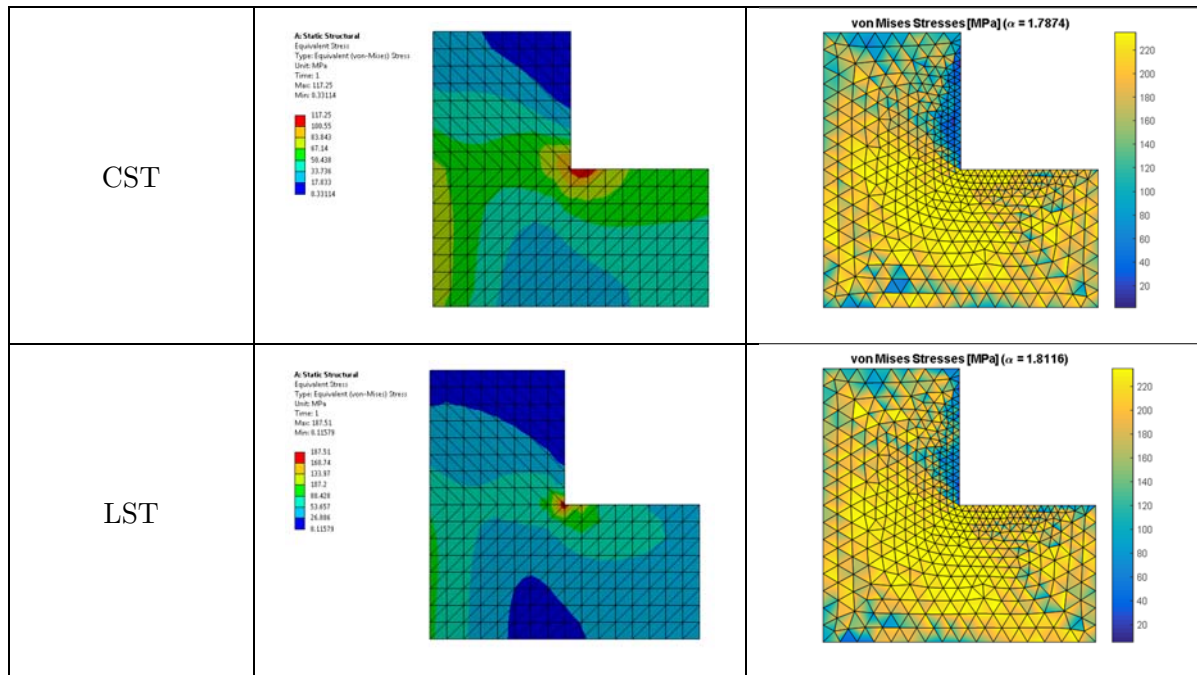


Figure 9.35. Submodel mesh

The results from the four analyses is seen in the table below.

Table G.7. Global model solutions and optimized submodel solutions for different element types.

Element Type of Global Model	Global Model Solution – von Mises Stress	Optimized Submodel Solution
Q4	<p>A: Static Structural Equivalent Stress Type: Equivalent (von-Mises) Stress Units: MPa Time: 1 Max: 148.82 Min: 8.38339</p> 	<p>von Mises Stresses [MPa] (<math>\alpha = 1.7469</math>)</p> 
Q8	<p>A: Static Structural Equivalent Stress Type: Equivalent (von-Mises) Stress Units: MPa Time: 1 Max: 223.67 Min: 8.889905</p> 	<p>von Mises Stresses [MPa] (<math>\alpha = 1.8235</math>)</p> 



The results from the analyses are listed in the table below.

**Table 9.8.** Maximum von Mises stress and load multiplier for the global model with different mesh elements

Element Type	Maximum von Mises [MPa]	$\alpha$ MATLAB MOSEK
Q4	148.82	1.7469
Q8	223.67	1.8235
CST	117.25	1.7874
LST	187.51	1.8116

The results are also illustrated in the following two graphs.

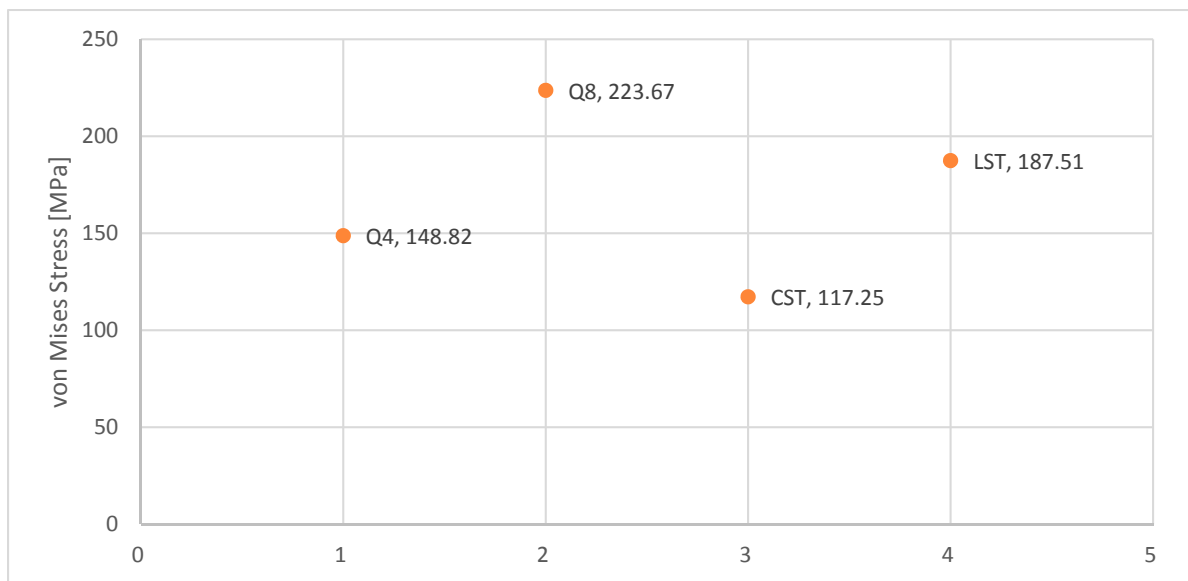


**Figure 9.36.** Maximum von Mises Stress for the global model with different mesh

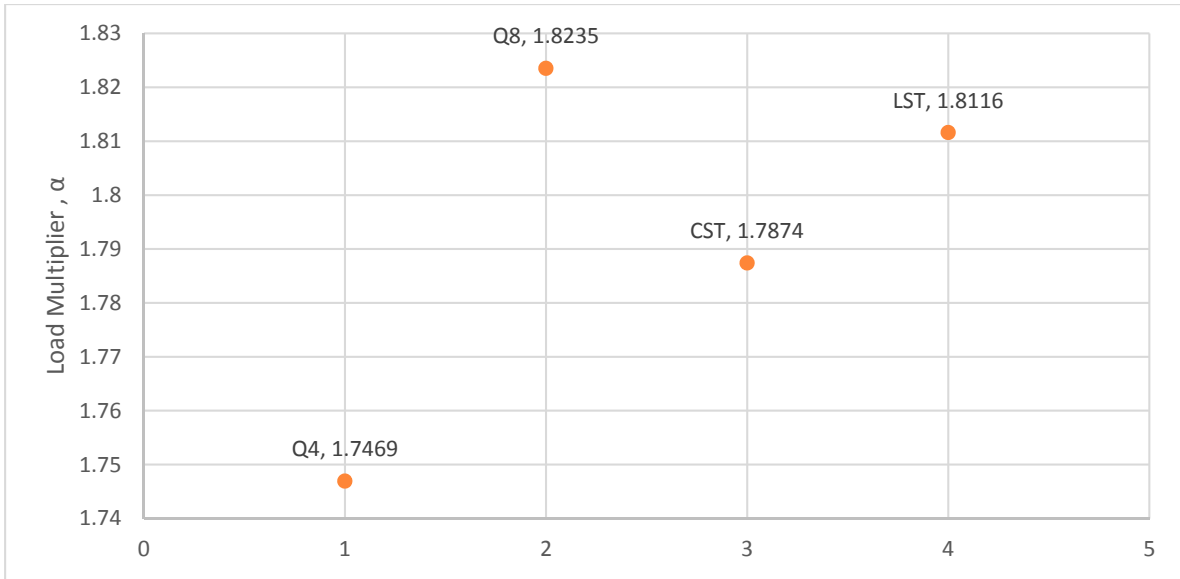


Figure 9.37. Load multiplier for global model with different mesh

From the above graphs it can be seen that the global model that is meshed with Q8 elements results in the highest load multiplier in the load optimization. When considering the maximum von Mises stress it is seen that the Q8 elements results in the highest value followed by LST, Q4 and CST elements.

In order to understand why the results are as they are, the three stress component at the cut boundary has to be evaluated. In the following figures a comparison of the two normal stresses and the shear stress has been investigated.

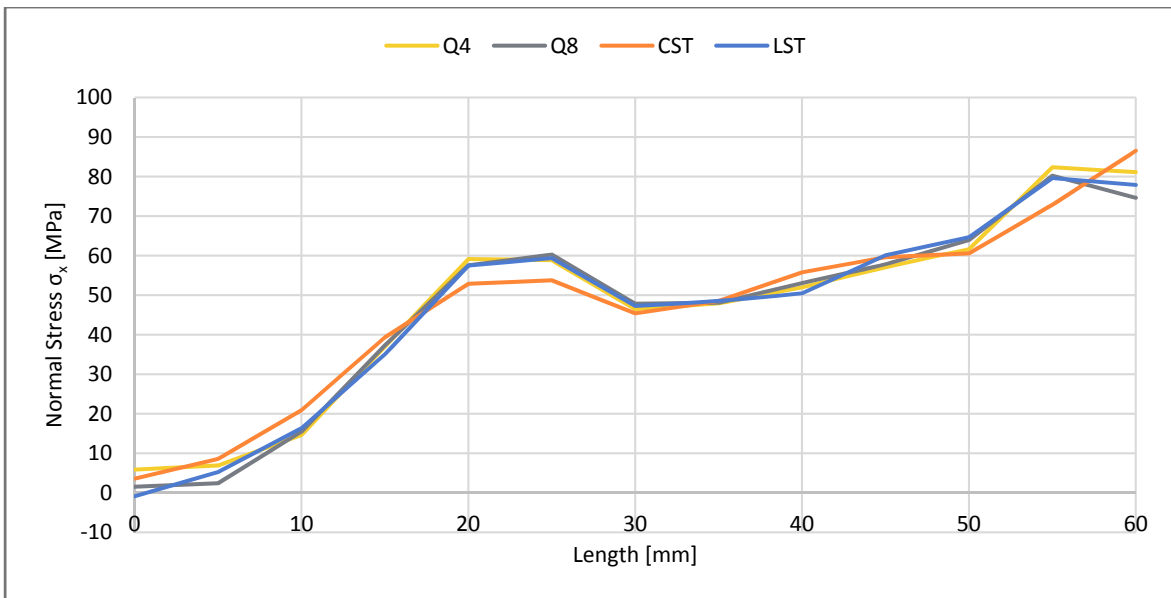
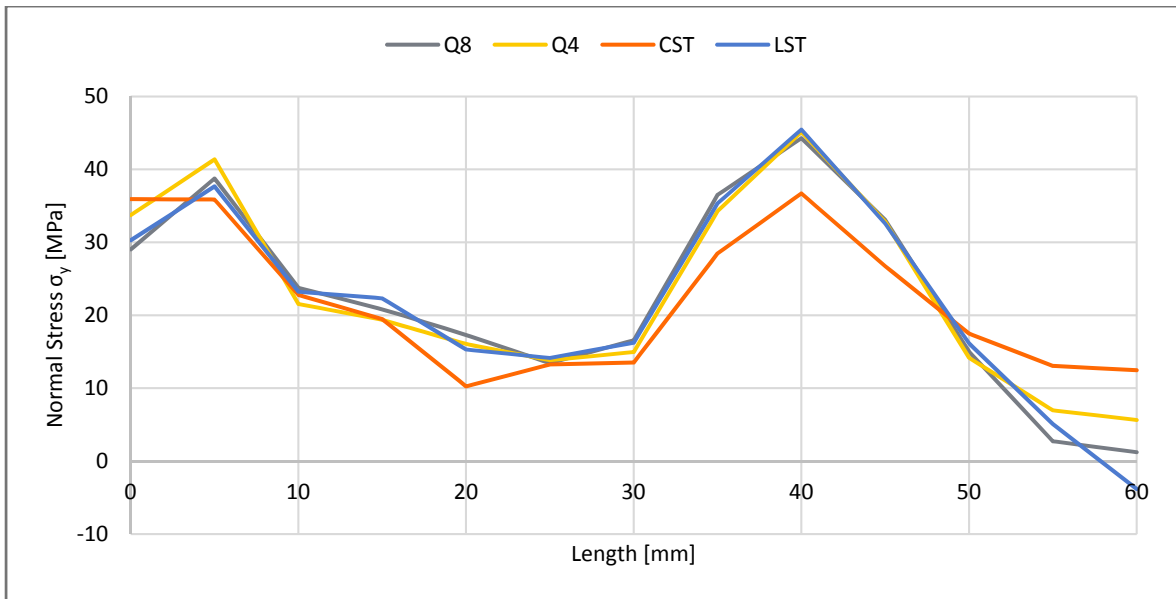
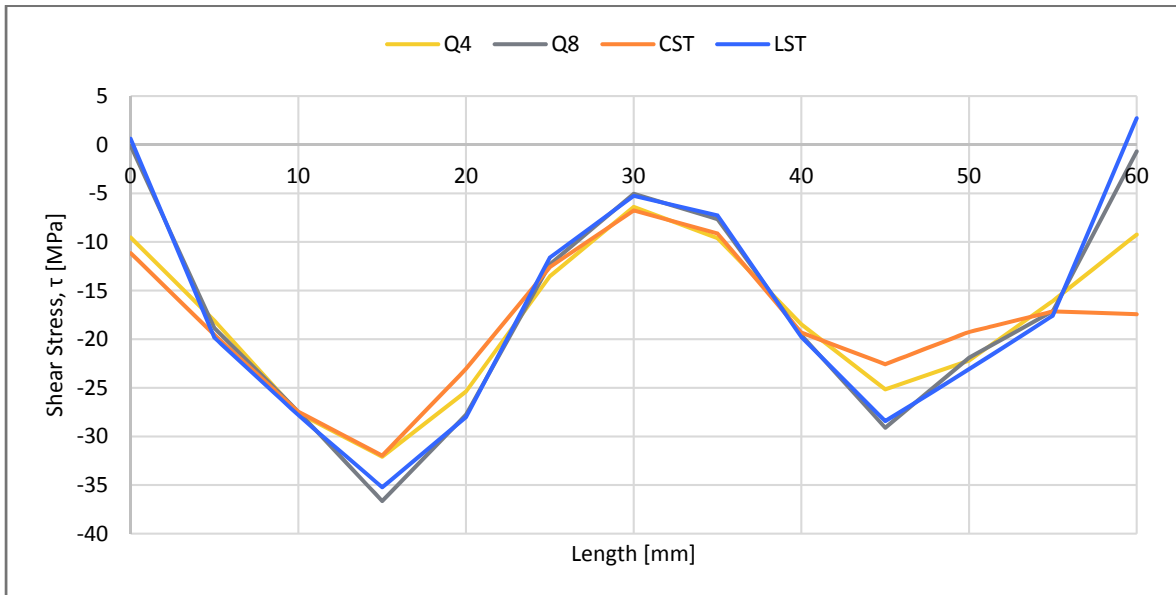


Figure 9.38. Normal stress distribution in the x-direction at the cut boundary



**Figure 9.39.** Normal stress distribution in the y-direction at the cut boundary



**Figure 9.40.** Shear stress distribution at the cut boundary

In the comparison it is seen that the cut boundary stresses don't have the same value. Especially CST elements have a large deviation compared to the other elements. The higher order elements produce the most similar stress components.

From the analysis of the model with stress singularity spot it can be concluded that the difference in the stress distribution is leading to the difference in the load multiplier. It is recommended to use Q8 or LST elements in the global mesh since they produce the most accurate stress values.

### Filletted Model (Stress Concentrations)

The considered model is shown in Figure 9.41. The only difference is the filleted edge. The plate is subjected to a tensional pressure of 25 MPa at the right edge, whereas the left edge is constrained in both the horizontal and vertical direction. The plate has a thickness of 1 mm and is made of steel with a yield strength of 235 MPa.

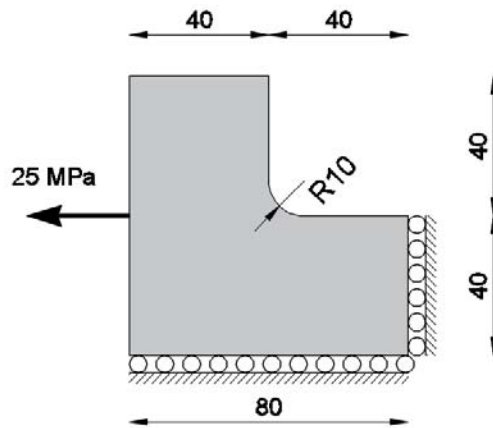
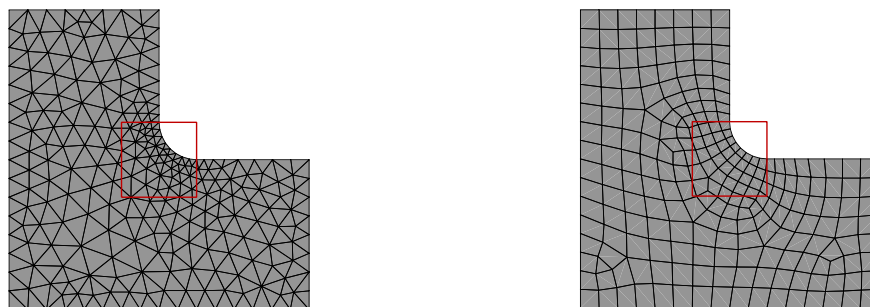


**Figure 9.41.** Free body diagram of global model

In the investigation a rectangular submodel is considered around the critical spot at the concave corner as seen in Figure 9.42. The rectangular submodel measures 20x20mm.



(a) Global model with CST or LST elements

(b) Global model with Q4 or Q8 elements

**Figure 9.42** Considered global model

Different element types are investigated when solving the global plate model. Q4, Q8, CST and LST elements are used, respectively, as indicated in Figure 9.42. It is not possible to assign two similar meshes when using square and triangle elements, respectively. The two different global meshes are shown in Figure 9.42. The triangular (CST and LST) mesh model contains 440 elements, whereas the square mesh (Q4 and Q8) model contains 233 elements.

The mesh of the submodel for each analysis contains 494 triangular stress-based elements. By having the same submodel mesh a true comparison can be conducted.

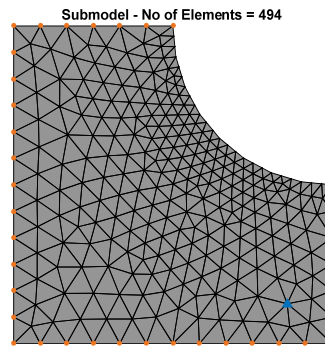
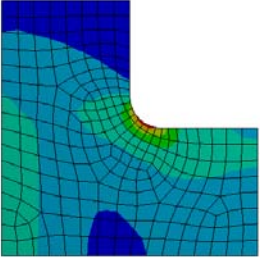
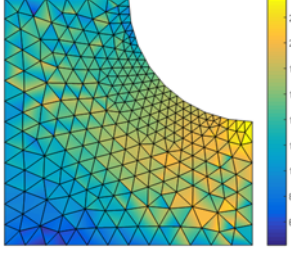
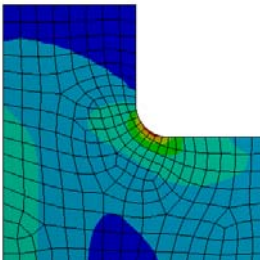
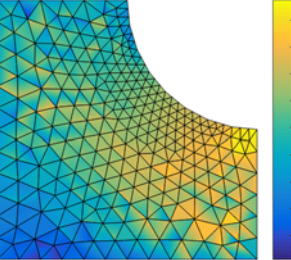
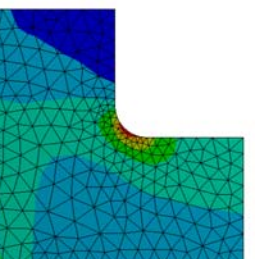
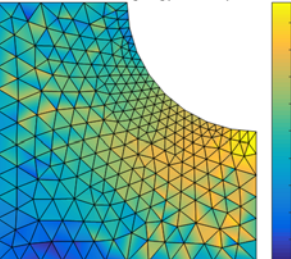
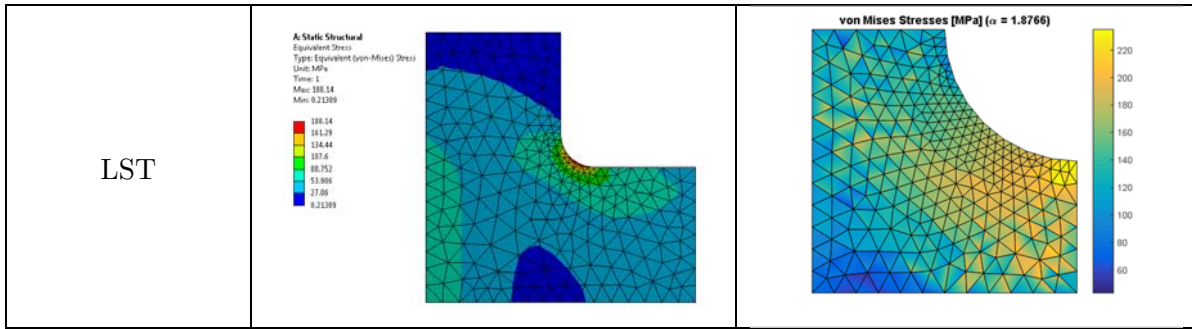


Figure 9.43. Submodel mesh

The conducted analyses for the four elements is shown in the table below.

<i>Element Type for Global Model</i>	<i>Global Model Solution – von Mises Stress</i>	<i>Optimized Submodel Solution</i>
Q4	<p><b>A: Static Structural</b>                      Equivalent Stress                      Type: Equivalent (von-Mises) Stress                      Unit: MPa                      Time: 1                      Max: 181.95                      Min: 0.49852</p> 	<p><b>von Mises Stresses [MPa] (<math>\alpha = 1.8902</math>)</b></p> 
Q8	<p><b>A: Static Structural</b>                      Equivalent Stress                      Type: Equivalent (von-Mises) Stress                      Unit: MPa                      Time: 1                      Max: 188.6                      Min: 0.097016</p> 	<p><b>von Mises Stresses [MPa] (<math>\alpha = 1.8922</math>)</b></p> 
CST	<p><b>A: Static Structural</b>                      Equivalent Stress                      Type: Equivalent (von-Mises) Stress                      Unit: MPa                      Time: 1                      Max: 157.71                      Min: 0.36833</p> 	<p><b>von Mises Stresses [MPa] (<math>\alpha = 1.9437</math>)</b></p> 



The results are listed in the table below.

**Table 9.9.** Maximum von Mises stress and load multiplier for a global model with different mesh elements

Element Type	Maximum von Mises [MPa]	$\alpha$ MATLAB MOSEK
Q4	181.05	1.8902
Q8	188.60	1.8922
CST	157.71	1.9437
LST	188.14	1.8766

The results are also illustrated in the following two graphs.

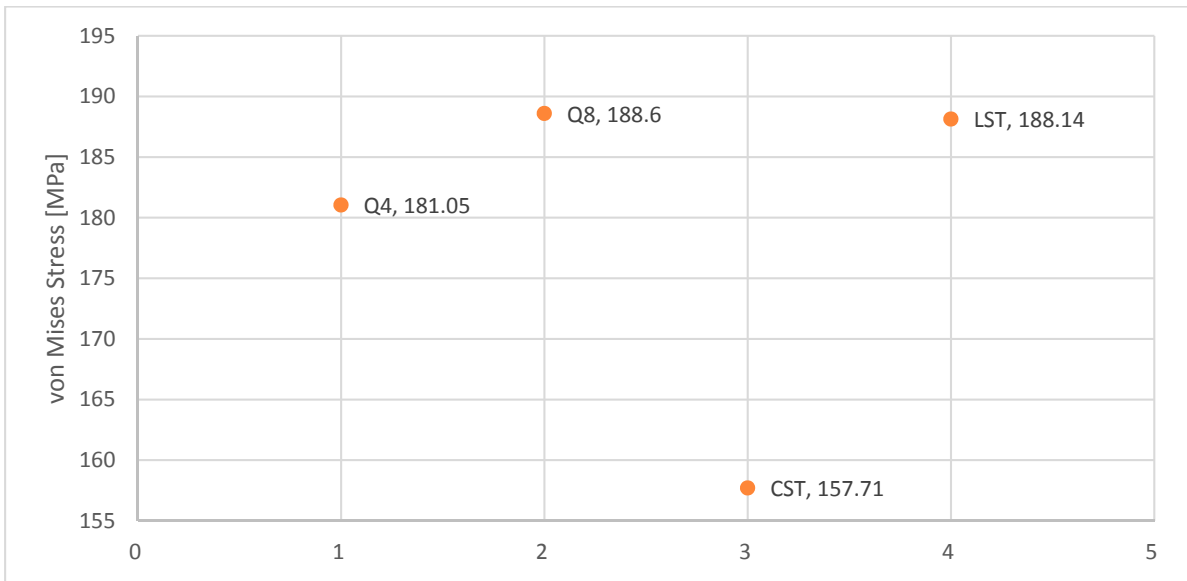


**Figure 9.44.** Maximum von Mises Stress for the global model with different mesh.

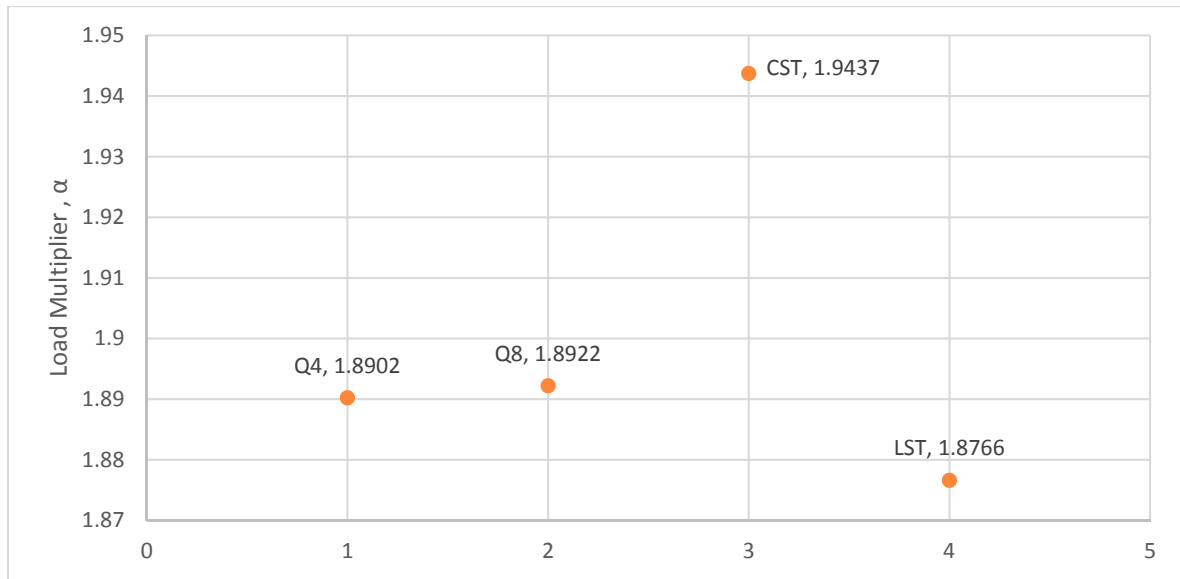


**Figure 9.45.** Load multiplier for the global model with different mesh.

It can be seen that the order of highest von Mises stresses is the same as in the example with the nonfilleted plate. The order of the load multiplier is in return completely different. A global model with CST elements gives by far the highest load multiplier.

In order to understand why the results are as they are, the three stress component at the cut boundary has to be evaluated. In the following figures a comparison of the two normal stresses and the shear stress has been investigated.

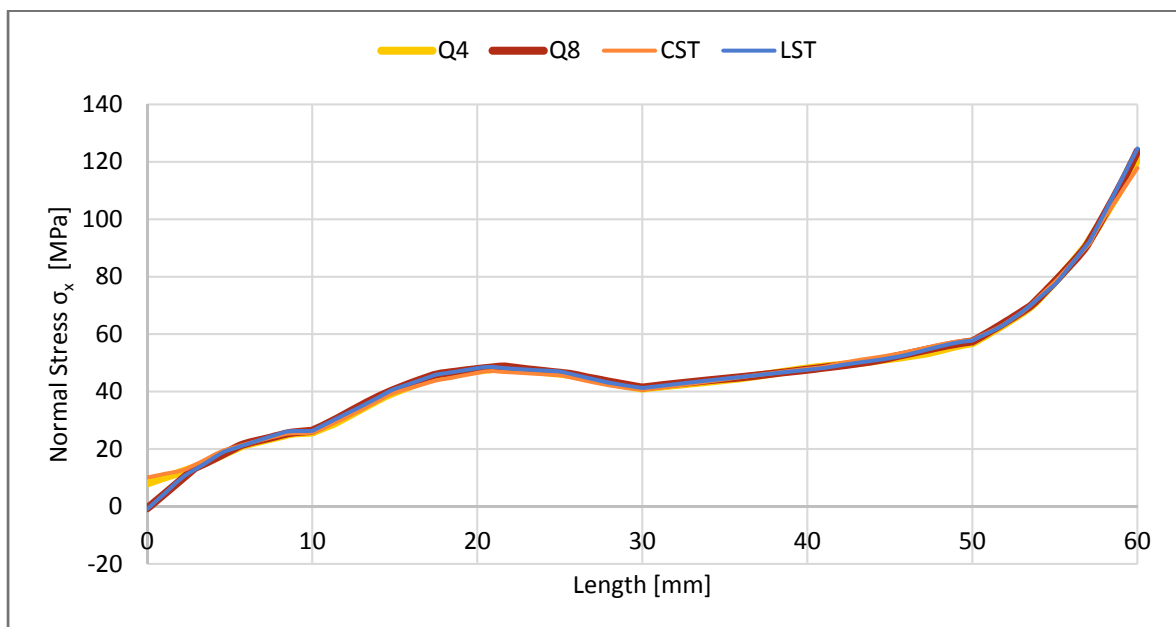


**Figure 9.46.** Normal stress distribution in the x-direction at the cut boundary.

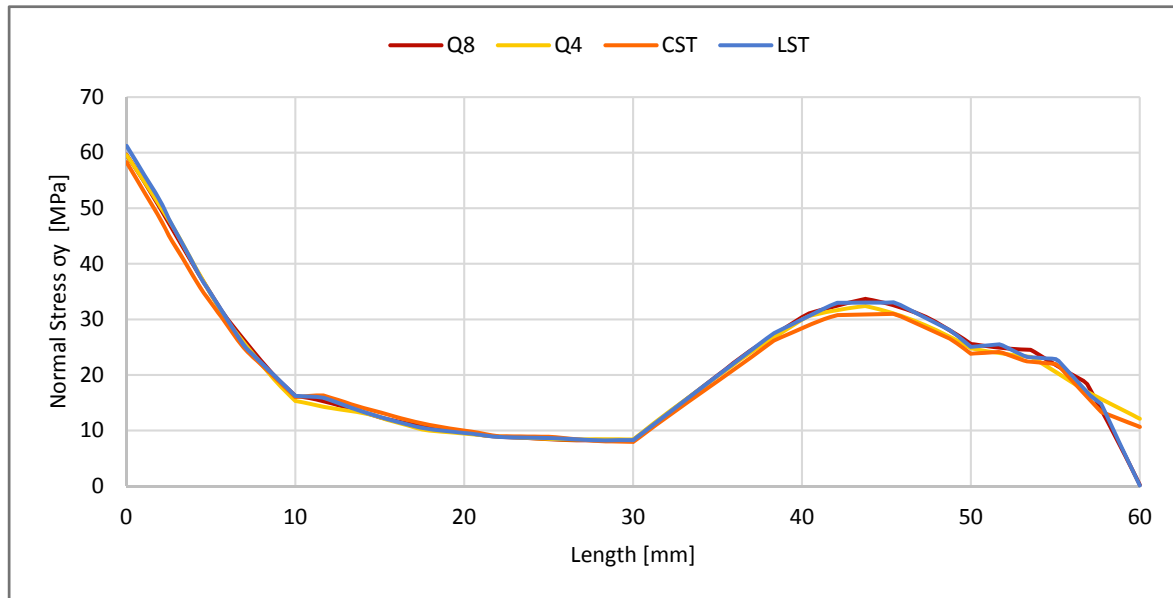


**Figure 9.47.** Normal stress distribution in the  $y$ -direction at the cut boundary.

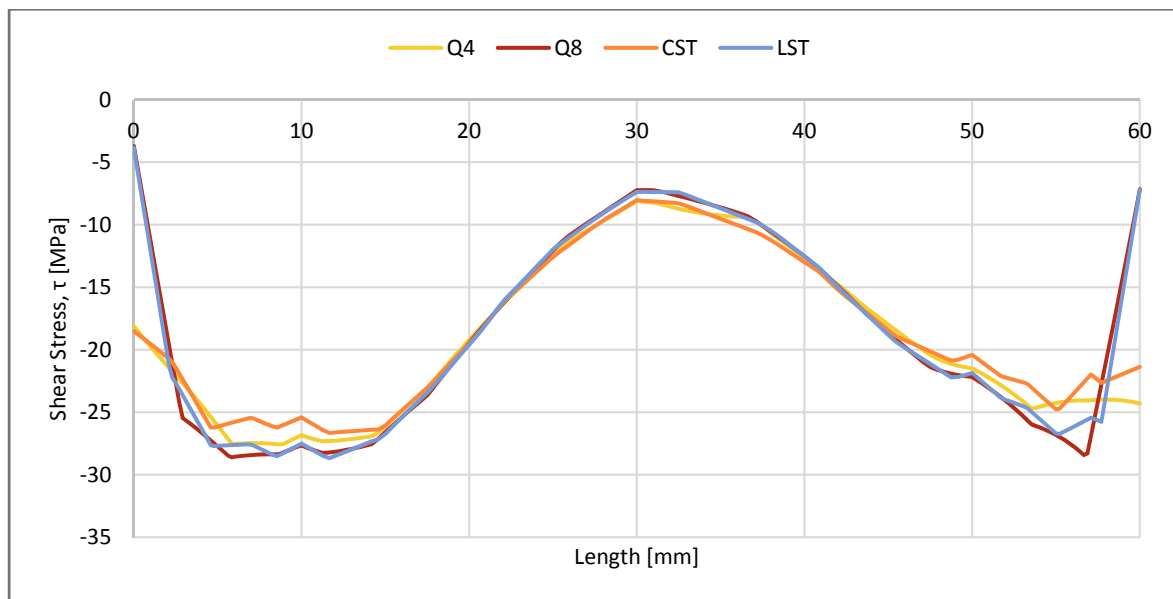


**Figure 9.48.** Shear stress distribution at the cut boundary.

When comparing the three stress components for the different meshes it can be seen that the stress distribution is very similar for the two normal stresses whereas the shear stress deviates much more. The higher order elements have very similar distribution in all three cases and that is why the load multiplier is almost identical. Once again it is not recommended to use CST elements in the analysis since it gives a poor stress distribution and can lead to that the load multiplier is higher than it really is even though it is a lower bound analysis. Therefore, higher order elements are recommended to obtain an accurate solution, and especially Q8 elements.

## Appendix H: Interaction of Elements

The upcoming appendix is used to demonstrate a correct interaction between the elements used for the optimization of reinforced concrete plates. The elements are recalled as a stress-based triangular element describing the behaviour of concrete, and a rebar element describing the concentrated reinforcement. Fundamental load cases are considered in order to demonstrate the interaction, which implies a load case resulting in pure shear stress states, and an example with compression. The material properties do not reflect realistic plate systems as the purpose is to solely validate a proper interaction.

### H.1 Example with Pure Shear Stress States

The example investigates a reinforced concrete plate with concentrated reinforcement along all edges as illustrated in the figure below. The idea is to load a rebar element such that a state of pure shear is obtained when assigning equal compressive and tensile strengths. The reinforcement properties are assigned such that collapse is not caused by failure in the rebar elements firstly, and thus collapse must occur in the concrete by a state of pure shear if the interaction between the elements are defined properly. The geometry, material properties, and boundary conditions can be seen in the figure below.

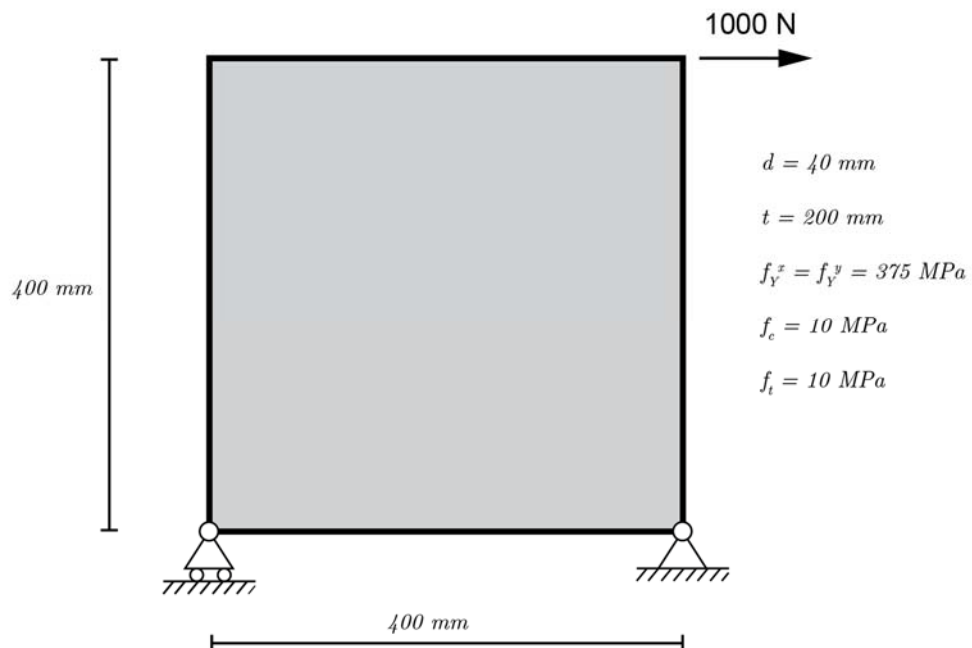


**Figure 9.49.** *Illustration of plate model.*

The model is implemented in MATLAB by discretizing the model as seen in the figure below.

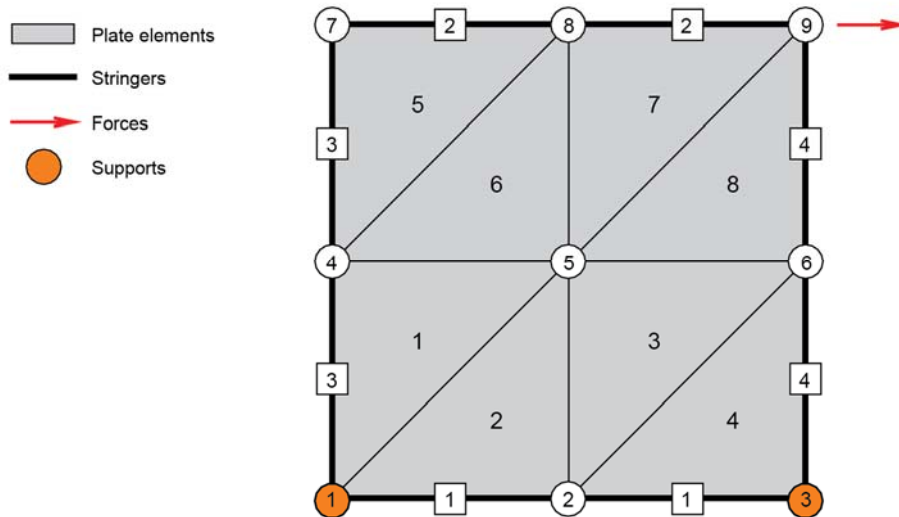


**Figure 9.50.** *Finite element discretization of plate model in MATLAB.*

When optimizing the structure, the load multiplier  $\alpha$  is found to 400, and the concrete is thereby exposed to a state of pure shear as illustrated below.

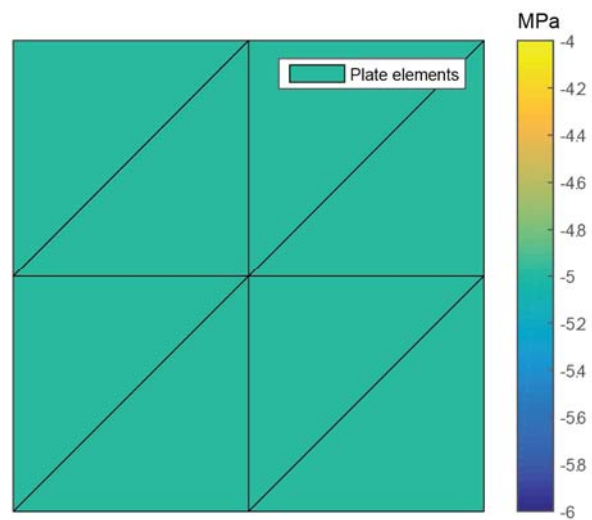


**Figure 9.51.** *Shear plot from MATLAB*

The normal force distribution is as seen in the figure below.

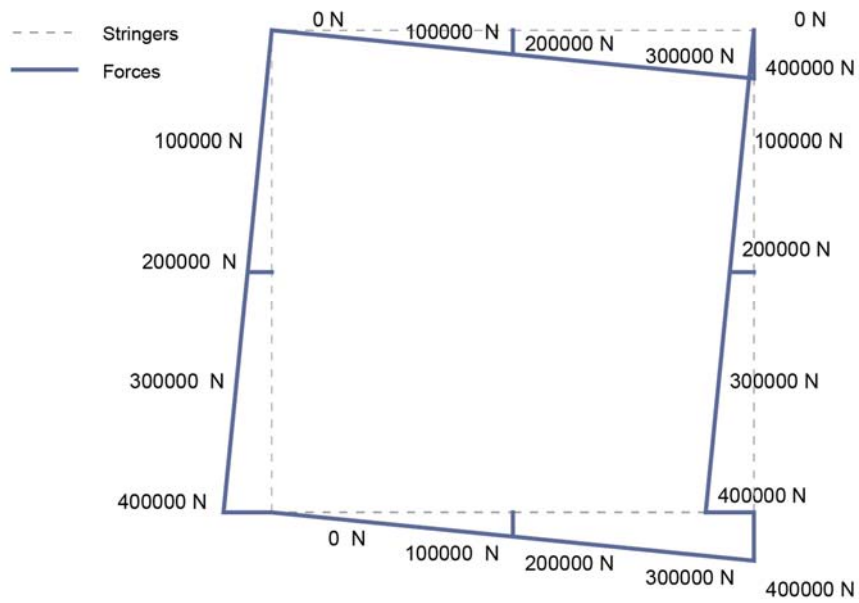
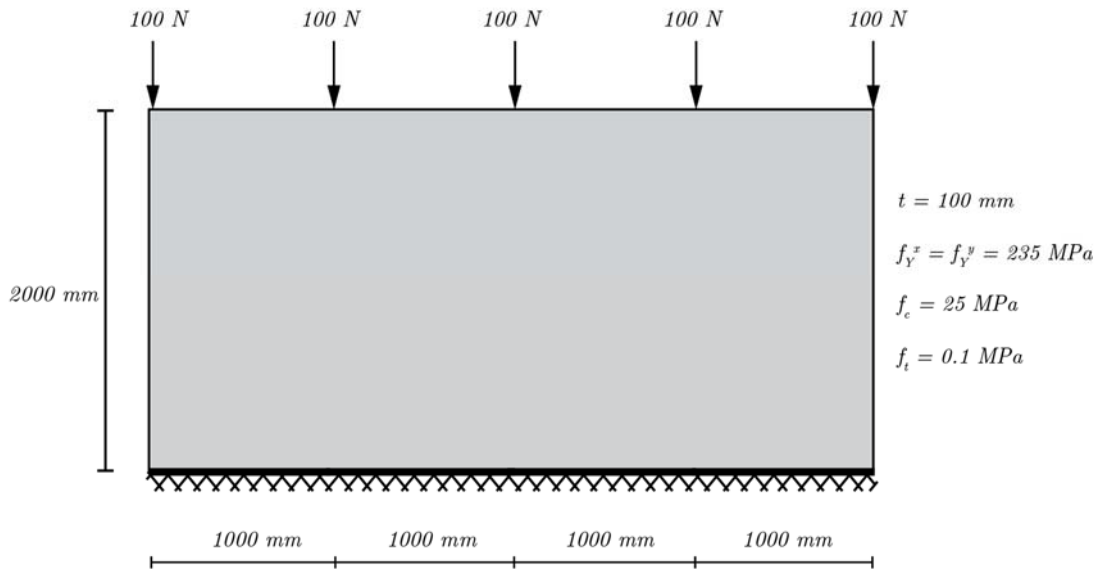


**Figure 9.52.** Normal forces in MATLAB

If integrating above the normal forces a shear stress corresponding to 5 MPa is likewise obtained.

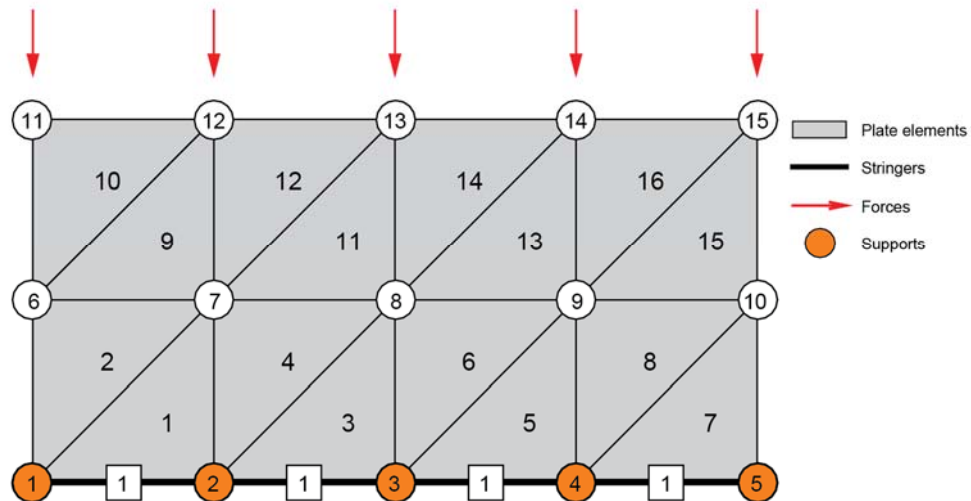
## H.2 Compressive Stress State

The second example examines a reinforced concrete plate with concentrated reinforcement located at the lower boundary of the plate. The plate is fixed at the bottom edge in the concrete, and forces are applied at the top of the structure as seen in the figure below.



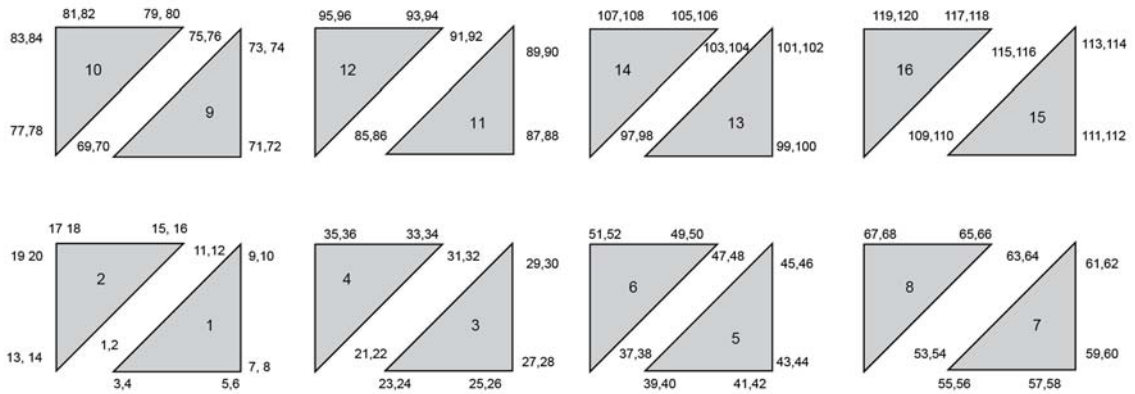
**Figure 9.53.** Free body diagram of the considered

The model is discretised in MATLAB by assigning 16 elements with the topology as seen in the figure below.



**Figure 9.54.** Discretization of the reinforced concrete model.

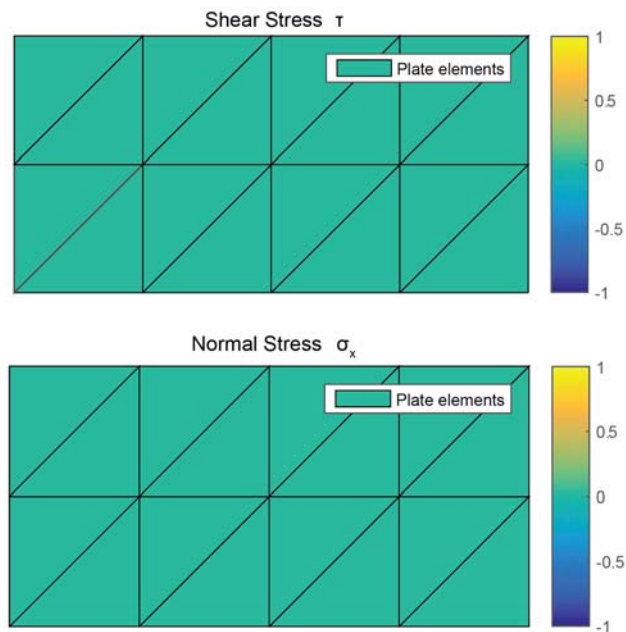
The forces and supports have to be assigned corresponding to the exact generalized forces. The numbering of the respective generalized forces for the plate elements is as seen in the figure below.



**Figure 9.55.** Equation numbers of the generalized forces for the triangular plate elements.

The forces are applied at equations: 79, 81, 93, 95, 105, 107, 117, 119, as seen in the figure above. The structure is supported by removing the following equilibrium equation: 3, 4, 5, 6, 23, 24, 25, 26, 39, 40, 41, 42, 55, 56, 57, 58.

By optimizing the structure in terms of second order cones in Mosek or by the nonlinear interior point optimizer in fmincon, a stress distributions field is obtained as seen in the figures below.



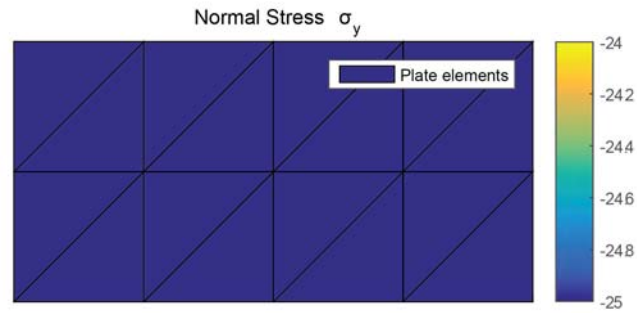


**Figure 9.56.** Stress distributions in the reinforced concrete plate.

From the stress plots it can be seen that only normal stresses in the y-direction appears as expected. The stress value for the normal stress is furthermore equal to 25 MPa, which is also defined as the compressive strength of the structures. This can also be seen in the figure below.

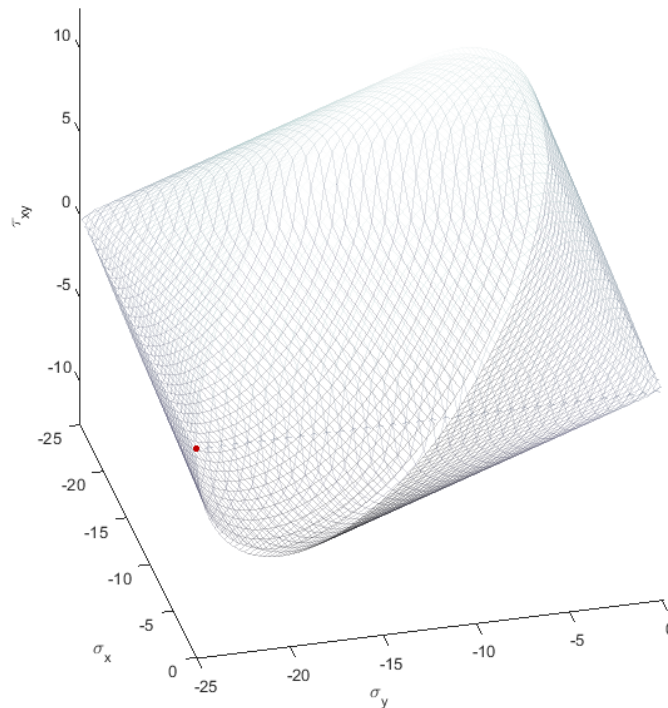


**Figure 9.57.** Stress states in the M.P. Nielsen yield criterion.

The value of the normal forces and moments in the reinforced bar in the bottom of the structure is zero as expected.

Thereby, a proper interaction between the reinforced bar element and the concrete elements is illustrated.

# Appendix I: Appended Paper

## Paper 1

A Program for Verification of Critical Stress Spots in Static  
Loaded Plates by the Lower Bound Limit Analysis

# A Program for Verification of Critical Stress Spots in Static Loaded Plates by the Lower Bound Limit Analysis

Ermin Sehovic, Rasmus Urhøj Hansen & Bo Rasmussen

*Department of Civil Engineering, Aalborg University Esbjerg, 6700 Esbjerg, Denmark*

---

## Abstract

An efficient program for verification of critical stress spots in perfect plastic steel plates subjected to static, in-plane forces is developed. The program is an interaction between ANSYS Workbench and MATLAB, in which ANSYS discretizes the problem to a submodel enclosing the critical region. Subsequently, the submodel is exported to MATLAB where a stress-based element is established for the submodel. A lower bound limit analysis is conducted by a nonlinear optimization algorithm based on the interior point method, which leads to a scalar load multiplier  $\alpha$  defining the maximum load bearing capacity.

Finally, the efficiency of the submodeling technique to verify critical stress spots is demonstrated by means of examples of plates subjected to in-plane forces resulting in either stress concentrations or stress singularities.

*Keyword: Critical Stress Spots; Submodeling; Finite Element Method; Load optimization; Static loading*

---

## 1. Introduction

In the finite element method it is frequently seen that fulfilling the ultimate limit state becomes a problem when designing static loaded plane structures by the theory of elasticity [1]. More specific, stress concentration and stress singularity spots (see Figure 9.58) often induce stresses exceeding the elastic load bearing capacity. As a consequence, the engineer often ignores the critical stress spots by the support of engineering experience instead of verifying the capacity by means of e.g. conducting a nonlinear plasticity analysis. The ignorance of the stress state in the yield region can potentially lead to structural collapse, and in some cases a documentation of the stresses is required to proceed with a project.

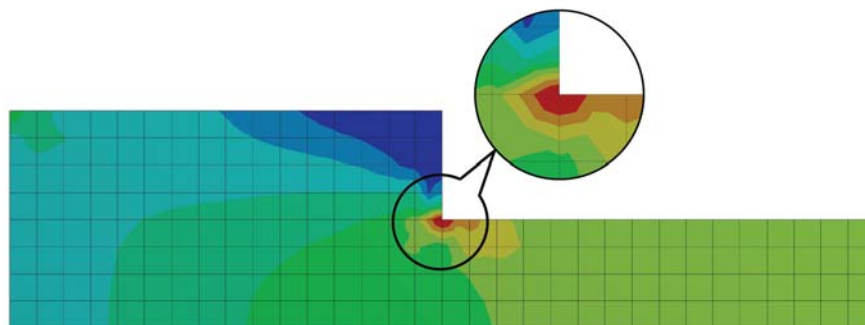


**Figure 9.58.** Example of a plane structure with a critical stress singularity spot.

To accommodate this problem, the study aims for an efficient method to verify critical stress spots by use of the theory of plasticity. Two objectives are therefore underlying for the investigation. First of all, the calculation has to provide a scalar load multiplier defining the optimal safety level, and secondly, the study has to strive towards developing a time-efficient program in comparison to the ones on the market today.

Calculation of the ultimate load bearing capacity of steel structures is often based on the assumption of a perfect plastic material model, which is also the case in this study. When considering a perfect plastic material model, the assumption of sufficient deformation capabilities in the structure is valid. This assumption is necessary in order to obtain stress redistributions.

When calculating the ultimate load bearing capacity either the upper bound theorem or lower bound theorem can be applied. The upper bound theorem is based on feasible collapse mechanisms where the load is minimal, whereas the lower bound theorem is based on a stress distribution that is in equilibrium and where the highest possible load bearing capacity is to be determined.

For solving numerical plate problems with a perfect plastic material model in this study, the lower bound method is implemented. The lower bound method has several advantages over the upper bound method, including the fact that the collapse load is on the safe side. The element formulation is stress-based in contrast to most elastic finite element formulations that are stiffness-based. In the calculations a linear stress field is described based on a finite element discretization where each element has a certain number of stress parameters. As only statically underdetermined structures are considered, it gives rise to stress redistributions at yielding spots in the structure. In the lower bound method, it corresponds to that only a part of the stress parameters has to secure equilibrium, whereas the rest of the stress parameters are used to redistribute the load in order to obtain the maximum load bearing capacity. The calculations are based on nonlinear optimization programming since von Mises yield criterion is used. The triangular plate element with linear stress variation that is used in this study was also used before in soil mechanics (Sloan, 1988 [14]) and linear optimization of concrete plates (Poulsen & Damkilde, 2000 [1]).

The advantage of the approach in this study is that only a subarea is considered and that the solver not only gives a lower bound solution, but it calculates the optimal stress distribution. Thereby, it is possible to determine whether critical stress spots lead to structural collapse.

### Nomenclature

$A$	area of element
$a_i, b_i$	coordinate difference in x- and y-direction for element side $i$
$C$	constraint matrix
$Cs$	strength vector
$f_y$	yield stress
$h$	element equilibrium matrix
$H$	assembled system equilibrium matrix
$l, l_i$	length of element and element side $i$
$p_x, p_y$	load intensity in the $x$ - and $y$ -direction
$Q$	element nodal force vector
$R$	system load vector
$Rc$	self-weight load vector

$T$	thickness
$B$	element stress parameter vector
$\alpha$	scalar load multiplier
$\beta_s$	system stress parameter vector
	in-plane stresses
$\sigma_x, \sigma_y, \tau$	

## 2. Method for Verification of Stress Spots

In this study the approach of verification of critical stress spots in static loaded plates is based on an interaction between ANSYS Workbench and MATLAB. Instead of ANSYS Workbench an arbitrary finite element software could have been used.

The overall proces of the program, from creating a global model to obtaining a submodel solution, is exemplified in Figure 9.59.

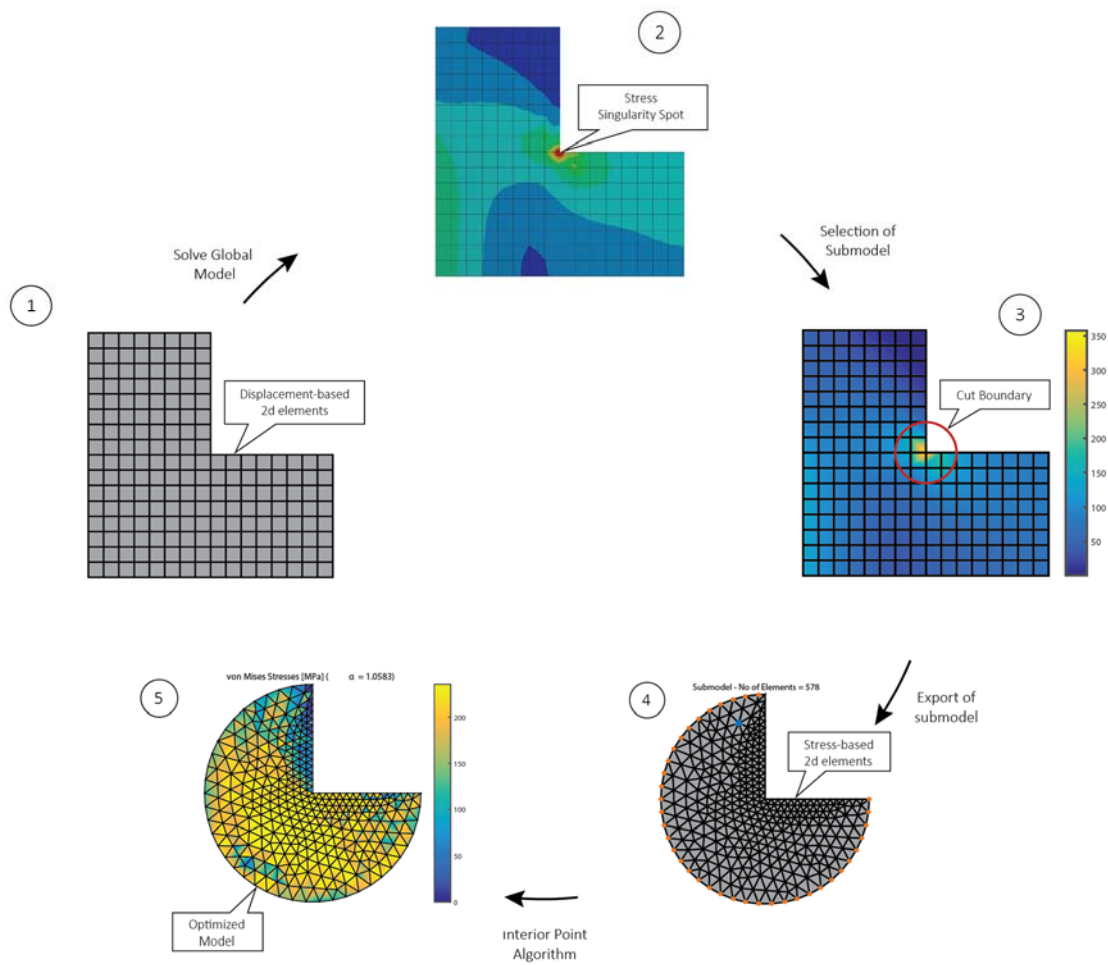


Figure 9.59. Overall process of the program.

In the first steps, ANSYS Workbench is used to solve a global user-defined model by means of a stiffness-based finite element method. By solving the global model, it is possible to conclude whether critical stress spots appear. To make the calculation more efficient the problem is discretized by a submodel considering only a specific region of the domain. In this region the problematic stress spots are solely located, why the problem is significantly reduced regarding calculation time and numerical errors.

The submodel is exported to MATLAB by an interaction with ANSYS Workbench that includes a direct transformation from a stiffness-based mesh utilized in ANSYS to a stress-based mesh generated in MATLAB. The problem is solved in MATLAB where a nonlinear load optimization is conducted by the interior point method. The optimization results in a scalar load multiplier  $\alpha$ .

### 3. Submodeling of Plates

In order to verify critical stress spots, the user has to discretize the global problem to a submodel that encloses the critical region. ANSYS Workbench is used to solve a global plate model and to create a submodel for the upcoming limit analysis in MATLAB. The global model in ANSYS is solved using stiffness-based elements where the structural stresses are related to the nodal displacements. After solving the global model, an APDL-script is implemented in ANSYS Workbench in order to create a submodel and to export the submodeling topology and boundary conditions for the 2D stress-based element formulated in MATLAB.

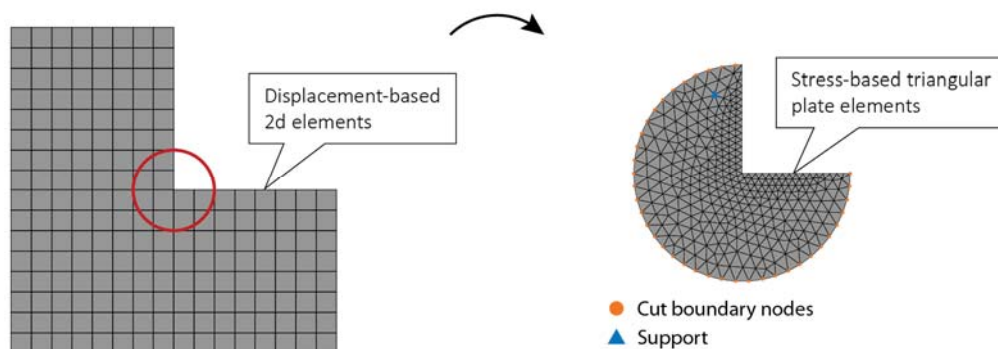


**Figure 9.60.** Example of the submodeling principle.

In order to conduct a lower bound limit analysis in the developed program, the following parameters are exported from ANSYS Workbench:

- node coordinates
- element topology
- plate thickness
- stress components at cut boundary
- density
- gravitational acceleration and direction

#### 3.1 Submodeling Procedure

The submodel is created based on a stress path that can be placed anywhere in the model independent of the global node and element position.

In the developed program, the submodel can either be defined from a *circular* or a *square* cut boundary as seen in Figure 9.61.



**Figure 9.61.** Principles illustrations of submodel geometries.

The size of the two submodel geometries is user-defined, which is done by importing an APDL-script in ANSYS Workbench. The rectangular submodel is defined based on the coordinates of the center in global Cartesian coordinates, and the length and width, whereas the circular submodel is defined by the circle radius and coordinates to the center.

When selecting the subarea, the user has to be aware of mainly two parameters that influences the scalar load multiplier  $\alpha$  in the limit analysis:

- Size of subarea
- Mesh of subarea

By defining a large subarea, a high scalar load multiplier is obtained, but the problem size also increases. If a fine mesh is assigned a more accurate scalar load multiplier is obtained, but it also increases the problem size and thereby the calculation time. Thereby, the load multiplier is an interaction between the size and the mesh of the submodel.

### 3.2 Mesh Generation for Submodel

The principle of making submodels is that the global model has to be meshed coarsely, whereas the mesh of the submodel has to be much more fine. The mesh of the submodel is made from a user defined edge sizing that is based on the number of division chosen for the path operation. This makes it possible to directly use the shear and normal stresses calculated for the stiffness-based elements in the stress-based element boundary nodes. This is due to that the stresses are assumed to vary linearly over the element edges, and that the stress-based elements are located at the same position as the stiffness-calculated path stresses. The fine submodel mesh is created with ANSYS Workbench by means of the input in the APDL-script where the mesh is assembled from CST-elements since triangular stress-based elements use the same topology. By having the same element geometry and number of nodes on the stiffness-based CST-elements as the stress-based elements, it is possible to directly import node coordinates and element topology from ANSYS to the program in MATLAB.

### 3.3 Export of Cut Boundary Stresses

A linear elastic analysis is conducted in ANSYS Workbench for a global model and from the analysis it is possible to obtain the stress state for the global model. After conducting the linear analysis, the stresses at the cut boundary are obtained by making a ANSYS finite element software only the three stress components at each node on the cut boundary is needed to perform the lower bound limit analysis in MATLAB. The stresses from the stress path are used as boundary conditions in the limit state analysis in MATLAB.

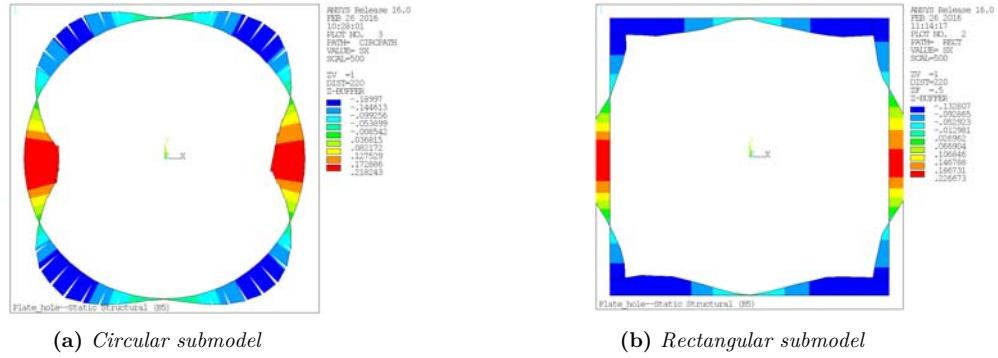


**Figure 9.62.** Example of stress paths with normal stresses along the submodel boundary, corresponding to the submodels in Figure 6.9.

#### 4. Limit State Analysis

##### 4.1 Lower Bound Formulation

The lower bound method is to be applied in the limit state analysis, where the aim is to determine an optimized stress distribution by maximizing the intensity of the predefined external load. In the lower bound method two conditions have to be satisfied in order to obtain a feasible stress state

- Equilibrium equations (Local equilibrium and equilibrium of stresses across element boundaries)
- Yield criterion

In this case the problem is accommodated by the finite element method with stress-based elements. Stress-based elements are used instead of the traditional stiffness-based elements since the problem is formulated as a lower bound method. In the finite element method, the discretized equilibrium equations are written as

$$\mathbf{H}\beta = \mathbf{R}_c + \alpha\mathbf{R}, \quad (\text{I.42})$$

where  $\beta$  is a column vector containing the stress parameters and  $\mathbf{H}$  is the global, assembled equilibrium matrix. The external load is divided into two parts, namely a constant part  $\mathbf{R}_c$  describing the self-weight of the structure and a part  $\mathbf{R}$  that is proportional to the scalar load multiplier  $\alpha$ . The global equilibrium matrix  $\mathbf{H}$  consists of contributions from all individual elements of a model. When the global equilibrium matrix  $\mathbf{H}$  is set up, the number of stress parameters have to be higher than the number of equilibrium equations, which results in a statically underdetermined structure.

Eq. (I.42) can be rewritten to (I.43), which is later written in a more conventional way.

$$\mathbf{H}\beta - \alpha\mathbf{R} = \mathbf{R}_c \quad (\text{I.43})$$

Two types of constraints have to be set up. The first set of constraints has the purpose of satisfying equilibrium equations, whereas the second set of constraints has to secure that von Mises yield criterion is not violated. The constraint securing that the yield criteria is not violated has to be checked in a number of points in each element. For all elements in a structure, the yield criteria can be expressed as

$$f_j(\beta) \leq 0, \quad j = 1, 2, \dots, p. \quad (\text{I.44})$$

The nonlinear optimization problem becomes a maximization problem since the lower bound method is considered. A scalar load multiplier  $\alpha$  has to be determined, which results in the optimal stress distribution of the structure.

The nonlinear lower bound load optimization problem is expressed as

$$\begin{aligned} &\text{maximize:} && \alpha \\ &\text{subject to:} && \mathbf{H}\beta - \alpha\mathbf{R} = \mathbf{R}_e \\ & && f_j(\beta) \leq 0, \quad j = 1, 2, \dots, p \end{aligned} \quad (\text{I.45})$$

As it is expressed in Eq. (I.45), the maximization problem is subjected to both equality constraints since the elements are formulated by linear stress variation, and inequality constraint since von Mises yield criteria is convex.

By solving the maximization problem in Eq. (I.45) with the corresponding linear and nonlinear constraints, it is possible obtain the optimal value for the load multiplier  $\alpha$  and the corresponding stress parameters  $\beta$ .

#### 4.2 Finite Element Formulation

The lower bound formulation is accommodated using linear triangle, stress-based elements as a part of an equilibrium based finite element method. Due to the triangular form of the plate element any irregular geometries can be modelled. In the program the stress-based element mesh and static boundary condition are automatically generated, created based on the information made by the ANSYS Workbench APDL-script.

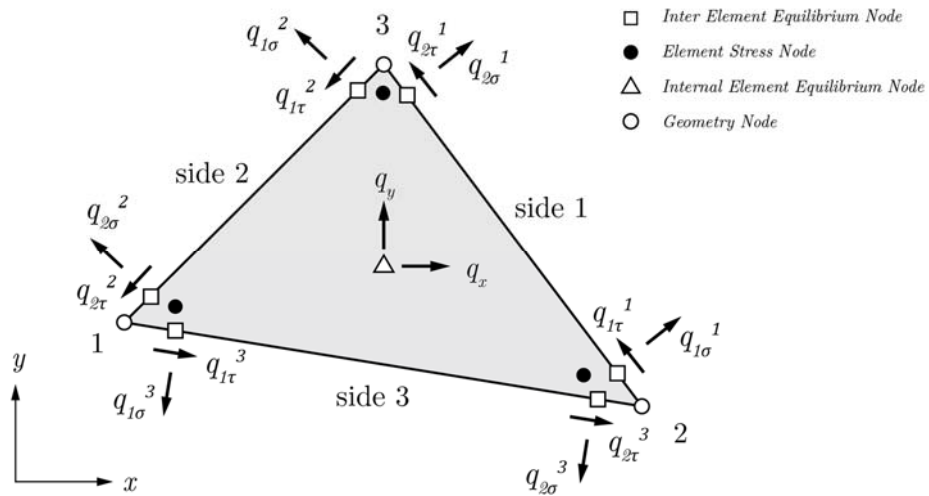


**Figure 9.63.** Triangle stress-based element.

The stress state of each element is described by the stresses at each element node. The stress variation in the element is assumed to vary linearly across the element and the equilibrium is satisfied in two points along each element side. From this assumption it is possible to directly re-formulate the sub-model boundary stresses to generalized nodal forces,  $q$ . Furthermore, the internal equilibrium of each element must be satisfied in order to obtain a statically admissible solution. This is done by satisfying the equilibrium equations in a single point lying within each element.

The lower bound load maximization problem in Eq. (I.45) includes the global equilibrium matrix  $\mathbf{H}$  that has to be set up. In order to set up the global equilibrium matrix  $\mathbf{H}$  it is first of all necessary

to express the equilibrium equations of a single element. In Eq. (I.46) the equilibrium equations are given in a compact form as

$$\mathbf{q} = \mathbf{h}\beta, \tag{I.46}$$

where  $\mathbf{h}$  is the local equilibrium matrix for an element,  $\beta$  is a vector containing the stress parameters, and  $\mathbf{q}$  are the generalized external nodal forces. [1]

When each local equilibrium element  $\mathbf{h}$  of a structure is formulated, it is necessary to assemble each element  $\mathbf{h}$  into the global equilibrium matrix  $\mathbf{H}$  just as it is the case in the finite element method. Based on the equilibrium matrix  $\mathbf{H}$  it is possible to solve the maximization problem.

#### 4.3 von Mises Yield Criterion in 2D

The paper is based on ductile steel plates that obeys von Mises yield criterion. A perfect-plastic material is considered and thereby the assumption of sufficient deformation capabilities in the structure is valid. The assumption is necessary in order to obtain stress redistributions.

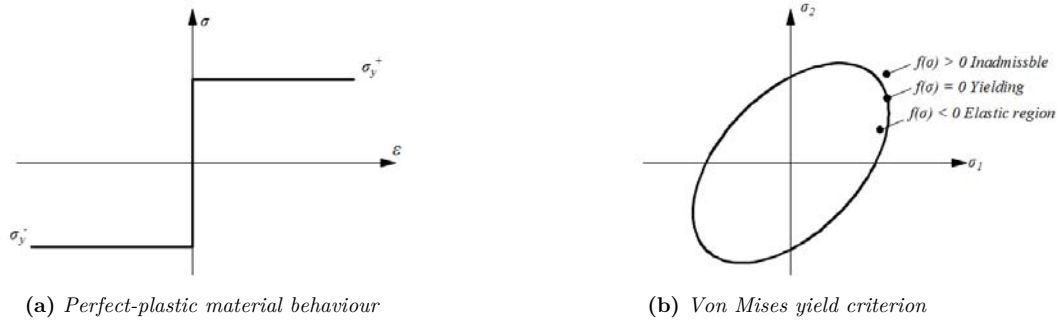


**Figure 9.64.** Material model and yield criterion.

Given that the material behaviour is perfectly-plastic the stress state  $f(\sigma)$  must be either below or equal to the elastic limit. If the limit is violated no information is known about the stress state, why it is considered inadmissible.

The problem solver for the lower bound formulation is for self-same reason described by the non-linear convex constraint given by

$$f(\sigma) = \sigma_{von\ mises} - Y_s \leq 0, \tag{I.47}$$

where  $Y_s$  defines the initial yield strength of the material and the von Mises stress can be found by

$$\sigma_{von\ mises} = f(\beta_i, \beta_j, \beta_{ij}) = \sqrt{\beta_i^2 - \beta_i\beta_j + \beta_j^2 + 3\beta_{ij}}. \tag{I.48}$$

When loading the construction into the plastic region the stress state can solely be modified by a stress rearrangement leading to a stress point located along or inside the yield surface. A load normally resulting in hardening will therefore not expand the yield surface and the stress point must for this reason still be located at the yield boundary that is shown in Figure 9.64. Although no expansion of the yield surface can occur due to the material behaviour, the stress point will still relocate according to the hardening rules as the load increases and the stresses are redistributing. [26]

## 5. Examples of Application

Two examples of application of the program is shown in the following sections.

### 5.1 L-Plates subjected to a tensional Pressure

The first example of application evaluates two similar L-formed 2D plates as seen in Figure 9.65. The geometrical difference between the two considered plate models is the fillet at the concave corner. By having a model with a sharp corner and a similar model with a filleted corner, it is possible to show the application of models with stress singularities and stress concentrations, respectively. Both plates are subjected to a tensional pressure of 30 MPa at the left edge. The plates are constrained in the vertical direction at the bottom edge, whereas the right edge is constrained in the horizontal direction. The plates have a thickness of 1 mm.

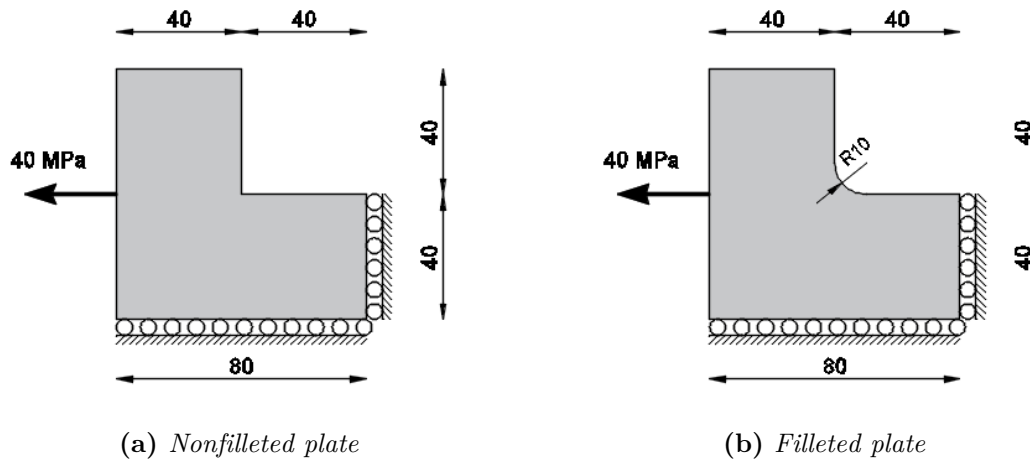


**Figure 9.65.** Free Body Diagram of Models (all dimensions in mm)

The plates are made of steel and the yield strength is assigned to 235 MPa.

#### 5.1.1 Linear Elastic Stress Analysis in ANSYS Workbench

An elastic stress analysis has been conducted in ANSYS Workbench based on the boundary conditions shown in Figure 9.65. The models are meshed coarsely with Q8-elements as seen in Figure 9.66.

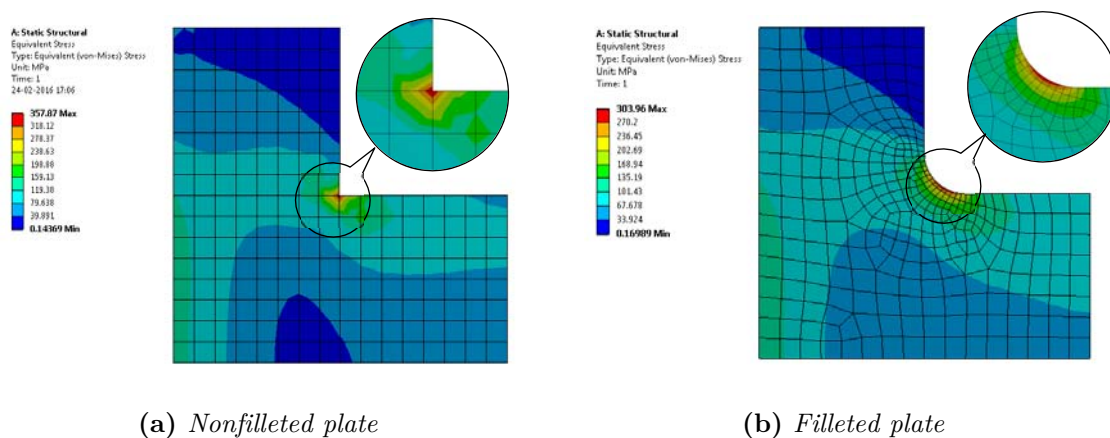


**Figure 9.66.** Plot of mesh and resulting von Mises stresses.

From the linear elastic stress analysis in ANSYS Workbench it is seen that the highest von Mises stresses are obtained in the region of the sharp corner and filleted corner, respectively, whereas the

stresses are much lower in the remaining part of the plate. This is due to stress singularities and stress concentrations, respectively.

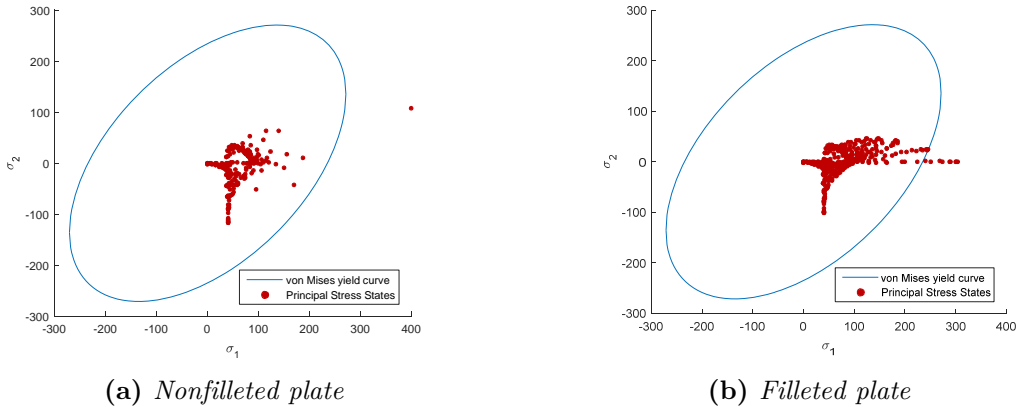


**Figure 9.67.** Plot of von Mises yield criterion and principal stress states for global model.

By plotting the principal stresses of each node of the global model as seen in Figure 9.67, it is seen that only a single stress state is critical for the nonfilleted model, whereas several nodes have stresses exceeding the yield criterion when considering the filleted plate. Since both models have a lot of capacity, the stresses at the critical areas can be redistributed such that an optimized allowable stress state is obtained.

### 5.1.2 Submodeling

In order to redistribute the stresses of the two considered models a circular and rectangular region is sliced, respectively. This is done to show that the program is able to handle both circular and rectangular subareas.

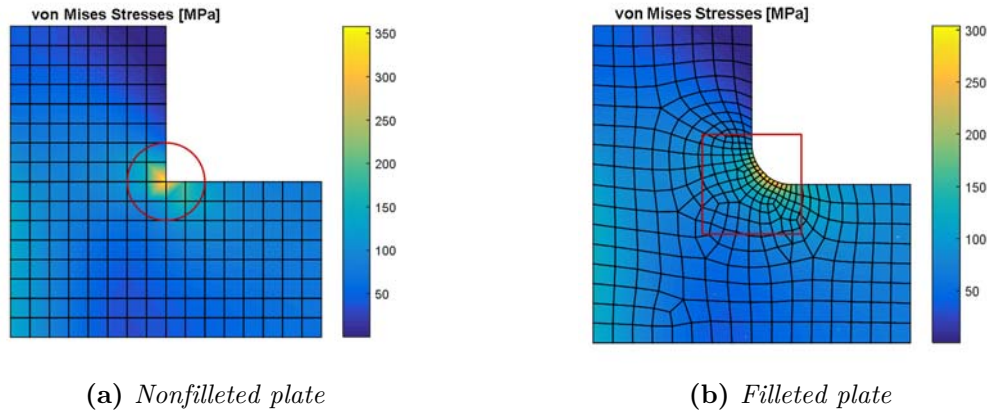


**Figure 9.68.** Global model with selected submodel Area.

For the submodel area a mesh is generated in ANSYS Workbench by means of an APDL-script. The external force is applied in the submodel at the nodes located on the cut boundary, see Figure 9.68.

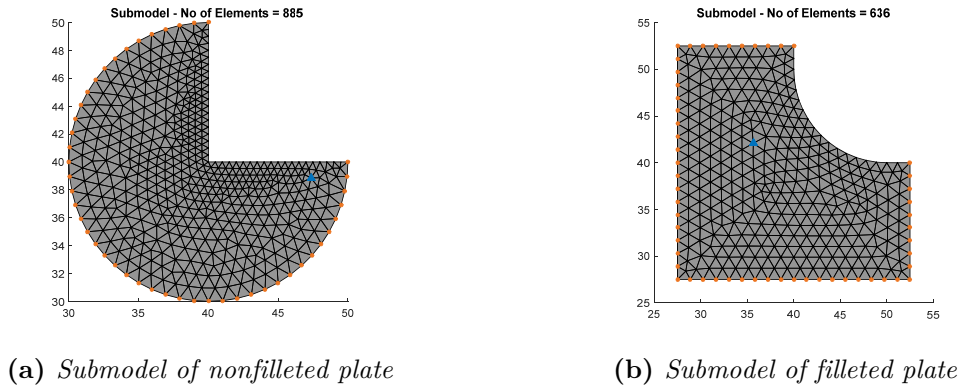


**Figure 9.69.** Submodel Mesh.

Both submodels are statically underdetermined, which gives rise to stress redistributions.

### 5.1.3 Verification of Critical Stress Spots

The scalar load multiplier  $\alpha$  is to be calculated for the submodels in order to clarify whether the given stress state results in structural collapse.

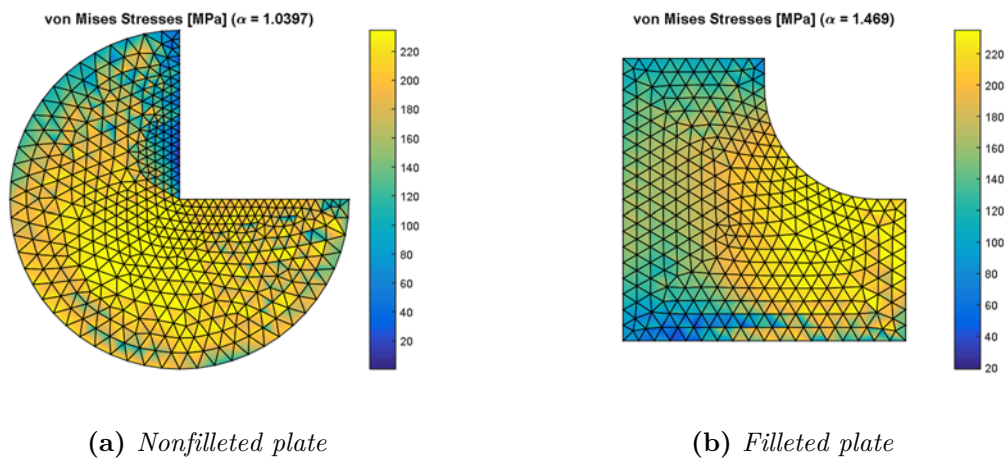


**Figure 9.70.** von Mises stress of optimized submodel.

The scalar load factor  $\alpha$  is above 1.0 and thereby it can be concluded that the applied force doesn't result in collapse for neither models, even though the elastic analysis shows critical stresses for the global model.

By plotting the principal stress states, as seen in Figure 9.71, it is seen that all stress states in the submodel satisfies von Mises yield criterion.

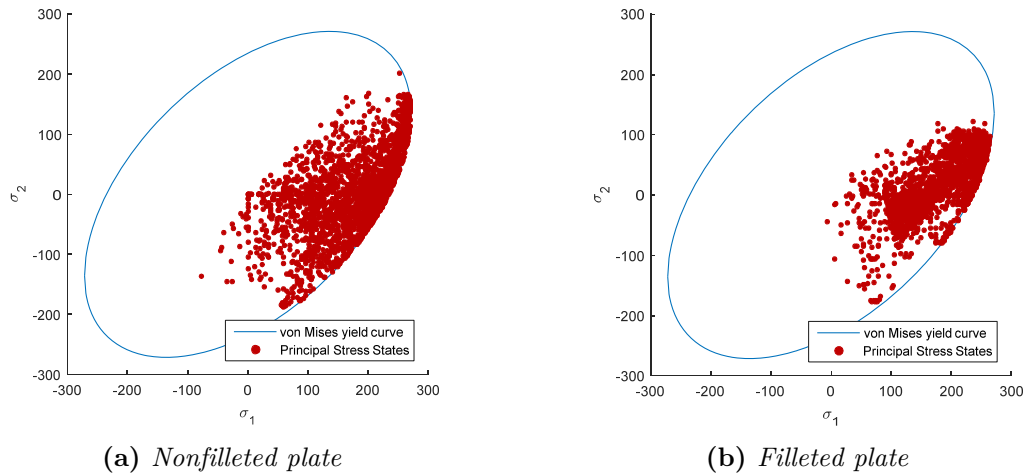


**Figure 9.71.** *Principal stress state of optimized submodel.*

## 6. Conclusions

A program that is able to verify critical stress spots in plates has been developed based on a sub-modeling principle, and lower bound limit analysis. In the lower bound limit analysis stress-based elements are used to calculate the scalar load multiplier  $\alpha$  in order to specify whether a stress state leads to structural collapse. The program appears to be very efficient since only a submodel is considered and only few steps are needed in the overall process.

By implementing an APDL-script in ANSYS Workbench, it is possible to export all the needed finite element information to set up the lower bound problem for the submodel. The maximization of the lower bound problem is conducted by means of nonlinear programming using an interior point solver in either MATLAB or MOSEK.

The generality and efficiency of the program has been presented by examples of plates subjected to stress singularities and stress concentrations, respectively.

## Acknowledgement

The authors devote a special thanks to professor Lars Damkilde for providing the idea with regard to the submodeling technique for verification of critical stress spots.

# Bibliography

- [1] P. N. Poulsen and L. Damkilde, "Limit state analysis of reinforced concrete plates subjected to in-plane forces," *International Journal of Solids and Structures*, vol. 37, p. 19, 2000.
- [2] HighestBridges.com, "Park Bridge," [Online]. Available: [http://www.highestbridges.com/wiki/index.php?title=Park\\_Bridge](http://www.highestbridges.com/wiki/index.php?title=Park_Bridge). [Accessed 29 May 2016].
- [3] Steinwart, "Det gamle København," [Online]. Available: <http://steinwart.dk/scalaxeltorv-kobenhavn-matrikel-nr-66-vestervold/axel-towers-set-fra-axeltorv-22-06-2015/>. [Accessed 29 May 2016].
- [4] M. Yu, G. Ma and J. Li, *Structural Plasticity Limit - Shakedown and Dynamic Plastic Analyses of Structures*, Berlin: Springer, 2009.
- [5] M. P. Nielsen, *Limit analysis and concrete plasticity*, Englewood Cliffs, NJ: Prentice-Hall, 1984.
- [6] L. Damkilde, J. F. Olsen and P. N. Poulsen, "A Program for Limit State Analysis of Plane, Reinforced Concrete Plates by the Stringer Method," *Bygningsstatistiske Meddelelser*, vol. 65, no. 1, p. 26, 1994.
- [7] K. P. Larsen, "Numerical Limit Analysis of Reinforced Concrete Structures," Copenhagen, 2010.
- [8] B. C. Jensen, *Betonkonstruktioner efter DS/EN 1992-1-1*, 2 ed., Valby: Nyt Teknisk Forlag, 2012.
- [9] L. Damkilde, *En introduktion til beregning af rammekonstruktioner med lineært-elastisk/ideal-plastisk materialeopførsel*, Lyngby, 1993.
- [1 E. Moersch, *Der Eisenbetonbau - Seine Theorie und Anwendung*, Stuttgart: Verlag Konrad Wittwer, 1922.
- [1 K. Johansen, "Brudlinieteorier," Gjellerup, København, 1943.  
1]
- [1 K. Johansen, "Yield-line theory," Cement and Concrete Association, London, 1962.  
2]

- [1 H. Lundgren, Cylindrical shells; application of the theory of elasticity and the theory  
3] of rupture to the design of cylindrical roofs, tanks, tubes, pipe lines, and other thin-  
walled cylindrical structures., Copenhagen: Danish Technical Press, 1949.
- [1 S. W. Sloan, “Lower bound limit analysis using finite elements and linear  
4] programming,” *International Journal for Numerical and Analytical Methods in  
Geomechanics*, vol. 12, no. 1, pp. 61-77, 1988.
- [1 P. A. Jensen and J. F. Bard, Operations Research Models and Methods, John Wiley  
5] & Sons, Inc., 2002.
- [1 M. Jirasek and Z. P. Bazant, Inelastic Analysis of Structures, Lousanne and  
6] Evanston: Wiley, 2001.
- [1 N. Karmakar, “A new polynomial time algorithm for linear pro-,” *Combinatorica* 4, p.  
7] 373–395, 1984.
- [1 K. Krabbenhoft and L. Damkilde, “A general non-linear optimization algorithm for  
8] lower bound limit analysis,” *International Journal for Numerical Methods in  
Engineering*, vol. 56, pp. 165-184, 2003.
- [1 The MathWorks, Inc., “Optimization Toolbox,” [Online]. Available:  
9] <http://se.mathworks.com/help/optim/index.html>. [Accessed 8 March 2016].
- [2 The MathWorks, Inc., “Choosing a Solver,” [Online]. Available:  
0] <http://se.mathworks.com/help/optim/ug/choosing-a-solver.html#brppuoz>. [Accessed  
9 March 2016].
- [2 The MathWorks, Inc., “Nonlinear Constraints with Gradients,” [Online]. Available:  
1] <http://se.mathworks.com/help/optim/ug/nonlinear-constraints-with-gradients.html>.  
[Accessed 10 March 2016].
- [2 The MathWorks, Inc., “Constrained Nonlinear Optimization Algorithms,” [Online].  
2] Available: [http://se.mathworks.com/help/optim/ug/constrained-nonlinear-  
optimization-algorithms.html#brnpd5f](http://se.mathworks.com/help/optim/ug/constrained-nonlinear-optimization-algorithms.html#brnpd5f). [Accessed 9 March 2016].
- [2 The MathWorks, Inc., “Writing Scalar Objective Functions,” [Online]. Available:  
3] [http://se.mathworks.com/help/optim/ug/writing-scalar-objective-  
functions.html#bsj1lqf](http://se.mathworks.com/help/optim/ug/writing-scalar-objective-functions.html#bsj1lqf). [Accessed 10 March 2016].
- [2 MOSEK, “The MOSEK C optimizer API manual,” [Online]. Available:  
4] [http://docs.mosek.com/7.0/capi/The\\_optimizers\\_for\\_continuous\\_problems.html](http://docs.mosek.com/7.0/capi/The_optimizers_for_continuous_problems.html).  
[Accessed 30 May 2016].

- [2 C. Frier and L. Damkilde, “A compact formulation of lower bound limit state  
5] problems using the interior point method,” *International journal for numerical  
methods in engineering*, vol. 00, pp. 1-6, 2000.
- [2 K. Krabbenhøft, Basic Computational Plasticity, Department of Civil Engineering  
6] Technical University of Denmark, 2002.
- [2 R. D. Cook, D. S. Malkus and M. E. Plesha, Concepts and applications of finite  
7] element analysis, 4 ed., Madison, Wisconsin: Publication Services, Inc., 2002.
- [2 N. S. Ottosen and M. Ristinmaa, The Mechanics of Constitutive Modeling,  
8] Amsterdam: Elsevier, 2005, p. 745.
- [2 Rambøll, “Projekter,” [Online]. Available: <http://www.ramboll.dk/projects>. [Accessed  
9] 2 March 2015].
- [3 Det Norske Veritas A/S, “DNV-OS-J101 - Design of Offshore Wind Turbine  
0] Structures,” 2014.
- [3 DNV GL, January 2011. [Online]. Available:  
1] [http://www.dnv.com/press\\_area/press\\_releases/2011/new\\_design\\_practices\\_offshore  
e\\_wind\\_turbine\\_structures.asp](http://www.dnv.com/press_area/press_releases/2011/new_design_practices_offshore_wind_turbine_structures.asp).
- [3 R. Davis, Plasticity and Geomechanics, 2002.  
2]
- [3 CRH Concrete A/S, “Elementet,” *Spar penge ved korrekt armering*, p. 12, October  
3] 2015.
- [3 K. W. Johansen, Yield-line formulae for slabs, London: Cement and Concrete  
4] Association, 1972.
- [3 D. E. Grierson and G. M. L. Gladwell, “Collapse Load Analysis using Linear  
5] Programming,” *Journal of the Structural Division*, vol. 97, pp. 1561-1573, 1971.
- [3 E. Anderheggen and H. Knöpfel, “Finite element limit analysis using linear  
6] programming,” *International Journal of Solids and Structures*, vol. 8, no. 12, pp.  
1413-1431, 1972.
- [3 A. F. Ashour and C. T. Morley, “The numerical determination of shear failure  
7] mechanisms in reinforced-concrete beams,” *The Structural Engineer*, vol. 72, no.  
23/24, pp. 395-400, 1994.
- [3 E. Madenci and I. Guven, The Finite Element Method and Applications in  
8] Engineering using ANSYS, 2 ed., Boston, MA: Springer US, 2015.

- [3 M. Nielsen and L. Hoang, *Limit Analysis and Concrete Plasticity*, 3 ed., Boca Raton, Fla.: CRC Press, 2011, p. 796 .
- [4 A. Makrodimopoulos and C. Martin, “Lower bound limit analysis of cohesive-frictional materials,” *International Journal for Numerical Methods in Engineering*, p. 604–634, 2006.